TASK 2 REPORT

EXTRACTING STRESS DATA FROM SEISMIC DATA

A Non-Invasive Approach for Elucidating the Spatial Distribution of In Situ Stress in Deep Subsurface Geologic Formations Considered for CO_2 Storage

DOE Award Number DE-FE0031686

Prepared by:

Battelle
505 King Avenue
Columbus, Ohio 43201

Principal Investigator: Mark Kelley
kelleym@battelle.org 614-424-3704

Project Manager: Christa Duffy
duffyc@battelle.org 614-424-5785

Authors: Bob Hardage[a], Richard Van Dok[b], Mike Graul[c], Allen Modroo[d], Valerie Smith[e], Mark Kelley[e]

a.   Consulting Geophysicist
b.   Sterling Seismic & Reservoir Services
c.   Texseis, Inc.
d.   Core Energy, LLC.
e.   Battelle

Submitted to:

National Energy Technology Laboratory
Technology Development and Integration Center
Carbon Storage Team
Project Manager: William W. Aljoe
412-386-6569
william.aljoe@netl.doe.gov

Date: October 30, 2020

BATTELLE

TABLE OF CONTENTS

Figures

Tables

ACRONYMS AND ABBREVIATIONS

2D	two-dimensional
3D	three-dimensional
CCS	carbon capture storage
CCW	counter-clockwise
CDP	common-depth-point
CMP	common mid-point
CO_2	carbon dioxide
CW	clockwise
DOE	U.S. Department of Energy
FMI	Formation Multi-Imaging
HTI	*horizontal transverse isotropy*
NETL	National Energy Technology Laboratory
NMO	normal moveout
PSDM	pre-stack depth migration
PSTM	pre-stack time migration
SNR	signal-to-noise ratio
TUV	triaxial ultrasonic velocity
VSP	vertical seismic profile
ZVSP	zero-offset VSP

EXECUTIVE SUMMARY

This report describes research accomplishments achieved with funding provided through Department of Energy (DOE) Contract DE-FE0031686. The purpose of this DOE funding is to develop methods that can provide key information about stress fields that act on deep rocks without invading the earth to acquire that information. The research objective was to demonstrate methods that extract the azimuth directions of SHmax and SHmin stress in deep rocks from traditional seismic reflection data like the data that are used to explore for deep oil and gas reservoirs.

Battelle performed two seismic investigations and achieved estimates of SHmax and SHmin azimuths in both efforts that agreed with local, non-seismic, ground-truth measurements of SHmax orientation. The first procedure utilized vertical seismic profiling (VSP) data; the second effort utilized three-dimensional (3D) seismic data. In each investigation, the seismic research data were generated by traditional, non-invasive, surface-based, seismic sources. The methodologies described in this report do not require that a special seismic source be deployed or that difficult seismic data-acquisition procedures be implemented.

The first study was done in the Illinois Basin. Common vertical-vibrator sources were used to generate down-going, illuminating, seismic wavefields and those down-going wavefields were recorded with standard three-component (3C) geophones deployed in a deep well. In other words, conventional VSP data that have been recorded in hundreds of wells across all major depositional basins were used. Use of these VSP data is considered to be a non-invasive procedure, a fundamental requirement for this DOE project, because legacy VSP data that had been acquired several years in the past were used. The earth was not invaded with a new well to acquire the VSP research data used for this study. This non-invasive-VSP procedure can be replicated in many locations by simply reprocessing existing legacy VSP data with the methodology that will be demonstrated in this report.

The second investigation was done in the Michigan Basin, where standard 3D seismic reflection data typical of the data that have been acquired by the oil and gas industry for several decades were used. These 3D data were generated by buried, shot-hole explosives and were recorded by vertical geophones. Data acquired with surface-based seismic sources and receivers, as these data were, certainly meet the criteria of being a non-invasive method for analyzing stress conditions in deep rocks. These 3D seismic data were also legacy data that were acquired several years before implementation of this study. There are thousands of similar sets of legacy 3D data in digital data-libraries around the globe. The methodology described in this report can be replicated with any of these legacy 3D seismic data volumes.

S-wave data were focused on in this VSP study because S waves are more sensitive to stresses and fractures than are traditional P waves used in seismic reflection seismology. Three new S-wave concepts were introduced that will be important in future applications of S-wave seismic data by reflection seismologists.

The first of these new S-wave concepts was that a traditional, horizontal-displacement S source, such as a horizontal vibrator, was not used to generate the down-going direct-S wavefields needed for this S-wave data analysis. Effective, horizontal-displacement, seismic sources are rare and expensive to deploy, which are major reasons why S-wave reflection seismology has

languished for years. Common, low-cost, vertical-displacement or impulsive, P sources (such as vertical vibrators or buried explosives) produce down-going direct-S wavefields, in addition to their well-known direct-P wavefields, and these direct-S wavefields can be used for S-wave imaging purposes. This important physics of using P sources for S-wave illumination of deep targets has been ignored by seismic reflection seismologists for decades. This work thus introduces an advance in S-wave reflection seismology that will benefit the global geophysical community: S-wave illumination of deep targets can be done with common, low-cost, and widely available P sources.

The second new advance in S-wave reflection seismology demonstrated is that S-mode reflection data are available in surface-based 3D seismic surveys that are generated by P sources and recorded with only vertical geophones. This important advance was demonstrated with the Michigan Basin 3D data. Traditional logic is that if you wish to capture any S mode with surface-based receivers, you must deploy horizontal geophones. Deploying horizontal geophones is an expensive, and often difficult, field procedure. At each reflecting interface, some of the energy carried by a down-going, direct-SV, illuminating wavefield produced by a P source reflects as an up-going SV reflected wavefield. This upgoing SV reflection indeed can be recorded, but only if horizontal geophones are deployed across the earth surface. However, some of the down-going SV energy converts to an up-going, reflected P wavefield. This reflected P wavefield is recorded by surface-based vertical geophones just as are up-going P reflections produced by a down-going P wavefield. The new S-wave imaging mode used in this study is this latter SV-to-P converted mode, which is designated throughout this report as **SV-P** data.

In common 3D, P-source, seismic surveys that utilize only vertical geophones, two images are thus embedded in vertical-geophone data. One image is the traditional P-P reflected wavefield that has been used for decades, and the second image is an SV-P reflected wavefield which carries stress-sensitive S-wave information. Both traditional P-P reflected wavefields and this new concept of SV-P reflected wavefields were utilized in this project. Hopefully, this work will encourage others to utilize SV-P reflections embedded in vertical-geophone data.

How to use this new concept of SV-P reflection seismology to detect SHmax azimuth is demonstrated by constructing SV-P trace gathers at imaging bins across a Michigan Basin 3D seismic survey. These SV-P trace gathers utilized only those source-receiver pairs that were constrained to be inside a narrow-azimuth corridor. That narrow stacking corridor was then rotated in a 360-degree circle to find the azimuth where a targeted SV-P reflection appeared at its earliest arrival time, and that azimuth where it appeared at its latest arrival time. The earliest arrival time of an SV-P reflection defines the azimuth of the fast-S mode, which is also the azimuth of SHmax. The azimuth of the latest arrival defines the azimuth of the slow-S mode, which is also the azimuth of SHmin.

The fundamental physics of fast-S wave modes is only one example of new rock information that becomes available when SV-P reflection physics is utilized. The existence of SV-P reflections in data generated by P-wave sources and recorded by vertical-geophone data has been ignored by geophysicists for decades. Because the combination of P sources and vertical geophones is used to collect almost all land-based 3D seismic data, this revelation that S-wave reflection seismology can be practiced with data generated by P sources and recorded by vertical geophones should reach beyond this DOE project and have an impact on worldwide seismic reflection imaging.

The third new concept introduced in this project was how to extract the azimuth of maximum horizontal stress (SHmax) by doing a simple, 360-degree, mathematical rotation of a down-going, direct-S, wavelet generated at the baseplate of a surface-based, vertical-vibrator, that travels through stressed rocks to a deep, horizontal, VSP geophone. This project shows that the azimuth where a polarity reversal occurs in this mathematically rotated S wavelet defines the azimuth of SHmax. This vertical-vibrator, direct-S, wavelet rotation method was tested for determining SHmax azimuth at the FutureGen2 site where VSP data were acquired by a previous DOE-funded project (Cornet, 2014). SHmax azimuths indicated by this simple wavelet-rotation method were determined when vertical vibrators were stationed at zero-offset, at far-offset, and at different azimuths around a VSP receiver well. These VSP-based SHmax azimuths agreed with the azimuth of SHmax found by traditional engineering mini-frac tests in the same VSP receiver well. This simple VSP data analysis procedure for detecting the azimuth of maximum horizontal stress has never been reported or discussed in geophysical literature. The publication of this technical finding should be of considerable interest to the worldwide geophysical community.

This study utilized existing VSP data that were acquired 7 years in the past and then were preserved in a digital seismic-data library. Others can use this same non-invasive strategy of extracting legacy VSP data from a digital-data library by reprocessing legacy VSP data to extract stress-sensitive S-mode attributes across an area of interest. A second non-invasive option for acquiring stress-sensitive VSP data would be to acquire new VSP data with a traditional P-wave source, preferably a vertical vibrator, in an existing well. This option would simply take advantage of an old invasion of a drilled well into the earth and would not require any new invasive drilling.

Because P sources (usually vertical vibrators) have been used to acquire almost all existing onshore VSP surveys, the new P-source concepts introduced by this project mean that a large number of legacy VSP surveys that have been acquired years in the past contain direct-S illuminating wavefields that can be processed according to this strategy to remotely define the azimuth of SHmax at sites of interest. It also means that future land-based VSP data-acquisition efforts will be implemented knowing that all P sources (vertical-vibrators, vertical-impact, and buried explosives) will produce direct-S illuminating wavefields in addition to direct-P illuminating wavefields.

1.0 Introduction

1.1   Overview and Purpose

This document presents a summary of Task 2 (Extracting Stress Data from Seismic Data) of the project titled "*A Non-Invasive Approach for Elucidating the Spatial Distribution of In Situ Stress in Deep Subsurface Geologic Formations Considered for CO_2 Storage (FE0031686)".* This three-year project is part of the U.S. Department of Energy (DOE) National Energy Technology Laboratory (NETL) Carbon Storage program to research and address gaps that affect the economics of commercial carbon capture storage (CCS) projects. One of these key gaps is the lack of certainty in predicting geomechanical impacts of pressure migration caused by carbon dioxide (CO_2) injection into a storage complex. The overall goal of this project is to improve technical and economic performance of state-of-the-art methods for determining in situ stresses. This project aims to develop methods for determining the spatial distribution, both laterally and vertically, of the magnitude and orientation of the three principal in situ stresses in the deep subsurface (depths greater than 1500 meters). Verification testing will be conducted at a field site. The results of this work will lead to an increased understanding of the geomechanical impacts associated with a CO_2 injection operation and therefore decrease the geomechanical risks throughout the life cycle of the project.

The project consists of five tasks over a three-year period from October 1, 2018 through September 30, 2021. This project is led by Battelle Memorial Institute (Battelle) in Columbus, Ohio. The project team includes Core Energy, LLC, The University of Pittsburgh, SINTEF, Bob Hardage, Ph.D., and Wayne Goodman, PhD. Other participants include Sterling Seismic and Reservoir Services, Texseis, and Schlumberger. A summary of the project tasks is provided in Table 1-1. This report documents results of Task 2.

Table 1-1. Project tasks.

Task	Task Description
Task 1	Project Management
Task 2	Seismic data processing for two field sites to determine the stress orientation (i.e., Shmax azimuth), anisotropy [Vs fast/Vs slow], and [Vp/Vs] in the area with seismic-data coverage.
Task 3	Laboratory experiment to establish experimentally-derived relationships between wave velocity/attenuation (anisotropy) and the triaxial stress state (magnitude and direction).
Task 4	Field well testing, logging, coring of the Core Energy LLC SOL 8-15A well in Otsego County, Michigan to obtain stress-related measurements and mechanical rock properties to use to build geomechanical model (Task 5) and to verify the seismic-derived stress results from Task 2.
Task 5	Geomechanical stress modeling of the spatial distribution of stress orientation and magnitude within the area with seismic data; incorporate stress magnitude-velocity anisotropy relationship(s) from triaxial ultrasonic velocity (TUV) lab experiments; compare/verify results with field data (stress measurements)

1.2   Task 2 Verification Sites

Task 2 involved demonstrating non-invasive methodologies for extracting stress data from two types of seismic data acquired at sites located in different geologic basins. Site 1 is the former FutureGen2 site in Morgan County, Illinois, in the western portion of the Illinois Basin (Figure 1-1). This site was selected because a comprehensive suite of characterization data is available

from the FutureGen2 test well drilled at the location. These characterization data consist of geophysical logs, core data, and well test data, including Shmax and Shmin measurements made at multiple depths by conducting open borehole hydraulic fracture stress tests. The seismic data at this site consist of a zero-offset vertical seismic profile (VSP) and 15 far-offset VSPs oriented in several azimuths away from the receiver well. Schlumberger recorded these VSP data in 2013, and thus this research was done with legacy VSP data that did not require invasive entry into any reservoir and its sealing unit. Figure 1-2 shows the VSP source locations and the test well at the FutureGen2 site.

Study site 2 is located in Otsego County, Michigan, in the northern part of the Michigan basin (Figure 1-3). This site was selected because a previously acquired, high-quality, large, three-dimensional (3D) seismic survey was made available by Core Energy, LLC, along with access to an open borehole (well State Otsego Lake 8-15A) within the seismic survey area that could be used to acquire stress measurements for comparison to seismic-derived stress results (Figure 1-4). Working with two different types of seismic data required developing a different seismic data-processing workflow for each site: one processing strategy tailored to VSP data recorded with three-component geophones placed in a deep well, and another strategy structured for 3D seismic data recorded by vertical geophones spread across a surface area spanning approximately 25 square miles.

A requirement for this project was that the developed method be non-invasive. Presumably, this requirement means no boreholes need to be drilled that penetrate the caprock or the storage reservoir. The approach demonstrated in this report meets this requirement because it uses seismic data as the primary data to characterize subsurface stress. If digital legacy seismic data already exist at a site of interest, are available for reprocessing, and are of suitable quality, they can be used in lieu of collecting new seismic data. Alternatively, if seismic data do not exist for a site, it will need to be acquired. This means the new seismic data must be surface reflection data, unless wells/boreholes already exist at the site that extend to the target storage reservoir and are appropriate for deploying downhole geophone arrays. It is likely there are many potential CO_2 storage locations where one or both of these conditions exist. In this project, legacy VSP data were used for Site 1, and legacy surface reflection data were used for Site 2.

Figure 1-1. The Illinois structural basin superimposed on a regional map showing approximate location of the FutureGen test well in Morgan County (modified from Buschbach and Kolata, 1991).

Figure 1-2. VSP well and source locations X01 through X17 at the FutureGen2 site. No data were generated at source stations X04 and X06.
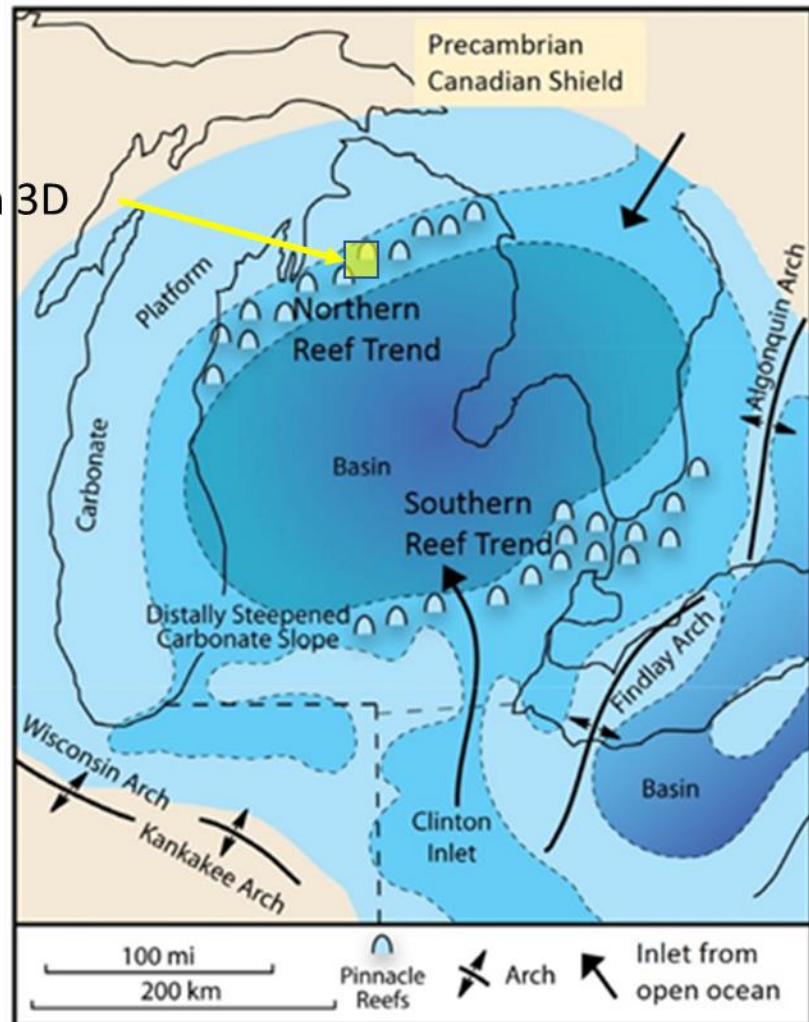
Figure 1-3. Approximate location of Site 2 in the Michigan Basin.
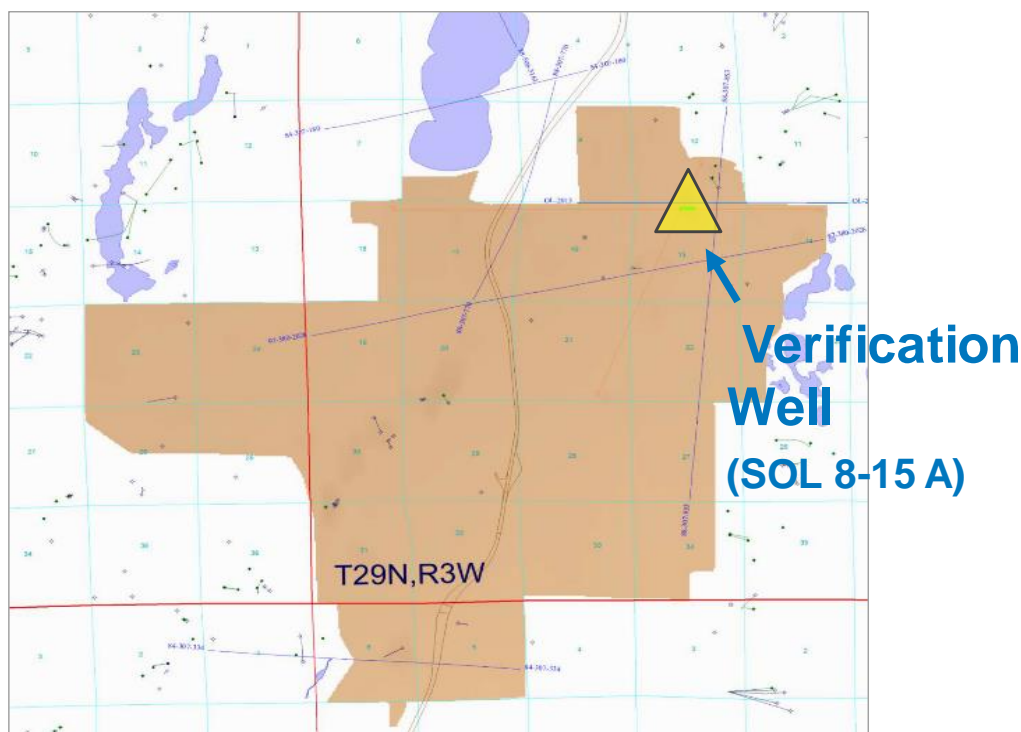
Figure 1-4. Perch 3D Seismic Survey Area at the Otsego County, Michigan Site. Each green square is 1 square mile.

1.3 Overview of Non-Invasive Methods for Extracting Stress Data from Seismic Data

This section describes methodologies used to extract stress orientation data from two types of seismic data: VSP data and surface-sensor reflection data. The former FutureGen2 site in Illinois was used to demonstrate the VSP method. The Perch 3D seismic survey in Otsego County, Michigan, owned by Core Energy, was used to demonstrate the methodology for seismic reflection data acquired with surface-based geophones.

1.3.1 Overview of Method for Extracting Stress Data from Vertical Seismic Profiling (VSP) Data

This study demonstrates a novel technique for determining the direction of maximum horizontal stress (Shmax) from VSP data that has never been demonstrated. This new approach involves only simple mathematical rotation of a down-going, direct-S, first-arrival wavelet recorded by a deep horizontal geophone. In this approach, no S-wave imaging was required to obtain estimates of Shmax. Later sections of this report explain the physics underlying this strategy and compare these VSP estimates of Shmax with ground truth measurements of Shmax provided by engineering stress tests conducted in the VSP well.

VSP estimates of Shmax azimuth can be used to orient VSP horizontal geophones in fast-S and slow-S polarization azimuths. Fast-S polarization direction and Shmax azimuth are equivalent compass angles. Once Shmax azimuth is known, fast-S and slow-S VSP images can be made to extend stress-sensitive information away from a VSP receiver well if desired.

However, extensions of stress information away from a VSP well can be done only if the difference in fast-S and slow-S velocities is large enough to create measurable differences in the arrival times of deep S-mode reflection events. VSP imaging efforts at the Illinois FutureGen2 site showed that slow-S images did not display measurable time delays in key reflection events when compared to their companion fast-S images. This approximate equivalence of fast-S and slow-S image times indicates that the difference between Shmax magnitude and Shmin magnitude at the FutureGen2 study site is not large. This fact increases the importance of the new direct-S wavelet-rotation method introduced in this project because, as will be shown in Section 3, this unique methodology provided correct estimates of Shmax azimuth even when the difference between Shmax and Shmin magnitudes was small.

An important concept introduced to the CO_2 sequestration community by this direct-S wavelet rotation method is proof and demonstration that only a simple vertical-displacement source, like a vertical vibrator, is needed to generate the down-going direct-S wavefield needed for S-wave data analysis. It is not necessary to deploy an expensive (and now almost non-existent) horizontal-displacement source, such as a horizontal vibrator, to generate direct-S illuminating wavefields.

2.0 Basic Concepts of Research Approach

Several fundamental concepts relate fractures and stresses in a seismic propagation medium to attributes of seismic waves that propagate through that medium. Fractures and stresses affect S waves more strongly than they do P-waves (Alford et al., 1989; Hardage et al., 2011; Mueller, 1992; Winterstein and Meadows, 1991; Xu and King, 1989), thus the focus of this study is on seismic S waves. It is appropriate to provide short descriptions of the basic relationships between stresses, fractures, P-wave attributes, and S-wave attributes in this early section so later writing can refer back to these fundamental principles to justify conclusions made about deep stress conditions when results of P- and S- seismic data processing and interpretation are presented. The rock physics and seismic wave propagation principles described here apply to P- and S- data acquired with vertical seismic profiling procedures and also to seismic reflection data recorded by surface-based geophones.

2.1 Extensional Fractures, Shear Fractures, and Maximum Horizontal Stress

Subsurface stress fields in the earth are described by using three orthogonal stress vectors: Shmax, Shint, and Shmin. In this notation, Shmax is the direction of maximum horizontal stress, Shint is the direction of intermediate horizontal stress, and Shmin is the direction of minimum horizontal stress. When stress-induced fractures are produced in rocks, the fracture pattern can be represented by three failure planes, A, B, C, which are related to each other as drawn on Figure 2-1. Failure plane B indicates the orientation of extensional fractures, which align with the direction of maximum stress Shmax. Failure planes A and C represent shear fractures that intersect the maximum horizontal stress vector at angle Φ, where Φ is approximately 30 degrees for most rocks. Twiss and Moores (1992) measured angle Φ between maximum stress vectors and shear-fracture planes A and C for numerous rock types, temperature conditions, and pore-fluid mixtures (a total of 130 tests). They found that Φ could be described as a distribution function that had a mean value of 28.7 degrees and a standard deviation of 7.4 degrees.

Horizontal stresses are studied in this project, which means fracture systems are viewed with seismic data when stress vectors σ_1 (Shmax) and σ_3 (Shmin) in the bottom-left and bottom-right diagrams of Figure 2-1 are horizontal. These two diagrams illustrate how the directions of extensional fractures and shear fractures are related to the azimuth of horizontally directed Shmax. The fast-S mode of seismic shear waves will orient its displacement vector in the same direction as Shmax azimuth. Thus, the emphasis of this research was to utilize seismic shear waves, and then to determine the polarization direction of the fast-S mode in deep rocks at two study sites, one site in Illinois and one site in Michigan. When this fast-S polarization direction is determined, then Shmax azimuth is defined.
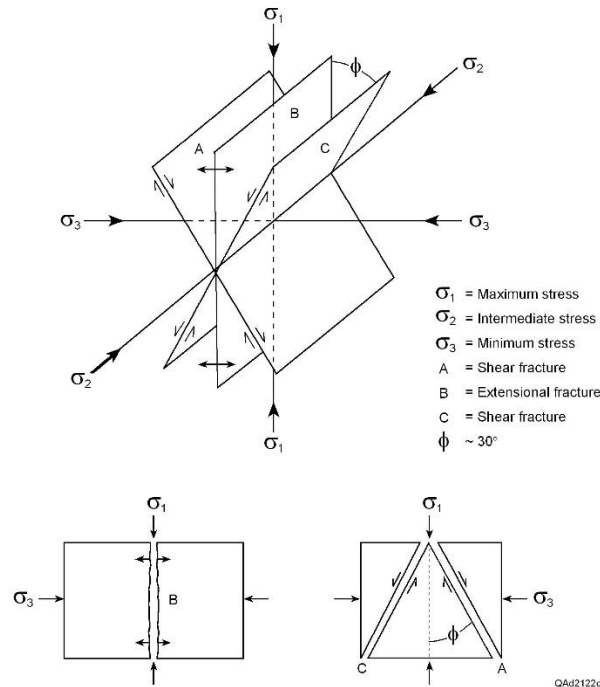
Figure 2-1. Relationships between horizontal stress fields and fracture planes. (Top) Oblique view of horizontal stress vectors and fracture planes. (Bottom left) Vertical view along the σ$_2$ (Shint) axis showing horizontal stress vectors σ$_1$(Shmax) and σ$_3$(Shmin) and fracture plane B (extensional fractures). (Bottom right) Horizontal view along the σ$_2$ (Shint) axis showing stress vectors σ$_1$ (Shmax) and σ$_3$ (Shmin) and fracture planes A and C (shear fractures). Extensional fractures B align with maximum stress vector σ$_1$ (Shmax). Shear fractures A and C intersect this maximum stress vector at an angle φ that is approximately 30 degrees. Horizontal stresses are studied in this project, which means fracture systems are viewed with seismic data when stress vectors σ$_1$ (Shmax) and σ$_3$ (Shmin) in the bottom-left and bottom-right diagrams are both horizontal. (Source: Hardage et al., 2011).

2.2   Accuracy of Fracture Properties Depends on Rock Volume Analyzed

An important principle that supports the concept of using S-wave seismic data to determine Shmax is: *as fracture orientations are measured in larger volumes of rock, the more confidence there is that the dominant population of fractures will be extensional fractures*. In other words, the larger the volume of rock that provides fracture-orientation information, the more confidence there is that the azimuth of fast-S polarization (i.e., Shmax azimuth and extensional-fracture direction) is reliable. Formation multi-imaging (FMI) data are popular well-log measurements used to describe azimuth orientations of fractures. However, FMI shows only those fractures that intersect a logged well, and a single borehole is a small sample of a fractured, deep-rock, volume. The population of fractures detected across a targeted depth interval in a single borehole is a small number, often being only a single digit. Such small-scale fracture sampling raises the question "*is a detected fracture an extensional fracture or a shear fracture* (Figure 2-1)?". Which type of fracture is imaged defines the interpreted azimuth of Shmax.

This caution about relying on Shmax azimuth measurements that involve only a small rock volume will be demonstrated using FMI log data collected in wells positioned inside a 1-mi^2 area of a West Texas fractured-carbonate oil field (Hardage et al., 2011). Azimuths of FMI-based, high-confidence fractures observed within this West Texas reservoir interval are plotted as rose

diagrams in Figure 2-2. When data are available from only one well (left diagram, 28 fractures) in this targeted 1-mi^2 study area, the dominant fracture population is oriented slightly south of east. If no other fracture-sensitive data were available, the maximum horizontal stress vector would be assumed to be pointed in the same direction, slightly south of east. If a seismic-based estimate of Shmax involving a large rock volume indicated a different azimuth for Shmax, some would suspect the seismic estimate rather than the borehole measurement.
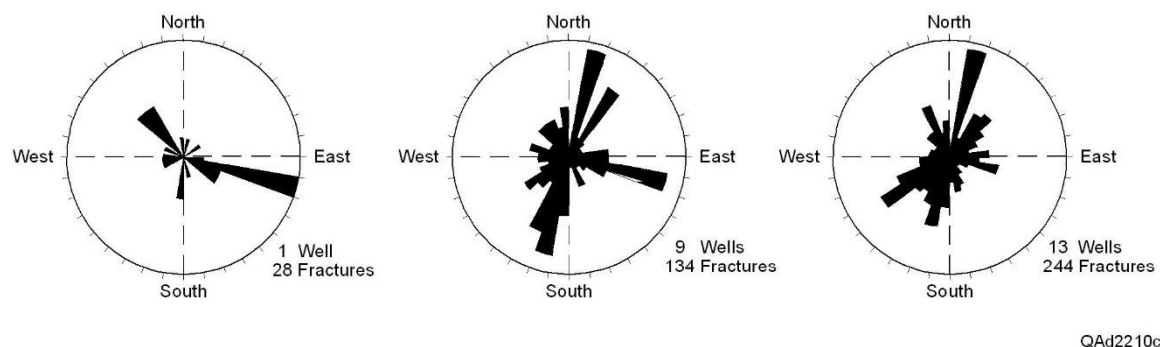
Figure 2-2. Azimuths of extensional and shear fractures become clearer as a fracture analysis is expanded from 1 well, to 9 wells, to 13 wells (or from 28 to 134 to 244 high-confidence fractures). The azimuth of the dominant fracture population (the azimuth of maximum horizontal stress) is obviously influenced by the physical size of the rock volume in which a fracture measurement is made (i.e. by the number of fractures that are involved in a measurement). (Source: Hardage et al., 2011).

When FMI is expanded across a larger portion of the 1-mi^2 study area to include data from nine wells (center diagram, 134 fractures), a large fracture population then appears that is oriented in a north-northeast to south-southwest direction. Now an investigator must decide if the direction of maximum stress is north-northeast to south-southwest, or east-southeast to west-northwest. When the analysis area is expanded again and three more wells are included, the original east-southeast orientation of observed fractures diminishes, other fracture orientations grow in importance (right diagram, 244 fractures), and a north-northeast to south-southwest orientation of σ_1 dominates the population and seems to be the correct choice for Shmax.

An interpretation of horizontal stress vectors based on the 13-well database is exhibited as Figure 2-3. With this maximum-size FMI database, the total fracture population segregates into a definitive picture of extensional fractures oriented north-northeast (failure plane BB) and shear fractures oriented approximately 30-degrees east and 30-degrees west of these extensional fractures (failure planes AA and CC). Note that this real-data result is almost a perfect replication of the theoretical relationship between extensional fractures and shear fractures illustrated on Figure 2-1.

Extensional fractures BB dominate the fracture population in Figure 2-3; however, many shear fractures (AA and CC) are also present. When fractured intervals are analyzed with data that investigate only small volumes of rock immediately adjacent to boreholes, the greatest population of fractures may be shear fractures local to a well, which will not be aligned with maximum horizontal stress. For example, if the only available FMI information at this West Texas field was that recorded in the single well displayed in the left diagram of Figure 2-2, an interpreter would define Shmax to be oriented east-southeast, which is the azimuth of minimum horizontal stress (Figure 2-3), not maximum horizontal stress. This interpretation would be the

worst possible conclusion about the azimuth direction of Shmax. The only evidence of correct Shmax fractures in the single-well data in Figure 2-2 is the small fracture population oriented slightly west of south. This misleading outcome is the risk of depending on fracture information extracted from only a small volume of stressed rock.
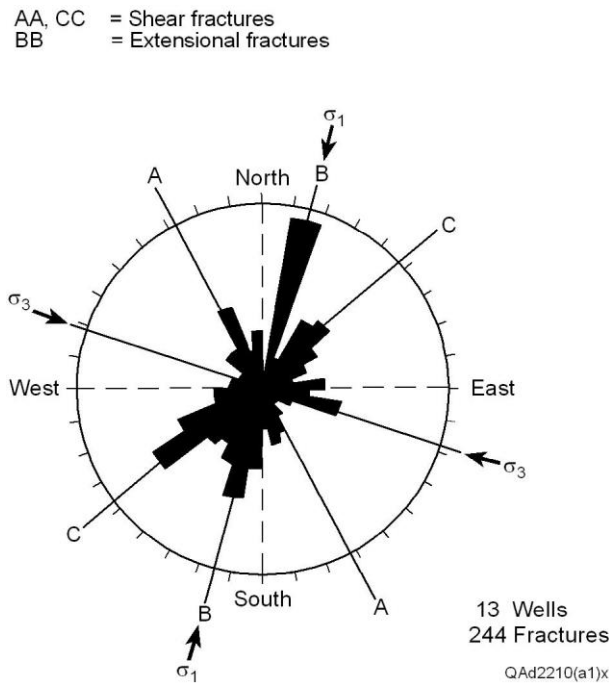
Figure 2-3. Horizontal stress model inferred by a significant number of fractures interpreted from FMI log data recorded in wells that spanned slightly more than 1-mi². (Source: Hardage et al., 2011).

This example emphasizes that fracture measurements involving large rock volumes are more reliable for defining Shmax than are measurements that involve small rock volumes. This logic implies that long-wavelength data that probe a large rock volume, as seismic data do, should be a reliable way to determine Shmax azimuth in deep rocks. This conclusion is particularly applicable to seismic shear waves because, as they propagate through stressed rocks, they segregate into a fast-S mode that is polarized in the azimuth of Shmax and a slow-S mode that is polarized in the azimuth of Shmin. In this methodology, the average wavelength of seismic S-waves used to probe deep rocks was approximately 100 m (305 ft). These long wavelength S-waves traveled slanted paths through deep, targeted, stressed rocks that were sometimes several thousands of feet thick. The end result was that a massive rock volume was probed in each of these investigations to determine Shmax azimuth.

2.3   Fast-S and Slow-S Wave Modes

Shear (S) waves have a unique property that sets them apart from compressional (P) waves. When an S wave encounters rocks that have azimuth-dependent variations in stiffness coefficients, it splits into two daughter S-wave modes that are polarized orthogonal to each other and that have different propagation velocities. The fast-S mode, often designated as S_1, is polarized so that its displacement vector is oriented in the direction of greatest rock stiffness, and the wave mode propagates with velocity V_{S1}. For fractured rocks, traditional S-wave physics

principles demonstrate that S_1 is polarized in the direction of maximum horizontal stress (Shmax), which is also the azimuth in which extensional fractures are oriented (Figure 2-1).

In contrast, a slow-S mode, commonly designated as S_2, is polarized so that its displacement vector is oriented in the direction of weakest rock stiffness, and this mode propagates with a slower velocity V_{S2}. For stressed rocks, traditional S-wave physics principles indicate S_2 is polarized in the direction of minimum horizontal stress (Shmin), which is the direction orthogonal to S_1 polarization (Figure 2-1). The difference in the magnitudes of propagation velocities V_{S1} and V_{S2} for fast-S and slow-S modes depends on the magnitude of the difference in rock stiffness in their respective polarization directions. This principle means that the ratio of fast-S and slow-S interval velocities, V_{S1}/V_{S2}, is a powerful indicator of fracture density within a fractured rock interval. Larger values of V_{S1}/V_{S2} indicate denser concentrations of fractures (higher fracture density), and smaller values of V_{S1}/V_{S2} indicate reduced fracture density. When a V_{S1}/V_{S2} ratio equals, or is close to, a value of 1, there probably are few, and perhaps even no, fractures. A V_{S1}/V_{S2} ratio of approximately 1 appears to be what exists at study site 1 in the Illinois Basin (Figures 1-1 and 1-2).

P waves also split into fast and slow modes when rocks have azimuth-dependent stiffness, but P-wave splitting is much weaker than S-wave splitting (Lynn, 2004a, 2004b). In practice, observable P-wave splitting is so minor that common practice (not necessarily correct practice) is to ignore that P-wave splitting occurs. This concept of wave splitting sets S waves apart from P waves and means that S waves provide unique information about deep-rock stress conditions, fracture physics, and rock stiffness properties that cannot be extracted from P waves. This S-wave physics is the reason S-wave modes were emphasized at each of the two deep, stressed-rock, study sites in this project.

2.4   Fast-S and Slow-S Propagation in Stress-Fractured Rocks

A rock-physics laboratory study by Sondergeld and Rai (1992) is particularly informative for understanding the physics of fast-S and slow-S propagation in stressed, fractured rocks. This laboratory test methodology was so simple, and so effective, that their laboratory test procedure was upscaled by a factor several thousand and replicated with VSP data at the FutureGen2 site in the Illinois Basin.

Test samples used by Sondergeld and Rai (1992) were horizontal cylinders cut from laminated shale. These shale cylinders were then oriented vertically, as illustrated in Figure 2-4, so that the laminae between shales layers simulated vertical fractures. A small piezoceramic element was secured to one end of this cylindrical volume of laminated shale and acted as an S source because it applied a horizontal pulse-displacement to the test sample. A similar piezoceramic element was positioned at the opposite end of the cylinder to imitate a horizontal geophone sensor.
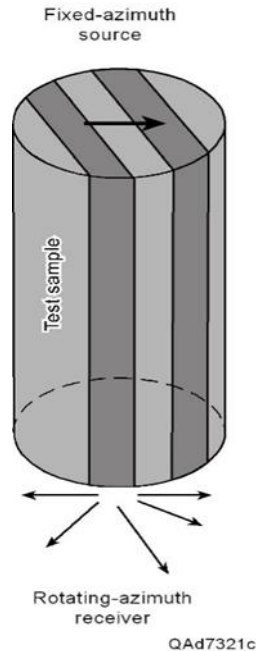
Figure 2-4. Laboratory measurements of S-wave propagation through a simulated medium of vertical fractures (Source: Sondergeld and Rai, 1992).

This vertically striated propagation medium, coupled with the fact that the source-receiver geometry caused S-waves to propagate parallel to embedded layer interfaces (i.e., parallel to simulated fractures), combined to create an excellent representation of S-wave propagation through a system of vertical fractures. Source and receiver elements used in this laboratory experiment were vector sensors, thus the polarities of recorded data depended on the orientations of the positive-polarity ends of the piezoceramic source and receiver elements. The vector nature of these piezoceramic sensors replicates vector-based seismic sources and receivers that are used in real-world acquisition of S-wave seismic data with horizontal vibrators and horizontal geophones.

In this laboratory experiment, the source on the upper end of the layered shale sample remained in a fixed orientation relative to the vertical planes of the simulated fractures (the laminae interfaces between shale layers) as data were recorded. The receiver element on the bottom end of the sample was then rotated in azimuth increments of 10 degrees to determine how the amplitude and phase character of the transmitted S wavelet varied with azimuth after the wavelet had propagated through the simulated fractured medium. Test results are illustrated on Figure 2-5 as a view from the source end of the test sample. In these measurements, the positive-polarity end of the source on the upper end of the sample was oriented in the direction indicated by arrow D. The positive polarity end of the receiver on the bottom end of the sample was oriented in directions shown by arrows labeled **R** drawn at positions 1, 2, 3, 4 in Figure 2-5.

This laboratory configuration simulates real-world ZVSP (zero-offset VSP) data in which a horizontal displacement is applied to the earth surface by a real seismic source, and the S-wave response is then recorded by a deep horizontal geophone positioned directly beneath the surface source. Time **t = 0**, when the source is activated, is shown by the dashed circle in Figure 2-5 that connects the start times of all receiver recordings. Wavefields that propagate

through this "fractured" medium are combinations of fast-S and slow-S wavelets. Fast-S wavelets are labeled S_1 in Figure 2-5, and slow-S wavelets are labeled S_2. Arrival times of S_1 wavelets are closer to the dashed circle, where travel time is zero, than are S_2 arrival times. This difference in arrival times means S_1 wavelets travel faster than S_2 wavelets because both wavelets are created at the same time, and then propagate the same distance in the same propagation medium. This type of wave splitting in fractured media, or in any anisotropic media, is unique to S waves.
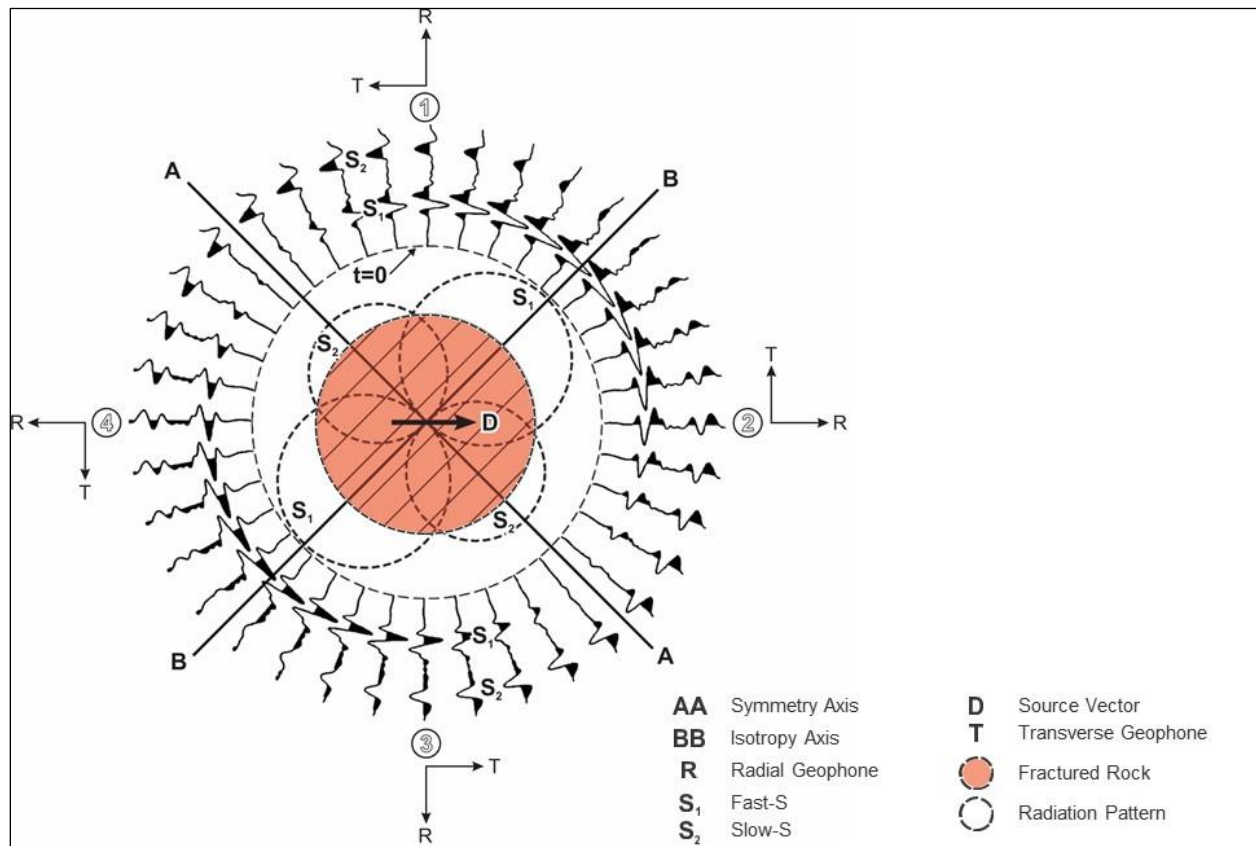
Figure 2-5. View of test sample from the source end. Source vector D is a shear displacement applied at an arbitrary angle relative to fracture planes. The source displacement remains fixed as the receiver at the opposite end of the sample is rotated at increments of 10 degrees. Only a S_1 (fast-S) mode propagates parallel to fracture planes (isotropy axis BB). Amplitudes of slow-S wavelets reduce to zero at axis BB and reverse polarity. Only a S_2 (slow-S) mode propagates perpendicular to fracture planes (symmetry axis AA). Amplitudes of fast-S wavelets reduce to zero at axis AA and reverse polarity. A mixture of S_1 and S_2 wavelets is observed at all other azimuths. (Source: Modified from Sondergeld and Rai, 1992).

The feature of S waves that is important to this DOE project is that whenever a horizontal-displacement S wave encounters a medium subjected to horizontal stresses, it transforms into two daughter S waves (S_1 and S_2) that are polarized in orthogonal directions and travel with different velocities. The length of the propagation path through test samples used by Sondergeld and Rai (1992) was sufficiently long so that the difference in S_1 and S_2 travel times did not allow S_1 and S_2 wavelets to overlap when they arrived at the receiver (illustrated by traces 1, 2, 3, 4). In contrast, when S waves propagate through a medium where there is not a large population of extensional fractures, or when the difference in Shmax and Shmin

magnitudes is small, an S-wave response will not be two distinct, time-separated wavelets as in Figure 2-5, but will be a single, complicated waveform composed of a first-arriving S_1 wavelet and a second-arriving S_2 wavelet that is only slightly delayed in arrival time relative to S_1. Distinct S_1 and S_2 wavelets that are well separated in travel time after propagating through stressed rocks are rarely observed in real seismic data. In this project, the difference in fast-S and slow-S velocities observed in VSP data at the FutureGen2 was negligible but was measurable at the Michigan Basin study site.

The laboratory procedure used by Sondergeld and Rai (1992) involved small rock samples, and source and receiver were separated several tens of centimeters. Their procedure was upscaled to real-world VSP data at study Site 1 (Illinois Basin) where source and rotating-receiver were separated distances of several thousands of meters. This is a laboratory-to-field upscaling of the order of 10,000 in its spatial dimensions. S wavelets generated by a surface-based seismic source, and then recorded by deep horizontal geophones in a VSP receiver well, were analyzed to determine the compass azimuths where rotated VSP direct-S wavelets produced at the baseplate of a vertical-vibrator source underwent polarity reversals, just as fast-S wavelets do at symmetry axis AA, and as slow-S wavelets do at isotropy axis BB, in Figure 2-5. The compass azimuths where these VSP direct-S wavelet polarity reversals occurred allowed Shmax azimuth to be identified in a non-invasive manner in deep rocks at the Illinois Basin study site. Examples of polarity reversals observed in direct-S wavelets embedded in the FutureGen2 legacy VSP data are presented in Section 3.

2.5   Vertical Vibrators Used as Horizontal-Displacement Sources

An important seismic source concept is introduced in the VSP portion of this project that overcomes the limitations of scarcity, high cost, and land-damage problems associated with traditional S sources. Specifically, this new source concept is that low-cost, widely-available, and land-friendly vertical vibrators are efficient S-wave sources in addition to being popular P-wave sources. The reasons why this important fact has been ignored by reflection seismologists is difficult to explain and justify. In Section 2.6 that follows, numerical calculations of P and S energy produced by vertical vibrators are shown that illustrate the attraction of practicing S-wave reflection seismology, and especially VSP data acquisition, with these popular P-wave land sources.

Historically, almost all land-based VSP data have been acquired with a vertical vibrator. This observation means that Shmax azimuth (i.e., the direction of isotropy axis BB in Figure 2-5) can be extracted from legacy, land-based, VSP recordings using the laboratory method described in Section 2.3. This was the research strategy that was implemented with legacy, vertical-vibrator, VSP data at the FutureGen2 study site in the Illinois Basin.

2.6   Direct-SV Radiation Patterns Produced by P Sources

Arguably, the most important technology introduced to the CO_2 sequestration community in this project are the concepts that common P sources generate down-going illuminating SV waves directly at their surface source stations, and that these direct-S wavefields allow S-wave reflection seismology to be practiced with common P sources. When this concept is understood, land-based S-wave reflection seismology can be practiced globally at low cost. In fact, in many areas of interest, data appropriate for S-mode investigations with VSP data, or S-wave two-

dimensional (2D) and 3D seismic reflection data, already exist at zero data-acquisition cost as legacy P-source data.

Two types of sources, either vertical vibrators or shot-hole explosives, have been, and still are, used to acquire almost all 2D, 3D, and VSP land-based P-wave seismic reflection data. In this project, vertical vibrators were used to generate the legacy VSP data at study site 1 (Illinois Basin) and shot-hole explosives were used to generate the legacy 3D seismic data at study site 2 (Michigan Basin). Evidence that each of these P sources produces direct-S illuminating wavefields is presented in the following two sections.

2.7   P and S Radiation Patterns Produced by Vertical Vibrators

This section explains the physics that underpins the fundamental, and long ignored, principle that vertical-vibrator sources are not only outstanding P-wave sources but are also effective S-wave sources.

Numerical modeling done in the 1950s established the concept that a surface-based, vertical-displacement seismic source (e.g., a vertical vibrator) produces more direct-SV radiation energy than direct-P radiation energy (Miller and Pursey, 1954). However, that modeling also showed that this robust amount of SV energy travels away from a P-source station at takeoff angles that are greater than 30 degrees from vertical, and that only a negligible portion of this radiating SV energy travels in the critical illumination cone that extends from vertical to +/-30 degrees from vertical. It is essential that significant down-going direct-SV energy propagate away from a source station at takeoff angles less than 30 degrees from vertical if that source is to be used as an S-wave source in seismic reflection seismology. Reflection seismologists have used this 1950s modeling result for decades to infer that vertical vibrators and other vertical-displacement P sources cannot be used for direct-SV illumination of deep targets.

Miller and Pursey's 1954 modeling of P and SV radiation patterns produced by a vertical-displacement source was done before there was computer technology that could be used to solve complex mathematical problems. Consequently, these researchers had to make assumptions that would permit them to calculate the geometry of expanding P and S wave fronts with pen-and-ink solutions of integrals that could be done on paper. To do so, they had to make simplifying assumptions about a vibrator source and about its propagation medium. Key assumptions were: (1) the earth surrounding a source station is perfectly homogeneous and isotropic, (2) the earth surface across a source station is perfectly flat, (3) the source displacement vector applied to the earth is perfectly vertical, and (4) there is only one source at a station, not an array of sources.

Most of these assumptions are not true at real-earth source stations. The earth immediately around a source station is rarely (and probably never) isotropic and homogenous. Instead, typical conditions at a source location include: stiffness coefficients that vary with azimuth because soil mineralogy changes over short distances, variable root depths of vegetation exist immediately around a source station, unseen buried objects are close to a source station, surface objects such as a fence post, small ditch, or parked vehicle are close to a source station, etc. Seldom is the earth surface perfectly flat at a source station. A minor inclination in the earth surface will cause the force vector created by a vertical-vibrator source to have a horizontal, shear-producing component and not to be true vertical. Most vibroseis data are also generated by an array of vibrators, not by a single vibrator. The influences of these real-world

conditions that exist at all, or nearly all, real-world source stations need to be included in numerical calculations of direct-P and direct-SV radiation patterns produced by P sources in order to depict the correct geometry of P and S radiation patterns that radiate into the earth.

Hardage and Wagner (2018a) revisited the issue of numerically calculating P and S radiation patterns produced by P sources by implementing finite-difference modeling that replaced the over-simplified assumptions Miller and Pursey (1954) were forced to use with more realistic earth and source conditions. In this finite-difference modeling, the propagation medium extended several kilometers laterally, and also vertically downward, from a source station so that no reflections from model boundaries would appear in calculation results. The X-Y dimensions of finite-difference cells across the entirety of propagation space were small fractions of seismic wavelengths. The propagation medium had no interfaces and was isotropic and homogeneous, just as Miller and Pursey (1954) assumed.

However, to account for the types of near-source irregularities mentioned above that exist at essentially all real-world source stations, the stiffness coefficients in a few model cells near a vibrator source station were either increased or decreased relative to the stiffness coefficients in the remainder of propagation space. These near-source irregularities were physically small (dimensions of only 3 or 4 meters) and their stiffness variations from the background stiffness values were small (plus or minus 30-percent change in stiffness).

Finite-difference modeling results are summarized in Figures 2-6a through 2-6d. Figure 2-6a shows the P and S radiation patterns that Miller and Pursey hand calculated in 1954. The vertical arrow indicates the source station where a surface-based vertical displacement is applied to a propagation medium that is isotropic, homogeneous, and has a fixed Vp/Vs ratio of 2. Almost no direct-S energy propagates away from the source station in the illumination cone extending from +30 degrees to -30 degrees from vertical. The fact that no significant S energy propagates away from the source station in this takeoff angle range has caused vertical vibrators to be ignored as potential S-wave sources since the 1950s.

Figure 2-6b is a finite-difference calculation for an isotropic, homogeneous medium with a Vp/Vs ratio of 2. These are the same physical conditions used for a propagation medium in the Miller and Pursey example in Figure 2-6a. This model was calculated to confirm that the finite-difference calculation procedure produced results similar to the Miller/Pursey results. The acceptable consistency in the calculated P and S radiation geometries in these two modeling approaches (hand-calculated results in Figure 2-6a and finite-difference calculation in Figure 2-6b) validates the conclusion that a surface-based, vertical-displacement source (i.e., a P source) is not an effective S source if a propagation medium has a flat surface and is perfectly isotropic and homogeneous. There is simply insufficient S energy traveling downward in the illumination cone extending from +30 degrees to -30 degrees from vertical to create effective S-wave reflections.

Figure 2-6c illustrates how a small, near-source, surface-exposed, irregularity affects P and S radiation patterns produced by a single vibrator in an otherwise isotropic and homogeneous medium. In this model, Vp and Vs are increased in a small, surface-exposed area that starts 5 ft from the right-side of the source station and extends to 15 ft from the station. Otherwise, all model conditions are exactly the same as the medium that produced the P and S radiation patterns in Figure 2-6b. Comparing Figures 2-6a, 6b, and 6c shows that this small, right-side irregularity in the earth causes S-wave radiation lobes to swing toward vertical. The result is that
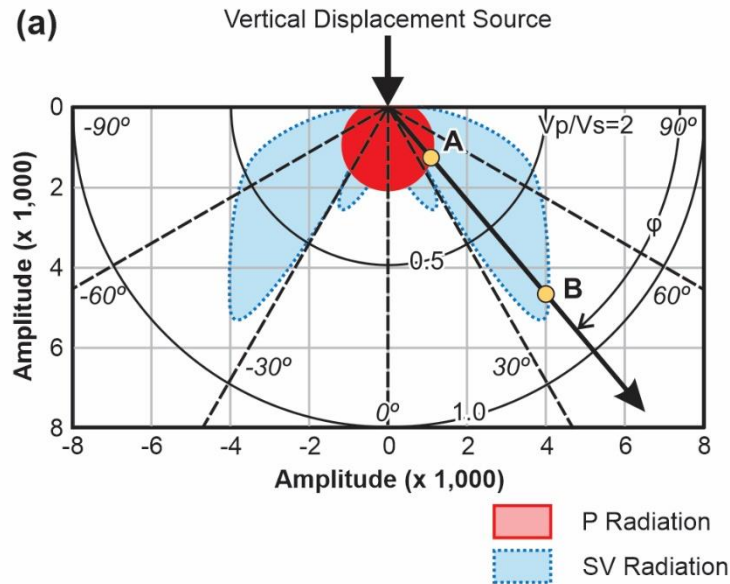
Figure 2-6a. P and SV radiation patterns calculated for a vertical vibrator source using equations similar to those developed by Miller and Pursey (1954). Propagation medium has a constant Poisson's ratio of 0.33 (V_P/V_S = 2). A and B = strengths of P and SV radiation at takeoff angle Ø, respectively. Polarity of right-side SV lobe is positive; polarity of left-side SV lobe is negative. (Source: Hardage and Wagner, 2018a).
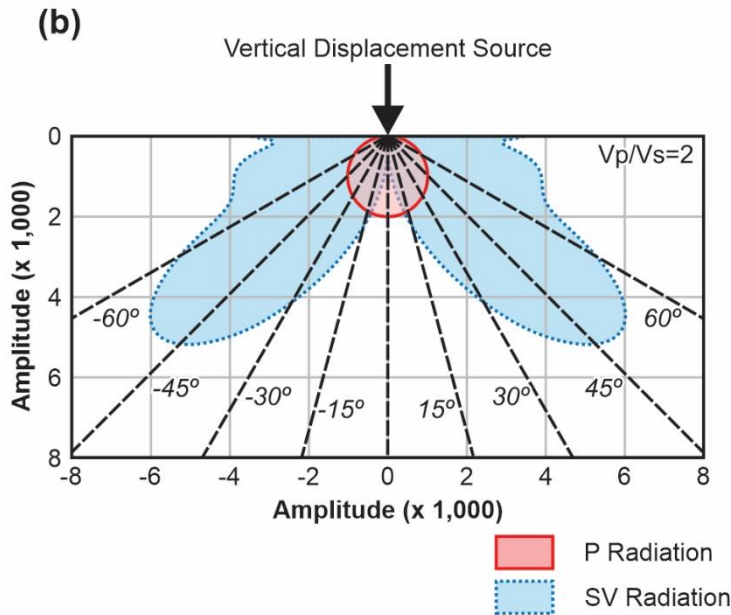
Figure 2-6b. Direct-P and direct-SV radiation patterns calculated by finite-difference modeling for a homogeneous, isotropic earth with a V_P/V_S velocity ratio of 2. Only a meager amount of S-wave energy propagates downward inside the takeoff angle range extending from +30 to -30 degrees from vertical, just as does the hand-calculated results in Figure 2-6a. Right-side SV lobe is positive polarity; left-side SV lobe polarity is negative. (Source: Hardage and Wagner, 2018a)
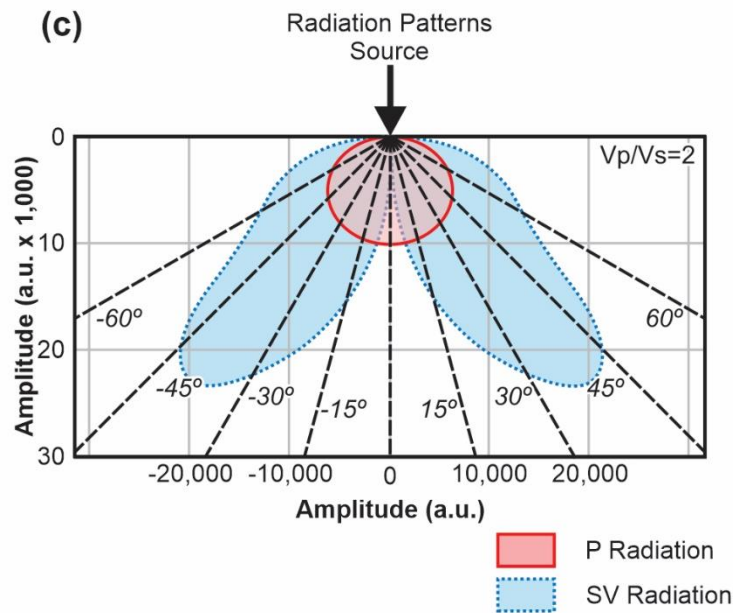
Figure 2-6c. P and SV radiation patterns when a small earth volume, with a 30-percent increase in stiffness, is on the right side only 5 ft from a vibrator base plate. Compared to Figures 2.6a and 6b, much more SV energy now propagates downward at near-vertical takeoff angles. (Source: Hardage and Wagner, 2018a)
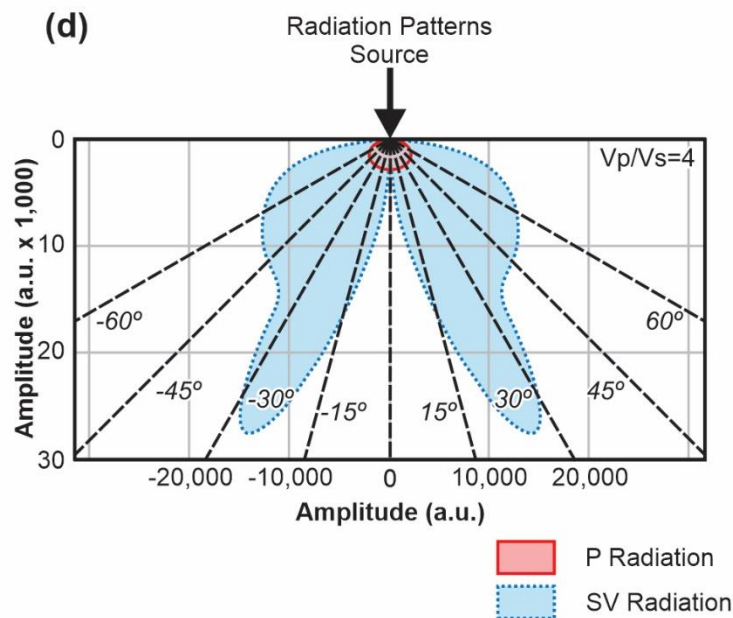
Figure 2-6d. A repeat of the model calculations used to produce the direct-P and direct-SV radiation patterns in Figure 2-6c, but now assigning a V_P/V_S value of 4 to the propagation medium rather than a value of 2. A V_P/V_S value of 4 is a better representation of soft sediment at a baseplate. A medium with a V_P/V_S value of 2 is more appropriate for consolidated rock. Now vertically traveling SV energy exceeds vertically traveling P energy. (Source: Hardage and Wagner, 2018a)

a considerable amount of direct-S energy now travels at near-zero takeoff angles, and a vertical vibrator becomes a reasonably efficient S-wave source for imaging deep geology. These kinds of small, near-source, irregularities are common at all seismic source stations. In this context, the term "small" means an irregularity is not only physically small, but its stiffness contrast with its surrounding medium is also small. Stiffness properties inside each near-source irregularity were allowed to be only 30-percent greater, or 30-percent smaller, than the same properties in the background homogenous medium.

The propagation medium in Figure 2-6d has the same small near-source irregularity as in Figure 2-6c, and the propagation medium is exactly the same as the medium in Figure 2-6c except the Vp/Vs ratio is now increased to a value of 4. A Vp/Vs value of 4 is more representative of unconsolidated soils found around most vibrator source stations than is a value of 2. A material with a Vp/Vs value of 2 is quite stiff and is more representative of a rather rigid elastic material than of a weak, unconsolidated soil. Comparing Figure 2-6c and 2-6d shows that direct-S illumination created by a vertical-vibrator source exceeds direct-P illumination at all takeoff angles, even true vertical, if Vp/Vs at a source station has a value of approximately 4, and if one or more small, realistic irregularities exist near the source station.

These modeling examples show that in real-world conditions, a vertical vibrator creates down-going direct-S energy at most source stations that is attractive for S-wave imaging purposes. This important principle is utilized in this study and is utilized in analyzing VSP data acquired at the FutureGen2 site in the Illinois Basin. The strong evidence assembled in this study that confirms that vertical vibrators are efficient S-wave sources, in addition to being established P-save sources, should be a valuable concept to publicize to the geoscience community.

2.8 SV-P Data Generated by Shot-Hole Explosives

At Site 2 of this study (Michigan Basin), stress data had to be extracted from 3D seismic data generated by buried explosives and recorded by vertical geophones. To determine Shmax azimuth, it is essential to extract S-mode reflections from seismic data. The source-receiver combination at Site 2 confronts two challenges that most geophysicists think will not allow S-wave reflections to exist in the Michigan Basin 3D data. Barrier #1 is the assumption that a buried explosive is a pure-P source because it is an expanding sphere of high-pressure gas. If true, no direct-S energy radiation is produced at a shot cavity. Barrier #2 is the assumption that S-wave reflections cannot be recorded by vertical geophones; S data can be recorded only by horizontal geophones.

This section presents evidence showing that Barrier #1 does not exist. A buried explosive is not a pure P source. Robust S-wave illuminating energy is definitely produced directly at shot cavities created by buried explosives, as will be shown in the following section. As a result of a buried explosive source creating both a direct-P wavefield and a direct-SV wavefield at its shot cavity, there are two sets of reflections embedded in vertical-geophone data. One set of vertical-geophone reflections is created by the down-going direct-P illuminating wavefield. These reflections are traditional P-P data. The other set of vertical-geophone reflections is created by the down-going direct-SV illuminating wavefield. These reflections are a new imaging mode option called SV-P data. Because SV-P data involve a down-going SV ray path, the data exhibit fast-S and slow-S behavior which allows Shmax azimuth to be determined. This project will be the first to demonstrate to the CO_2 sequestration community that S-wave data that react to

stress conditions in deep, stressed rocks exist in 3D data created by a buried-explosive source and recorded by vertical geophones.

2.9   Evidence of Shot-Cavity Shearing and Direct-S Generation

Kusubov (1976) verified that shearing was created by buried shot-hole explosives by first detonating explosive charges at depths of approximately 2 meters at a Yucca Lake test site. He then excavated lake-bed sediment and created vertical planes of exposure passing through subsurface cavities formed by several buried shots. A photograph of one shot-cavity cross-section is displayed in Figure 2-7. First, note that this cavity is not a perfect sphere, which indirectly implies shearing has happened. Second, and more important, obvious and extensive fractures radiate away from the cavity into surrounding sediment layers. More photos of shot cavities are shown in Kusubov's (1976) Lawrence Livermore report.

An earlier Lawrence Radiation Laboratory report by Short (1961) shows other photos of a shot cavity created by a large buried-explosive deployed to a deep depth via a large-diameter borehole. This shot hole was drilled into a sedimentary section not far from a deep salt-mine shaft, which allowed investigators to dig a lateral shaft to examine the shot cavity. The cavity was large enough for investigators to get inside the void space created by the explosion and analyze fracture systems and shear failures created by cavity formation. Researchers concluded that fractures and shearing were created at any zone of weakness that was contacted by the expanding, high-pressure, gas volume produced by the chemical explosion. Horizontal interfaces between thin-layered sedimentary units were common origin points of shearing. Collectively, photos of excavated shot cavities documented in these two government lab reports are compelling proof that the medium around a buried explosion undergoes severe fracturing and shearing. As a result, direct-SV wave fronts must necessarily propagate away from buried-shot cavities in addition to direct-P wave fronts.
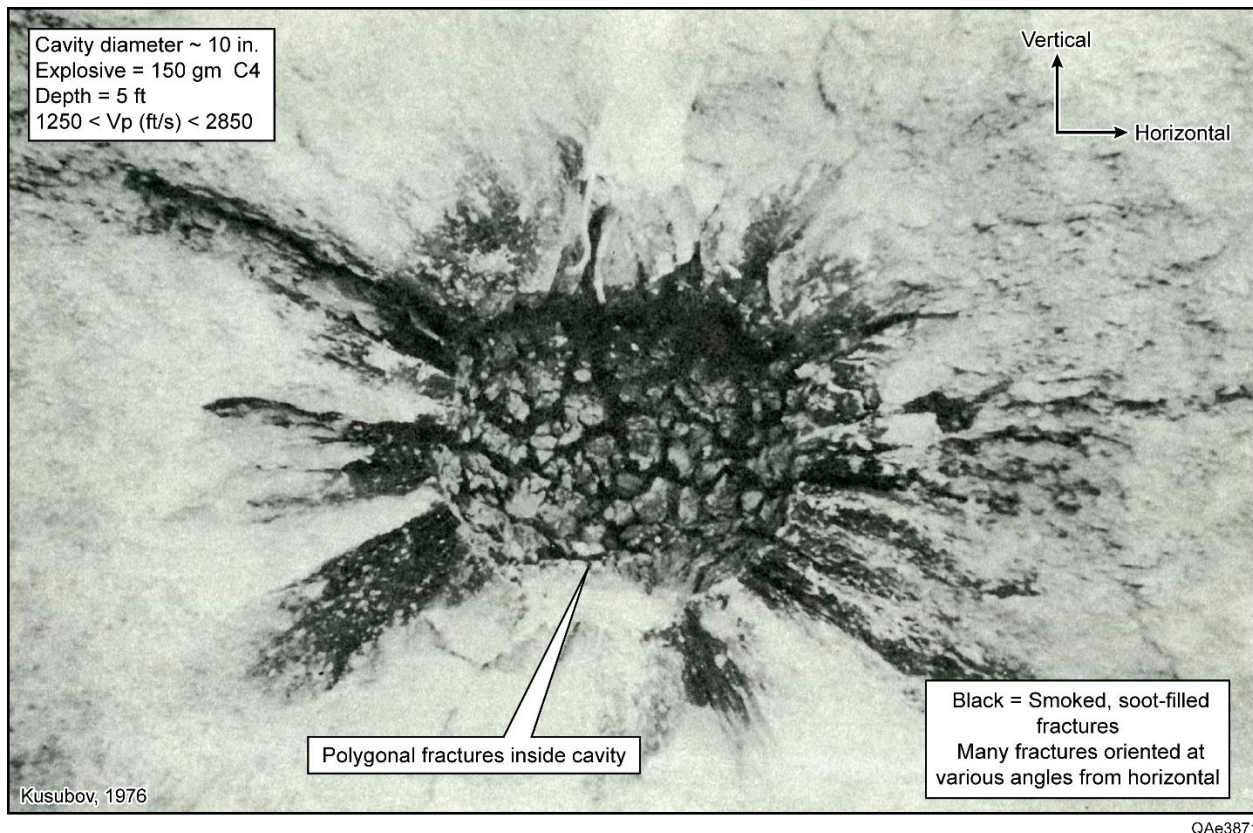
Figure 2-7. Shot cavity created in lake-bed sediment, Yucca Lake, Nevada. The cavity is not spherical, and numerous extensive fractures radiate into the surrounding soil. The walls of the fractures are blackened by exploding gas residue. This fracturing is evidence of strong shearing of the medium surrounding a buried explosive (Kusubov, 1976).

2.10   Evidence of Direct-SV Mode Produced by Buried Explosives

A field test done by Hardage and Wagner (2018b) confirmed that direct-SV illuminating wave fields are produced by a buried explosive. The diagram in Figure 2-8b shows the source-receiver geometry. First, explosive charges were placed at different depths in drilled shot-holes. In this test, 1-kg explosive charges were positioned at depths of 20, 50, and 100 ft. The 50-ft and 100-ft charges were in the same shot-hole. During data recording, the 100-ft charge was shot first, and then the 50-ft charge was detonated to create a separate data record from the same shot-hole. The explosive at a depth of 20 ft was in a separate shot-hole offset only 10 ft from this dual-charge shot-hole.

Second, 3C VSP receivers were positioned in the subsurface to record the down-going wavefields created by these buried explosives. In this experiment, there was a long vertical array of 42 stations of 3C geophones in a nearby well. Conventional rotation of the 3C geophones in this extensive vertical array of 42 receivers segregated the test data into three data panels that, respectively, emphasized: (1) down-going, direct-P arrivals, (2) down-going, direct-radial-S arrivals, and (3) down-going, direct-transverse-S arrivals. The data in Figure 2-8a show the down-going, direct radial-S response at one deep, far-offset, receiver.
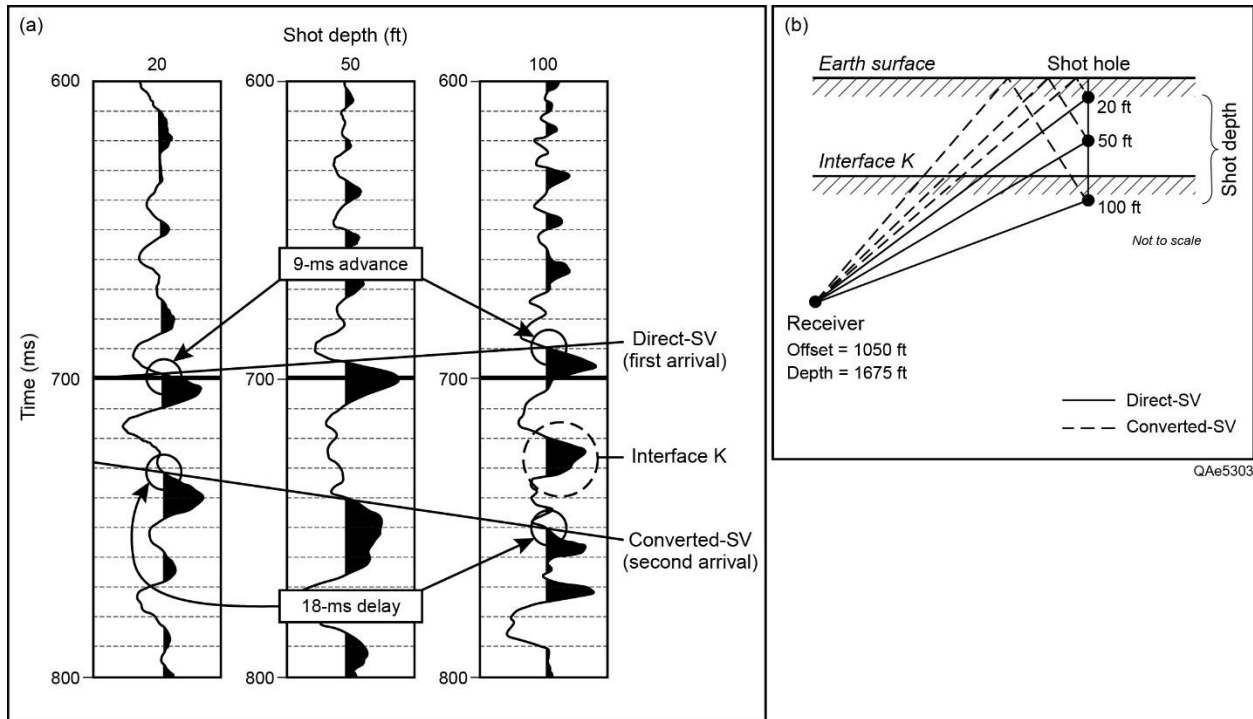
Figure 2-8. (a) Data recorded by rotated horizontal geophones that illustrate down-going direct-SV first arrivals produced by buried explosives at different depths and their subsequent, down-going, converted-SV reflections from the earth surface. (b) The source-receiver geometry used to acquire the data. Solid-line ray paths are direct-SV arrivals. Dash-line ray paths are converted-SV arrivals produced at the earth surface. Travel times in (a) are measured along slant travel paths to a deep, far-offset, VSP geophone. From Hardage and Wagner (2018b).

If an SV wavefield is produced exactly at each shot cavity, the arrival time of that direct-SV wavelet at this subsurface receiver will decrease as shot depth increases because the shot-to-receiver distance decreases. A decrease in arrival time with increasing shot depth (9-ms in this case) is exactly what was observed for the first SV arrival in Figure 2-8a.

Down-going SV wavefields are also created by mode conversions when up-going P and SV wavefields generated at a shot cavity encounter reflecting interfaces above a buried shot (Figure 2-8b). Significant reflected SV modes occur at the earth-air interface. In contrast to the decreasing arrival times of a direct-SV mode, an SV mode reflected from the earth surface arrives at a deep receiver at increasing travel times as shot depth increases because the shot-to-surface distance increases as shot depth increases. Time-delayed converted-SV wavelets created at the earth surface are the second set of labeled SV arrivals in Figure 2-8a. When drilling the 100-ft shot-hole, a hard sandstone layer was encountered approximately halfway between drilling depths of 50 ft and 100 ft (exact depth was not documented). This hard layer is labeled as **Interface K** in Figure 2-8b. Upgoing P and SV waves from the 100-ft shot produced a significant, down-going converted-SV wavelet at this K interface. Converted-SV energy created at the K interface is labeled in Figure 2-8a.

This simple field test can be easily replicated by anyone interested in documenting SV illumination created by buried-explosive sources. Such tests will provide compelling evidence that a buried explosive produces a down-going SV illuminating wavefield directly at its shot

cavity, which is a physics principle that has not been fully recognized by exploration geophysicists to date. A buried explosive also produces down-going P-SV and SV-SV converted modes at the earth surface. Any of these down-going S wavefields can be used in S-wave reflection seismology.

2.11   Extracting S-wave Data from 3D P-source Seismic Data

A general consensus across the geoscience profession is that S waves are more sensitive to stress effects in rocks than are P waves. It is thus essential to extract S-wave modes from data generated by P sources. Traditional 3D seismic practice has been to acquire P-SV data. This term "P-SV" refers to data that are created when a down-going illuminating P wave converts to up-going SV-shear reflections at rock interfaces. These SV reflections can be recorded only with horizontal geophones. When 3D data are recorded with vertical geophones, as was the case for the Michigan Basin 3D seismic data used in Phase 2 of this study, it is not possible to utilize P-SV data.

In Phase 2 of this project, it was necessary to implement the new concept of SV-P reflection imaging in order to acquire S-wave information for determining Shmax azimuths (whereas P-SV data involve a down-going illuminating P wave and an up-going SV reflected wave, SV-P data involve a down-going illuminating SV wave and an up-going P reflected wave). Up-going P reflections in SV-P data are embedded in the same vertical geophone data where up-going P reflections of P-P data are found.

The energy sources used to generate the 3D vertical-geophone data used in Phase 2 of this study were buried explosives. Preceding Sections 2.7 through 2.9 were included in this report to illustrate direct-SV generation by buried explosives. The robust nature of SV energy produced by shot-hole explosive implies there should be acceptable SV-P reflection data across the Michigan Basin 3D seismic study area.

2.12   Processing 3D SV-P Data to Determine Sh$_{max}$ Azimuth

The first data-processing step for determining Shmax azimuth from 3D SV-P data is to create trace gathers that allow the azimuths of fast-S and slow-S polarization directions to be recognized. Unfortunately, the concept of extracting SV-P data from vertical-geophone data is so new in the reflection seismology community that there are no published examples of azimuth-dependent SV-P trace gathers. This project will be the first-ever effort to construct SV-P trace gathers for the explicit purpose of illustrating the azimuth dependency of S-wave velocity. Likewise, this study will be the first-ever effort to use SV-P trace gathers from 3D data to define Shmax azimuth.

It is thus necessary to defer to traditional P-SV trace-gather analyses, a practice that has been used with P-source data recorded with 3C geophones for more than two decades, to illustrate the concept of investigating azimuth-dependent SV velocity behavior. One of the earliest of such P-SV analyses is illustrated in Figure 2-9. At the location where this late 1990s study was done, 3D data were recorded using 3C geophones and buried explosive sources, the same source that generated the 3D vertical-geophone data at Study Site 2 in Michigan. The objective was to map azimuth orientation of extensional fractures in carbonate units **A** and **B** labeled on the data so that a horizontal well could be drilled in an azimuth direction that would intersect a maximum number of extensional fractures.
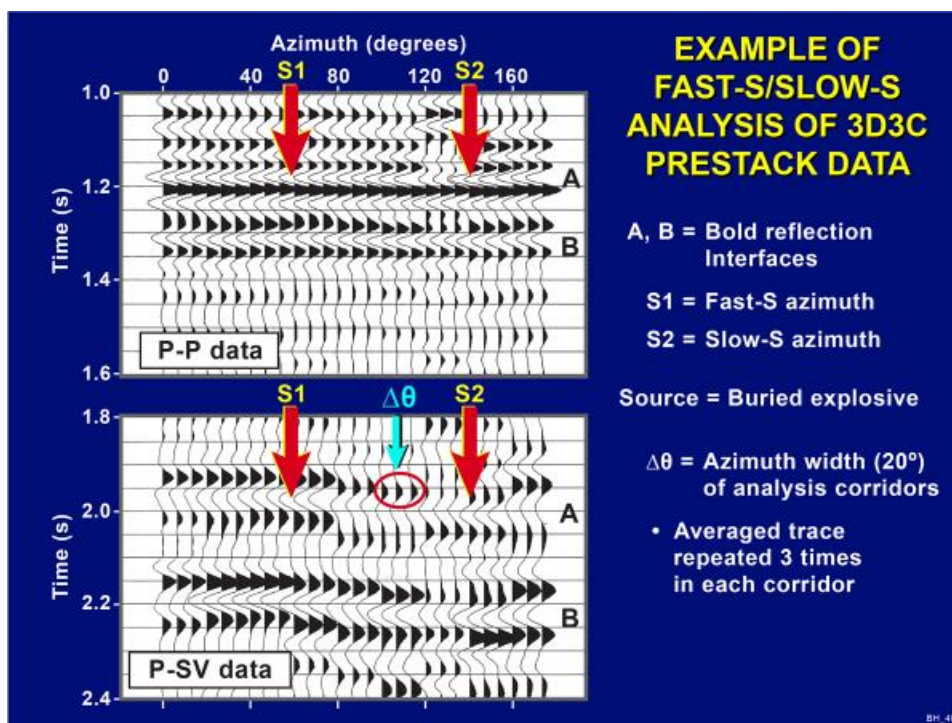
Figure 2-9. Pre-stack P-P (top) and P-SV (bottom) trace gathers constructed at a single stacking bin in a 1990s Shmax investigation. The azimuth width of stacking corridors was 20 degrees. The summed trace in each azimuth corridor is repeated 3 times in this display format. Fast-S (Shmax) azimuth is labeled S1. Slow-S (Shmin) azimuth is labeled S2. These data are powerful evidence that P-P data exhibit almost no fast/slow velocity behavior, but, in contrast, S-mode data show strong fast/slow velocity behavior. (Source: Hardage et al., 2011)

In this first-generation study, both P-P and P-SV trace gathers were created to compare P-wave and S-wave sensitivity for detecting aligned fractures and oriented stress fields. The azimuth width of analysis corridors was 20 degrees, and the stacked trace in each oriented corridor was repeated three times to enhance visual analysis of wavelet character. This three-repeated-traces format was an arbitrary decision done only in this particular study and has rarely been repeated. The display in Figure 2-9 involves 180 degrees of azimuth rotation around a single stacking bin that is used for illustration. Because both positive-offset sources and receivers and negative-offset sources and receivers are utilized at each stacking bin, there is actually a full 360-degrees of azimuth analysis of P-SV arrival times included in this data display.

P-P trace gathers in Figure 2-9 show no sensitivity to azimuth orientation of the trace-gather corridor used to construct each P-P trace. In contrast, P-SV trace gathers show that reflections **A** and **B** occur at different arrival times for different stacking-corridor azimuths at the same stacking bin. The earliest P-SV arrival time (which is the fast-S azimuth, and also the Shmax azimuth) is labeled **S1**, and the latest P-SV arrival time (which is the slow-S azimuth, and also the Shmin azimuth) is labeled **S2**. FMI and dipole sonic log data recorded in the only available well inside this 3D seismic image space showed that most fractures intersected by the wellbore were also oriented in azimuth **S1**. All evidence at this study site indicated that Shmax stress was oriented in azimuth **S1** shown in Figure 2-9.

Figure 2-10 extends this narrow-azimuth-corridor strategy for detecting Shmax and Shmin azimuths to SV-P data such as were used in the Michigan Basin study. In this figure, source

lines are oriented north-south, and source stations are shown as red Xs. Receiver lines are oriented east-west, and vertical-geophone receiver stations are shown as solid yellow circles. In this example of a stacking corridor, source stations are shown only on the left-hand side of the stacking bin, and receiver stations are shown only on the right-hand side. In practice, source stations on the right-hand side of a stacking bin and receiver stations on the left-hand side also contribute to trace gathers constructed inside an azimuth corridor. Only those source-receiver pairs that place an SV-P reflection point inside a stacking bin contribute to an SV-P trace gather at that super bin.

A vertical view of a typical, full-azimuth, direct-SV radiation pattern produced at a source station is shown as a spoke-wheel pattern of black arrows positioned a short distance northwest of stacking bin **SB.** The length of each arrow indicates the strength of direct-S radiation traveling in the direction of arrow orientation. An attraction for using direct-SV from a P source for fast-S/slow-S analyses is that the full-azimuth takeoff-angle directions of direct-SV radiation from a P-source station ensures that every azimuth corridor around a P-source station will be illuminated with down-going SV energy.
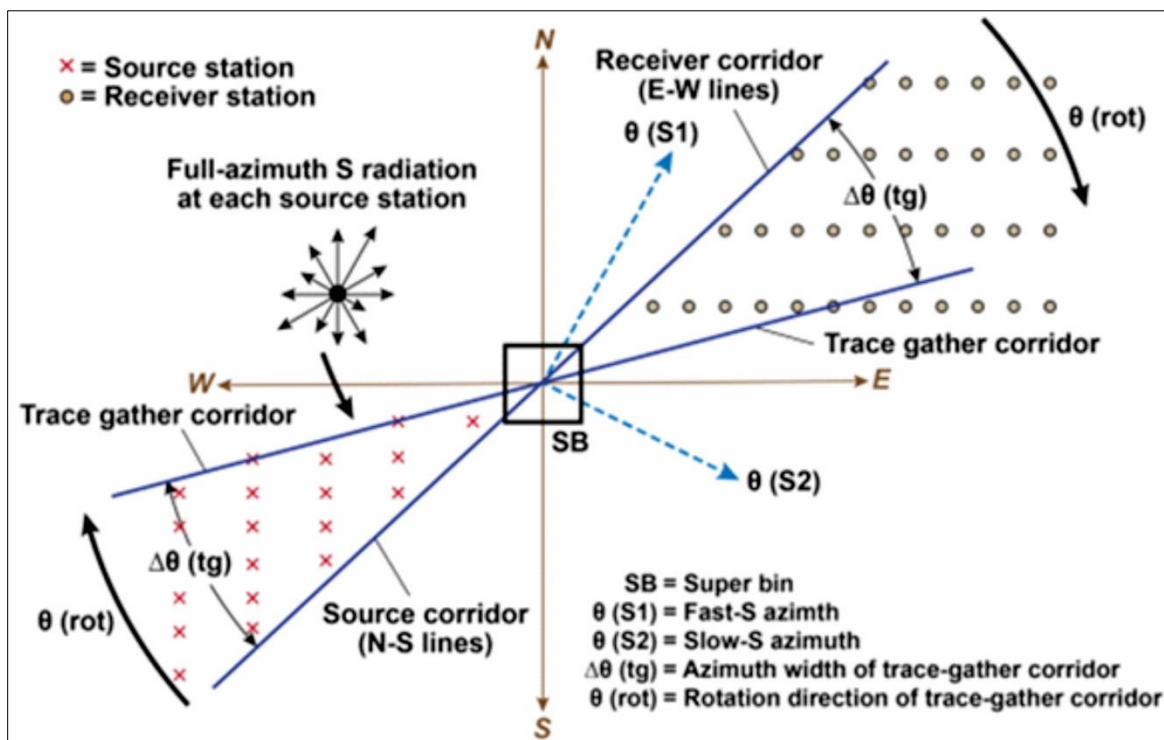
Figure 2-10. Strategy used to create pre-stack SV-P trace gathers in narrow, rotating, azimuth corridors that define fast-S and slow-S polarization azimuths. Fast-S azimuth will also be the azimuth of Shmax. The area spanned by the stacking area labeled SB can be a single stacking bin or a super-bin spanning a small area of several normal-size stacking bins.

It is essential that traces in a stacking-bin gather exhibit one or more reflection events close to, and preferably immediately above and below, an interval of interest. Data processors may have to produce trace gathers using several choices for stacking-bin size to decide what the

dimensions of a satisfactory stacking bin should be. Feature **SB** in Figure 2-10 represents a selected stacking-bin size that will be used to construct a trace gather. If subsurface geology is reasonably uniform across the full extent of a 3D survey, it may be sufficient to construct only one super bin positioned near the center of the 3D source-receiver spread. If structural differences, or significant changes in geological conditions, occur across a 3D area, at least one stacking bin analysis should be done in each unique geological domain.

Another variable that requires data-processor experience is the width of the azimuth corridor used to construct a trace gather (feature **Δθ(tg)** in Figure 2-10). Wide data corridors cause more data traces to contribute to a trace gather and increase the signal-to-noise ratio of reflection events. However, wide stacking corridors also make it difficult to define fast-S and slow-S polarization azimuths with precision. Data processors must do experimentation to decide what an appropriate azimuth-corridor width should be.

After stacking-bin size and corridor width are selected, the stacking corridor in Figure 2-10 is rotated in a clockwise direction around stacking bin **SB** as shown by arrows labeled **θ(rot)**. It is wise to position adjacent azimuth corridors so that they overlap. For example, if corridor width is 20 degrees, then the neighboring corridor could be rotated perhaps 15 degrees so that there is a 5-degree overlap between neighboring trace-gather corridors. This particular choice of corridor overlap would create a 15-degree azimuth sampling of fast-S/slow-S polarization behavior rather than a 20-degree azimuth sampling. Data processors have to experiment to decide how much corridor overlap should be used.

This type of azimuth-dependent trace-gather procedure was applied to SV-P traces extracted from 3D vertical-geophone data at the Michigan Basin study site to determine if fast-S and slow-S azimuths can be determined at this location with SV-P data.

Table 2-1. Recap of major principles underlying the method for processing seismic data for extracting stress data.

Section	Major Points
2.1 Extensional Fractures, Shear Fractures, and Maximum Horizontal Stress	Extensional fractures align with Shmax. Shear fractures do not.
2.2 Fast-S and Slow-S Wave Modes	When rock stiffness varies with azimuth, S waves split into fast and slow modes. Fast-S polarization aligns with Shmax. P wave splitting is much weaker than S wave splitting
2.3 Fast-S and Slow-S Propagation in Stressed Fractured Media	Azimuths of fast-S and slow-S polarizations are identified by polarity reversals of direct-S wavelets.
2.4 Vertical Vibrators Used as Horizontal Displacement Sources	S sources are scarce, expensive, cause land damage, and can be replaced by vertical vibrators
2.5 Direct-SV Radiation Patterns Produced by P Sources	Modeling and testing show that vertical vibrators and buried explosives are effective S sources
2.6 P and S Radiation Patterns Produced by Vertical Vibrators	Finite difference modeling shows that small irregularities in the earth near a baseplate cause direct S radiation to travel vertically

Table 2-1 (continued). Recap of Major Principles underlying the method for processing seismic data for extracting stress data.

Section	Major Points
2.7,8,9 Direct-S Modes Produced by Buried Explosives	Field tests and photos of shot cavities show direct S wavefields are produced at shot cavities
2.10,11 Extracting Shmax Azimuths from 3D P-Source Trace Gathers	Shmax azimuth can be determined from azimuth-dependent SV-P trace gathers. Concept is to find the azimuth where a targeted SV-P reflection arrives earliest. This azimuth is fast-S azimuth, which is also Shmax azimuth.

3.0 Non-invasive Extraction of Stress Information from VSP Data: Methodology

The procedural steps used to estimate Shmax azimuth from vertical seismic profile (VSP) data at Study Site 1, Illinois Basin, are illustrated in this section. These procedures are first applied to zero-offset VSP data in Section 3.5, and then expanded to far-offset VSP data in Section 3.8.

The wave physics basis of the analysis procedure has been described in Sections 2.1 through 2.3. The field procedure was to expand sub-meter distances between a laboratory S source and S receiver (as used by Sondergeld and Rai (1992) and illustrated in Figures 2-4 and 2-5) by a factor of several 1000s to represent source-receiver separation distances encountered in real-world VSP data acquisition. Sondergeld and Rai (1992) determined fast-S and slow-S polarization directions (i.e. Shmax and Shmin azimuths, respectively) in a laboratory environment by analyzing phase/amplitude behavior of direct-S wavelets that traveled between an S source and an S receiver positioned at opposite ends of small samples of a fractured shale. Differences between their lab test method and this project's upscaling of their test procedures to real-world VSP data are summarized in Table 3-1.

Table 3-1. Comparisons between features of laboratory test and VSP-data procedures.

Wavelet	Direct S, high frequency	Direct S, low frequency
Propagation medium	Finely-bedded shale	Thick layered rocks (e.g., limestones, shale, sandstone)
Source-receiver separation	Several centimeters	Several kilometers
Source	Centimeter-scale piezoceramic element	12,000-kg vertical vibrator at the earth surface
Receiver	Centimeter-scale piezoceramic element	Traditional 3C VSP geophone positioned at depths of 1000-1500 meters
Receiver rotation	Manual repositioning on test sample	Mathematical rotation of recorded S wavelet
Qualitative description of fast-S/Slow-S wavelets	Arrival time of fast-S and slow-S wavelets well separated (strong anisotropy)	No, or minor, difference in fast-S and slow-S arrival times (weak anisotropy)

3.1   Procedure

A graphical depiction of a mathematical rotation of a down-going direct-S wavelet recorded at a deep VSP receiver station at the FutureGen2 project site is displayed as Figure 3-1. The direct-S wavelet used in this rotation was generated at the earth surface by a 12,000-kg vertical-vibrator source positioned 195 ft (59 m) from a VSP receiver well and was recorded by a horizontal geophone positioned at a depth of 4225 ft (1288 m). These VSP, zero-offset, source-

receiver conditions are a significant up-scaling of Sondergeld and Rai's laboratory test conditions.

The fact that a vertical vibrator generates a down-going, direct-S, illuminating wavefield that propagates vertically from a vibrator baseplate is a recent concept that was introduced, tested, and proven during the 9-year period from 2011 to 2018 by researchers at The University of Texas at Austin. The concept is described in Section 2.6, and examples of direct-P and direct-SV radiation patterns created by a vertical vibrator are shown in Figures 2-6a through 2-6d. This new vertical-vibrator illumination physics provides the deep-rock, direct-S, wavelets that were utilized in the VSP data examples exhibited in this section.
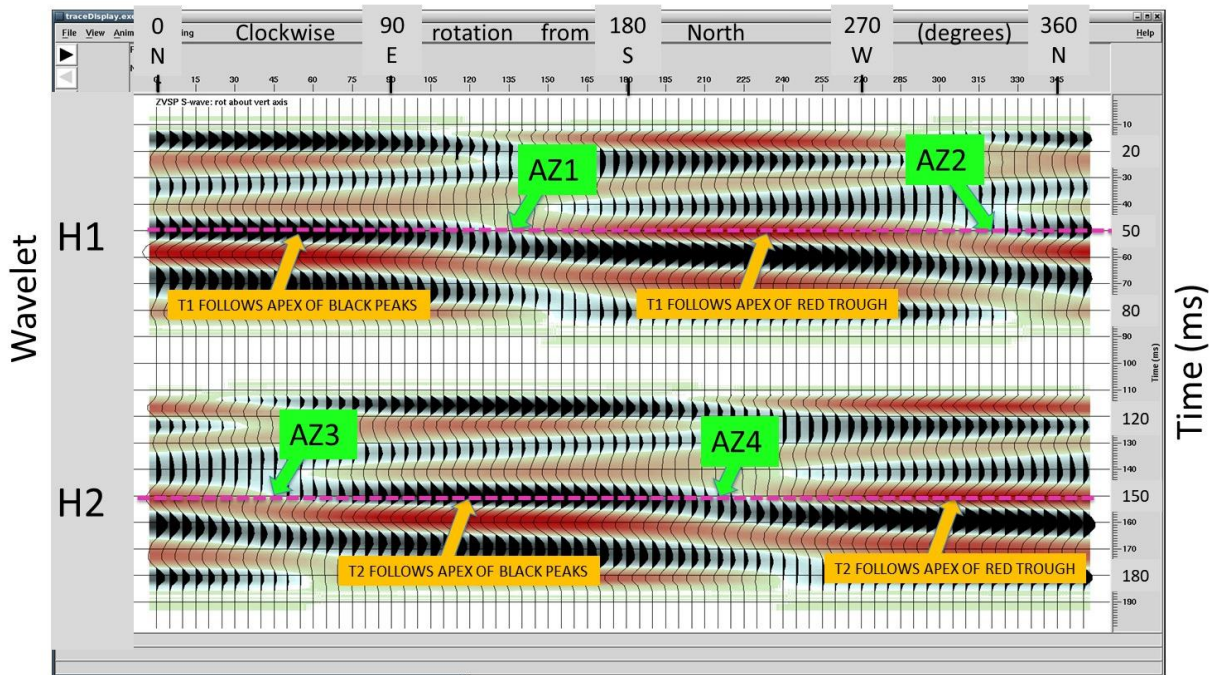
Figure 3-1. Mathematically rotated H1 horizontal-geophone (top) and H2 horizontal-geophone (bottom) VSP wavelets. Data are shown, from left to right, as functions of the azimuth direction in which each geophone's response axis is oriented. Red dash line T1 in the top panel is both the zero-time line and the zero-phase line for measuring phase behavior of rotating H1 (transverse geophone) wavelets. Red dash line T2 in the bottom panel is both the zero-time line and the zero-phase line for measuring phase behavior of rotating H2 (radial geophone) wavelets. When wavelet polarity is examined from left to right, AZ1 and AZ2 are azimuths where polarities of H1 VSP wavelets reverse on the T1 reference line, and AZ3 and AZ4 are azimuths where polarities of H2 VSP wavelets reverse on the T2 reference line.

A fundamental requirement for generating an accurate mathematical rotation of a down-going VSP direct-S wavelet is that the wavelet that is subjected to rotation must be a high-quality, zero-phase wavelet that has an optimal signal-to-noise ratio (SNR). A zero-phase wavelet is defined as a wavelet that is symmetrical about its zero-time line. This is why the red dash lines in Figure 3-1 are defined as being both a zero-time line and a zero-phase line. Ideal zero-phase wavelets have a robust, strong-amplitude, symmetrical peak (or trough) centered at zero time and only one reduced-amplitude lobe on each side of this large-amplitude central lobe. All of these wavelet properties apply to the black, central-lobe, H1 wavelets between north (N) and

east (E) azimuths in Figure 3-1, as well as to the red, central-lobe, H1 wavelets between south (S) and west (W) azimuths.

Data examples that follow will illustrate that down-going VSP direct-S wavelets generated by a vertical vibrator, the energy source that generated the FutureGen2 VSP data used in this study, are usually excellent zero-phase wavelets. Another important concept that will be illustrated is that VSP wavelets recorded by transverse-horizontal geophones have a higher SNR than do down-going, direct-S wavelets recorded by radial-horizontal geophones. VSP wavelets recorded by radial-horizontal geophones at various depths are often contaminated by up-going P-SV reflections (and sometimes by up-going P-P reflections) that distort down-going, direct-S wavelets and destroy their zero-phase character.

The direct-S VSP wavelet used in the wavelet rotation display in Figure 3-1 is the response of a H1 (transverse) horizontal geophone at geophone depth 4225 ft (1288 m) after that geophone has been rotated to be perpendicular to a vertical plane oriented 52-degrees clockwise (CW) from north. This vertical plane passes through both the X-Y coordinates of the down-hole VSP receiver station and the X-Y surface coordinates of the zero-offset source station and is the directional orientation of the radial-horizontal geophone. When this receiver-to-source orientation of VSP horizontal geophones is done, the axis of the H1 (transverse) horizontal geophone is oriented 38 degrees counter-clockwise (CCW) from north (or 322-degrees CW from north). The companion H2 horizontal geophone is orthogonal to the H1 horizontal geophone. Its axis is thus oriented in azimuth 52-degrees, which makes the H2 geophone be a radial-horizontal geophone pointing directly at the X-Y coordinates of the zero-offset source station.

The rotated H1 and H2 wavelets in Figure 3-1 are plotted from left to right as functions of azimuth measured CW from north. Data traces start at 0-degrees azimuth at the left end of each data panel, increase at 5-degree increments toward the right, and stop at 355-degrees azimuth. The real VSP wavelet that was mathematically rotated to create both data panels is the 8-th wavelet from the right in the H1 data panel. This wavelet is the one that the H1 horizontal geophone recorded when it was oriented in azimuth 322-degrees and was activated by the transverse component of the direct-S wavelet produced by the vertical vibrator positioned at the zero-offset source station.

The wavelets in the H2 data panel of Figure 3-1 are rotated H1 wavelets that are delayed by 90 degrees of compass rotation at each azimuth coordinate. This procedure for creating the H2 data panel ensures that VSP fast-S wavelets and VSP slow-S wavelets have identical waveshapes. Examination of Sondergeld and Rai's laboratory test data in Figure 2-5 shows that their fast-S and slow-S wavelets have identical waveshapes, and that their slow-S wavelets lag their fast-S wavelets by 90-degrees of compass-rotation azimuth. The VSP direct-S wavelet rotation procedure used to construct data panel H2 in Figure 3-1 thus exactly replicates the lab test data exhibited in Figure 2-5.

Correct positioning of zero-time (zero-phase) reference lines T1 and T2 in Figure 3-1 is critical for interpreting phase behaviors of rotated versions of H1 and H2 wavelets. It is essential that these reference-time (reference-phase) lines pass through the center of the peaks and troughs of H1 and H2 wavelets in those azimuth zones where central peaks and troughs of rotated wavelets have maximum amplitudes. In Figure 3-1, the arrow pointers extending away from the four, orange-colored, T1 and T2 labels identify these key azimuth zones where decisions can be made if T1 and T2 lines are properly positioned on zero-phase wavelets. When T1 and T2 reference time lines pass through the apex of central peaks and troughs of H1 and H2 wavelets

in their high-amplitude azimuth zones, as they do in Figure 3.1, then wavelet phase decisions made across other azimuth zones, where wavelet amplitudes are weak and wavelet shapes change rapidly with azimuth, will be reliable.

Using these wavelet interpretation guidelines, important principles of seismic S-wave physics exhibited by the data in Figure 3-1 are:

- Fast-S (H1) wavelets reach maximum amplitudes on the T1 red-dash zero-time (zero-phase) line at the same azimuths where slow-S (H2) wavelets undergo a polarity reversal on the T2 red-dash zero-time line.
- Slow-S polarity reversals labeled AZ3 and AZ4 thus define fast-S polarization direction; i.e., Shmax azimuth.
- Slow-S (H2) wavelets reach maximum amplitudes on the T2 red-dash zero-time (zero-phase) line at the same azimuths where fast-S (H1) wavelets undergo a polarity reversal on the T1 red-dash zero-time line.
- Fast-S polarity reversals labeled AZ1 and AZ2 thus define slow-S polarization direction; i.e., Shmin azimuth.

These four principles are exactly the key findings in Sondergeld and Rai's laboratory test (Figure 2-5). Verifying that the same behaviors observed in laboratory measurements of S-wave propagation in small fractured-rock samples also occur in real-world, mathematically-rotated, direct-S, H1 and H2 VSP wavelets is a major technology deliverable in this project.

The implications of these VSP research findings are significant. Prior to the proof-of-concept of predicting Shmax by simple rotation of a down-going, VSP, direct-S wavelet that is now established in this project, the options for determining fast-S (Shmax) and slow-S (Shmin) azimuths from VSP data were limited, and usually required:

- Deployment of an S-wave source that can generate a horizontal source displacement in different azimuth directions at a single source station, or

- Using down-going P wavefields generated by traditional P sources (vertical vibrators) located in several azimuth directions away from a VSP receiver well, and then

- Constructing S images from data generated by these azimuth-dependent sources and comparing azimuth-dependent arrival times of mode-converted S reflections to determine fast and slow azimuths.

This project shows that all that is needed to generate data appropriate for estimating Shmax azimuth is a single, traditional, P source positioned at a single, surface station, and a mathematical rotation of a direct-S wavelet produced by that P source and recorded by a deep VSP horizontal geophone. This latter option is much simpler, and considerably less costly, than traditional VSP methods that have been used up to this time to determine Shmax and Shmin azimuths. Perhaps more importantly, the procedure described in this section can be applied to legacy VSP data that likely have already been acquired at a site of interest.

3.2   What and Where Are Direct-S Wavelets in Rotated-Wavelet Displays?

The term "direct-S wavelet" is used repeatedly in this report, and it is critical that readers understand what and where direct-S wavelets appear in the rotated-wavelet displays that will be presented in this section. Inspection of fast-S and slow-S wavelets used in the laboratory test

that inspired the research procedure implemented in this project (Figure 2-5) shows that those lab-test wavelets were compact, noise-free, and ideally symmetrical, as zero-phase wavelets should be, and that fast-S and slow-S wavelets were totally separated from each other in travel time when they arrived at the receiver location. Direct-S wavelets of this nature leave no doubt as to what fast-S and slow-S wavelets are, and where each type of wavelet (fast or slow) is located, in essentially any type of data displays that one may construct.

In contrast, in VSP rotated-wavelet displays in this report, a reader will not find solitary S wavelets that are totally isolated in travel time from other geophone-recorded S wavelets. Instead, rotated data will be displayed as 80-ms windows of rotated VSP trace data, as exhibited in Figure 3-1. These data windows will span approximately four wavelet peaks and four wavelet troughs (typically). When a horizontal VSP geophone is mathematically rotated, the entire VSP data trace associated with that geophone is rotated, not just a single wavelet, and not just a selected 80-ms data window. After mathematical rotation, a small data window is then extracted from each rotated full trace, that to the best skill of the person processing the VSP data, is centered on the down-going, direct-S wavelet at a chosen geophone station. These data windows are the 80-ms windows that will be presented in each display of rotated H1 geophone and H2 geophone data in this section.

At each geophone station where rotated direct-S VSP wavelets are presented, the zero-phase reference time for each down-going, direct-S, VSP wavelet is defined by a red-dash line drawn across each wavelet display (Figure 3-1). If a VSP data processor has defined direct-S wavelets correctly and applied appropriate signal processing, each H1 red-dash line will pass exactly through the apex of maximum-amplitude H1 wavelet peaks and troughs that occur at fast-S (Shmax) azimuths, and each H2 red-dash line will pass exactly through the apex of maximum-amplitude H2 wavelet peaks and troughs that occur at slow-S (Shmin) azimuths. In this study, ray tracing was done to assist in the selection of the proper direct-S wavelet embedded in far-offset VSP data. This ray tracing used interval velocities determined from zero-offset VSP data.

Fast-S wavelets consist of only that single central peak (trough) that is centered on a T1 red-dash line, plus the left-side and right-side troughs (peaks) associated with that central peak (trough). Similarly, slow-S wavelets consist of that single central peak (trough) that is centered on a T2 red-dash line, plus the left-side and right-side troughs (peaks) associated with that central peak (trough). Data trace peaks and troughs that span the remainder of each 80-ms data window are not a part of a direct-S VSP wavelet.

When proper wavelet-amplitude conditions exist, then polarity reversals of fast-S wavelets are defined as any H1 wavelet behavior where H1 minimum-amplitude, black peaks (red troughs) shift to minimum-amplitude, red troughs (black peaks) exactly on the T1 red-dash line. Similarly, polarity reversals of slow-S wavelets are defined as H2 wavelet behaviors where H2 minimum-amplitude, black peaks (red troughs) shift to minimum-amplitude, red troughs (black peaks) exactly on the T2 red-dash line. Polarity reversals in data that occur above and below these T1 and T2 red-dash lines are not associated with direct-S wavelets and must be ignored.

These data interpretation principles are used to define Shmax and Shmin azimuths in each rotated-wavelet display that appears later in this section.

3.3   Source and Receiver Deployments at FutureGen2 VSP Data

The procedures used to interpret rotated direct-S VSP wavelets described in the preceding section are now applied to VSP data acquired across the FutureGen2 project area described in

Section 1 to estimate Shmax and Shmin azimuths. The map in Figure 1-2 that illustrates where VSP source stations are positioned around the FutureGen2 VSP receiver well is repeated here as Figure 3-2 for reader convenience.

Figure 3-2. Map showing locations of VSP source stations around the FutureGen2 VSP receiver well.

3.4   Independent Ground Truth Measurement of Shmax at FutureGen2 Site

Seven open-borehole hydraulic fracture tests were conducted in this FutureGen2 VSP receiver well in 2013 as a part of the FutureGen2 research program. The field-testing program included three tests in the near-basement Mount Simon Sandstone and five tests in the underlying crystalline basement formation. The maximum horizontal principal stress direction (Shmax) was determined to be: N 51± 4°E, in the Mount Simon; N 63±9°E for three of the tested intervals in the Pre-Cambrian and N77°E for the other two tests in the Pre-Cambrian. This difference in Shmax directions suggests the existence of local, small-scale, stress heterogeneities within the basement rock formation. These Mount Simon test results (51°± 4°) provide an independent ground-truth measurement of Shmax azimuth that will be used to judge the reliability of Shmax azimuths predicted by rotation of VSP direct-S wavelets.

3.5   Determining Shmax for Vertical Travel Paths (Zero-Offset VSP Data)

Shmax azimuths were first determined from VSP data generated at zero-offset source station ZVSP. This source-station label (ZVSP) does not appear in Figure 3-2 because the zero-offset station was only 195 ft (60 m) northeast of the VSP receiver well. A zero-offset VSP source-receiver geometry replicates the vertical source-to-receiver travel path used in Sondergeld and Rai's laboratory testing (Figure 2-4). Displays of zero-offset VSP data generated at source station ZVSP are shown as Figure 3-3. These zero-offset VSP data traces begin at a shallow depth of only 75 ft (23 m) and continue at intervals of 50 ft (15 m) to a depth of 4475 ft (1364 m).

At this receiver well location, granitic basement begins at a depth of 4250 ft (1295 m), so these zero-offset VSP data extend 225 ft (68 m) into basement rocks.
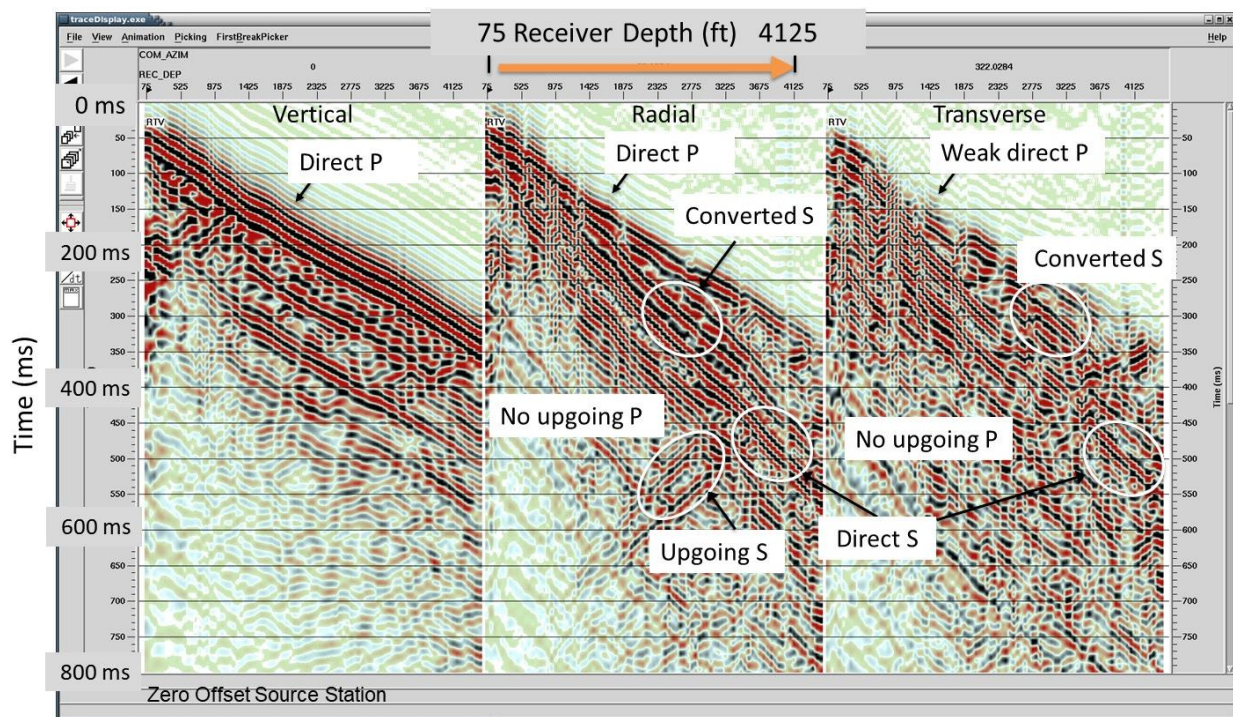
Figure 3-3. VSP data produced at zero-offset source station ZVSP and sorted into three panels according to which receiver in the down-hole 3-component geophones recorded the data.

The ZVSP data in Figure 3-3 are presented after performing standard VSP data-processing practices of:

1. Mathematically rotating each 3C geophone so that its H1 geophone axis points in the direction of down-going transverse-S displacement vectors, and its H2 geophone axis points in the direction of radial-S displacement vectors,

2. Applying a time-dependent gain function that boosts deep wavelet amplitudes to values equivalent to shallow wavelet amplitudes, and

3. Segregating data traces into three data panels according to which receiver in each 3-component geophone recorded the data.

Key features of the data are labeled on each data panel.

3.6   Selecting Appropriate Direct-S Wavelets to Rotate

Raw, unprocessed, down-going, direct-S VSP wavelets were used in the wavelet rotations done in this study. This choice to use unprocessed VSP wavelets can be adjusted by others who wish to apply VSP wavefield separation procedures, optimize VSP wavelet shapes, or to apply filters that eliminate tube wave interference and other damaging noise modes that distort VSP wavelet shapes.

To test the validity of direct-S VSP wavelet rotation as a method for defining Shmax azimuth, it was essential to utilize direct-S wavelets that were not contaminated by interfering events and that had minimal waveform distortions. Visual examination of the ZVSP data in Figure 3-3 shows that there are depth intervals where down-going ZVSP direct-S wavelets satisfy these requirements. One ideal ZVSP direct-S wavelet recorded by a transverse-horizontal geophone was selected at receiver depth 4225 ft (1288 m) for Shmax analysis. This is the same direct-S wavelet that was used to explain the principles of direct-S wavelet rotation in Figure 3-1. The H1 and H2 rotated-wavelet data panels from Figure 3-1 are now used again in Figure 3-4 to estimate Shmax azimuth at source station ZVSP.
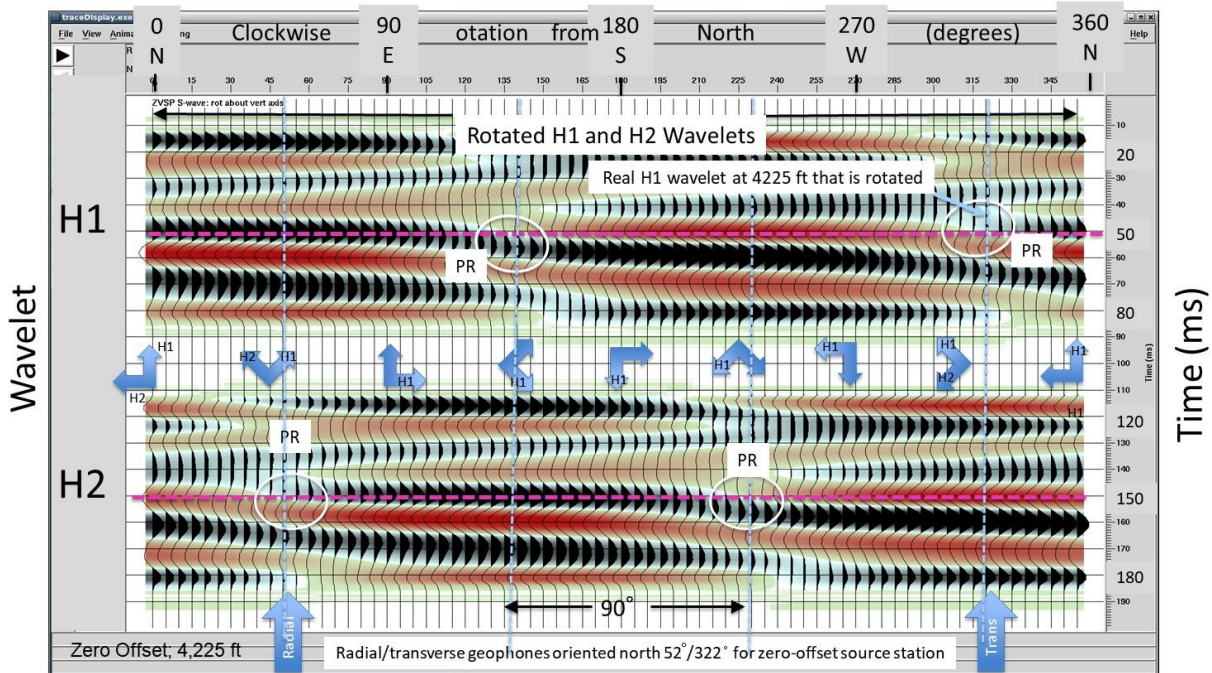
Figure 3-4. Estimate of Shmax azimuth using direct-S wavelets produced at source station ZVSP and recorded by a transverse-horizontal geophone at receiver depth 4225 ft (1288 m). Shmax azimuth is shown to be 50º (+/- 5º), the azimuth where H2 (slow-S) wavelets undergo a polarity reversal (PR oval at the left end of the H2 wavelet panel). The azimuth orientations of H1 and H2 geophones that produced the rotated wavelets are shown by the orthogonal, blue, rotating arrows positioned between the H1 and H2 data panels.

3.7   Understanding Geophone Orientations in Rotated Wavelet Displays

A row of blue, rotating, orthogonal arrows are positioned between the H1-horizontal geophone and H2-horizontal geophone data panels in Figure 3-4. These blue arrows imitate map views (looking down from the zero-offset source station) of a mathematical set of rotating H1 and H2 geophones at a depth of 4225 ft (1258 m). The azimuth orientations of the axes of these H1 and H2 horizontal geophones are displayed at 45-degree azimuth increments during their 360-degree, full-azimuth, mathematical rotation. The blue arrow set on the far-left shows H1 and H2 orientations at 0 degrees compass azimuth where the wavelet rotation starts. Here the H1 geophone axis is pointing north and the H2 geophone axis is pointing west. The second arrow set shows H1 and H2 orientations at 45 degrees of compass-azimuth rotation. Here the H1 geophone is oriented 45º CW from north and the H2 geophone is oriented 45 degrees CCW from north. The third arrow set defines the orientations of H1 and H2 at 90 degrees of compass-azimuth rotation. Here H1 is pointing east and H2 is pointing north. These rotating arrow sets

should help readers understand why H1 and H2 wavelet polarities and amplitudes behave the way they do along their two red-dash H1 and H2 zero-phase lines (Figure 3-4).

The two vertical blue arrows below the H2 data panel identify the azimuths of the actual radial and transverse geophones at a depth of 4225 ft that were used to generate the radial and transverse data panels in Figure 3-3. The wavelets that were mathematically rotated to create the full H1 and H2 wavelet panels were the transverse and radial geophone wavelets recorded at a depth of 4225 ft (1258 m). These wavelets are identified by the vertical blue arrows positioned at azimuths of 52 and 322 degrees at the base of Figure 3-4.

Data panels H1 and H2 in Figure 3-4 are rotated fast-S and slow-S wavelets, respectively. Examination of Sondergeld and Rai (1992) test results (Figure 2-5) shows that when a down-going fast-S mode is recorded with a horizontal sensor that rotates in a full 360-degree azimuth circle around the down-going direct-S ray path, the following wavelet behaviors should be observed:

1. A fast-S mode (H1 panel) will exhibit two polarity reversals, separated by 180 degrees of azimuth. These fast-S polarity reversals define the azimuth plane of slow-S polarization, the azimuth plane where fast-S (H1) amplitude vanishes.

2. A slow-S mode (H2 panel) will exhibit two polarity reversals, separated by 180 degrees of azimuth. These polarity reversals define the azimuth plane of fast-S polarization, the azimuth plane where slow-S (H2) amplitude vanishes.

3. A fast-S mode (H1 panel) achieves maximum amplitude at the same two azimuths where its companion slow-S mode undergoes a polarity reversal. Fast-S maximum amplitudes have opposite algebraic signs at these two slow-S azimuths.

4. A slow-S mode (H2 panel) achieves maximum amplitude at the same two azimuths where its companion fast-S mode undergoes a polarity reversal. Slow-S maximum amplitudes have opposite algebraic signs at these two fast-S azimuths.

These four direct-S wavelet behaviors are exactly replicated when a zero-offset, down-going, direct-S, VSP wavelet is mathematically rotated (Figure 3-4). Particularly important is the fact that a slow-S polarity reversal occurs at 50 degrees (+/-5º) on the H2 data panel of Figure 3-4. This slow-S polarity reversal indicates that the direction of fast-S polarization (i.e., Shmax azimuth) is 50 degrees (+/-5º), a result that is essentially the same Shmax azimuth [51 degrees (+/-4º)] that was indicated in earlier borehole breakout tests at this test site.

This research project thus demonstrates that VSP-scale, direct-S, wavelet rotation provides correct definitions of Shmax azimuth when the travel path from source to receiver is vertical as it is in zero-offset VSP data. This is a seminal finding in the area of non-invasive measurement of stress field properties in deep rocks.

3.8 Determining Shmax Azimuth from Slanted Travel Paths (Far-Offset VSP Data)

Although data presented to this point verify that laboratory-scale, direct-S, wavelet rotation physics can be upscaled to traditional, zero-offset-VSP, source-receiver dimensions, these foundational tests and proofs have exactly mimicked lab measurements and involved only vertical, straight-line, travel paths. When a well is available for non-invasive deployment of down-hole 3C VSP geophones, as was the situation at the FutureGen2 site, it is common

practice to generate VSP data at far-offset source stations and to not limit data collection to only zero-offset VSP data. It is therefore important to determine if direct-S wavelet-rotation provides correct estimates of Shmax when a direct-S ray path from source to receiver is not a vertical, straight-line, ray path as in zero-offset VSP data, but is slanted and curved, as is the case for S-wave propagation from a far-offset source station to a deep VSP geophone.
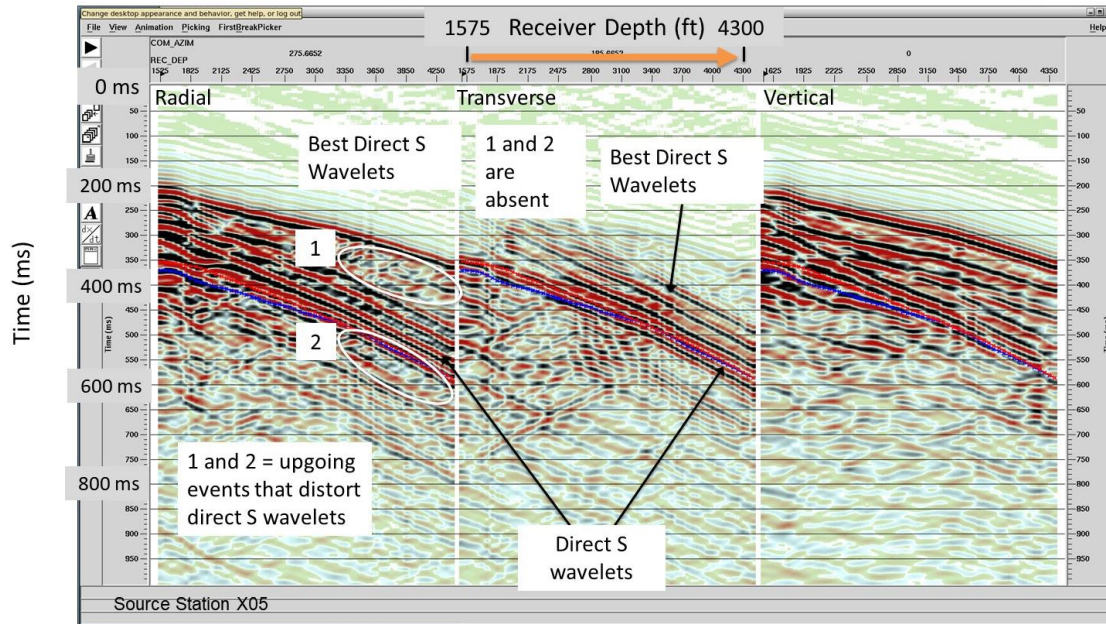
Figure 3-5. VSP data produced at far-offset source station X05.

VSP data generated at offset source station X05 (Figure 3-2) are displayed in Figure 3-5. This source station is 2041 ft (622 m) from the receiver well in an azimuth direction of 278 degrees CW from north (see map in Figure 3-2). A source offset of approximately one-half of the depth to the deepest receiver station in a VSP well usually results in good-quality data, and this is the case for data generated at source station X05. Examination of Figure 3-5 shows that direct-S wavelets are particularly good quality on both the transverse and radial geophone data panel. This high-quality signal-to-noise behavior occurs because direct-S energy strength usually increases significantly when a source-to-receiver ray path involves a takeoff angle that exceeds 15 degrees from vertical (Figures 2-6c and 2-5).

The direct-S wavelet recorded by the VSP receiver at depth 3750 ft (1143 m) was used for wavelet-rotation analysis along the slanted travel path from source station X05 (Figure 3-6). An important principle about the position of the red-dash, zero-phase, reference line for rotated wavelets is illustrated by this data example. This principle requires that VSP data interpreters must use great care to position this red-dash reference line so that it passes through zero-phase points of rotated wavelets. Even when a data processor uses raytracing to indicate the position of a direct-S arrival at a far offset VSP receiver, a zero-phase line created during VSP data processing may still have to be slightly adjusted to be a true zero-phase reference line for interpreting rotated wavelets. In this case, the original red-dash lines, which were positioned at 50-ms on the H1 wavelet panel and at 150-ms on the H2 wavelet panel in Figure 3-6, need to be moved down about 4 ms so that they pass precisely through the apices of H1 and H2 wavelets. These adjusted zero-phase lines are the dash lines shown in Figure 3-6. Polarity reversals are now identified by these time-shifted zero-phase reference lines, not by the original

red-dash line provided by the VSP data processor. This new phase-reference line indicates Shmax azimuth is 50° (+/-5°), the same Shmax azimuth results obtained for the ZVSP vertical travel path results at receiver station 4225 ft (Figure 3-4).
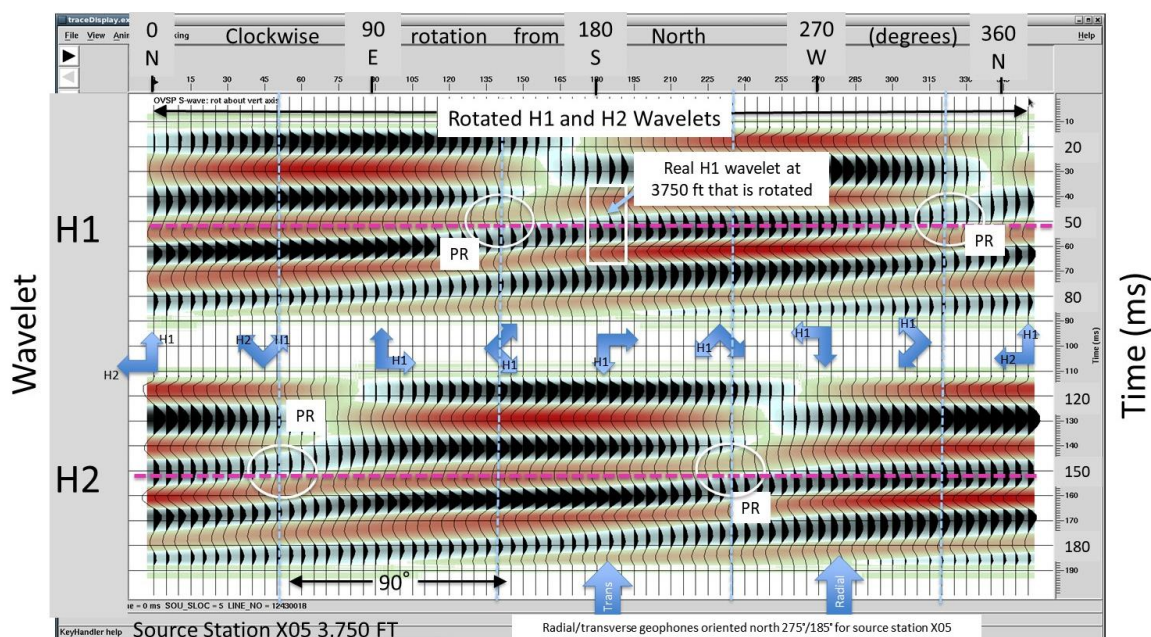
Figure 3-6. Estimate of Shmax azimuth using direct-S wavelets produced at source station X05 and recorded at receiver depth 3750 ft (1143 m). Shmax azimuth is measured on an adjusted zero-phase reference line which has been shifted down 4 ms to serve as a correct zero-phase line for the zero-phase wavelets embedded in these VSP data. This adjustment results in Shmax azimuth being 50 degrees (+/- 5°), the azimuth where H2 (slow-S) wavelets undergo a polarity reversal.

3.9   Determining Shmax from Selected Far-Offset Azimuths

Another variable that needs to be investigated is to determine if rotation of direct-S VSP wavelets provides consistent estimates of Shmax for source stations that are positioned at significantly different azimuths around a receiver well. Effects of source azimuth positions relative to a VSP receiver well were examined by doing a rotation of a direct-S wavelet created at source station X10 (see source station map in Figure 3-2) and then comparing estimates of Shmax azimuths from that source station's data with estimates of Shmax estimates made from data generated at source station X05. Source station X10 is positioned in an azimuth direction of 311 degrees from the receiver well (Figure 3-2), and source station X05 is in an azimuth direction of 278 degrees, an azimuth difference of 33 degrees. Source station X10 is also 634 ft (193 m) farther from the receiver well than source station X05 and has a longer slanted travel path to VSP receiver stations.

Source Station X10

VSP data generated at source station X10 are shown as Figure 3-7. Transverse (H1) direct-S wavelet quality is again generally good. Direct-S wavelet rotations of the transverse-geophone response recorded at depth 3750 ft (1143 m) are displayed as Figure 3-8. In this instance, there is no need to adjust the position of the red-dash zero-phase time line as was done in Figure 3-6.

These wavelet rotations infer that Shmax azimuth is 50 degrees (+/-5°), the same Shmax azimuth prediction obtained with direct-S wavelets generated at source station X05 (Figure 3-6).
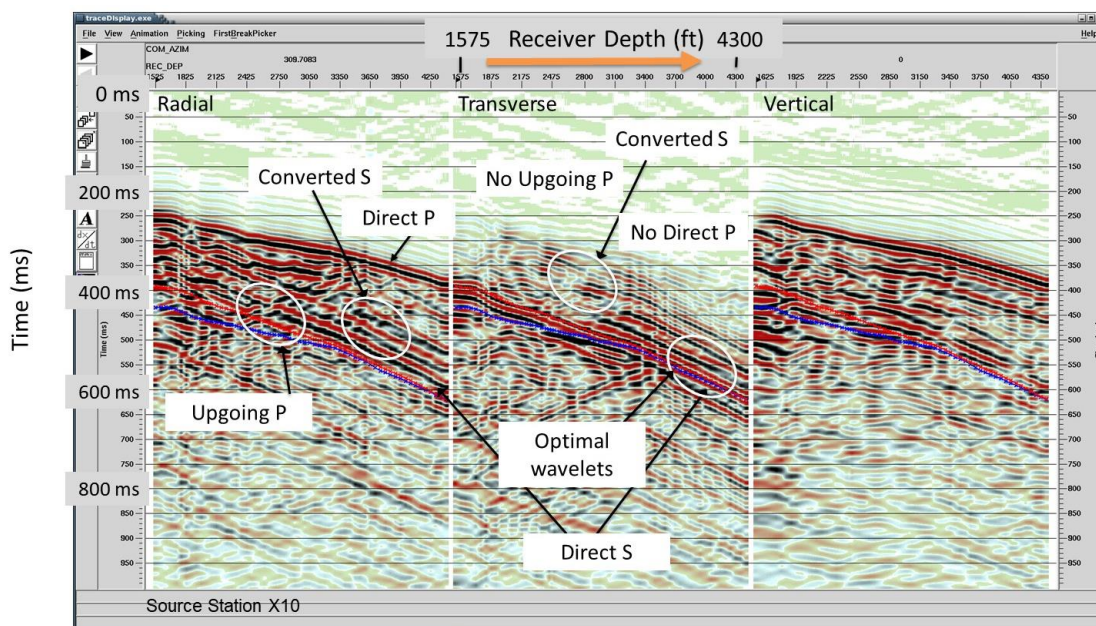
Figure 3-7. VSP data produced at far-offset source station X10.
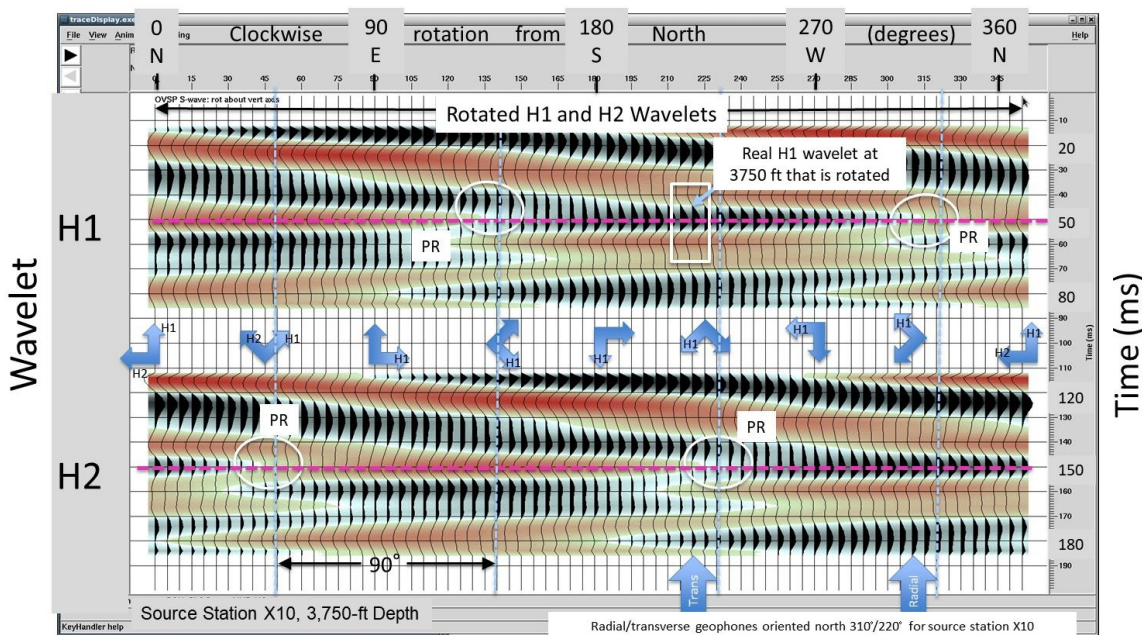
Figure 3-8. Estimate of Shmax azimuth using direct-S wavelets produced at source station X10 and recorded at receiver depth 3750 ft (1143 m). Shmax azimuth is 50 degrees (+/- 5°), the azimuth where H2 (slow-S) wavelets undergo a polarity reversal.

Source Stations X07, X15, and X16

Display formats used in these last four, far-offset, VSP data examples will be simplified now that data analysis procedures have been illustrated for rotated direct-S wavelets in Figures 3-4, 3-6,

and 3-8. Specifically, only H1 wavelet panels will be displayed. In preceding examples, H2 data panels were used only to identify slow-S polarity reversals, and then applying the principle that Shmax azimuths were identical to the azimuths where these slow-S polarity reversals occurred. These last three examples show an alternate way to predict Shmax. This alternate approach is to use only H1 wavelets to identify azimuths where fast-S wavelets undergo a polarity reversal, and then use the principle that the azimuth of Shmax is (plus/minus) 90 degrees from the azimuths where these polarity reversals of fast-S wavelets occur. The validity of this alternate approach is established by the lab test results exhibited in Figure 2-5 and by the preceding interpretations of real VSP data (Figures 3-4, 3-6, and 3-8).
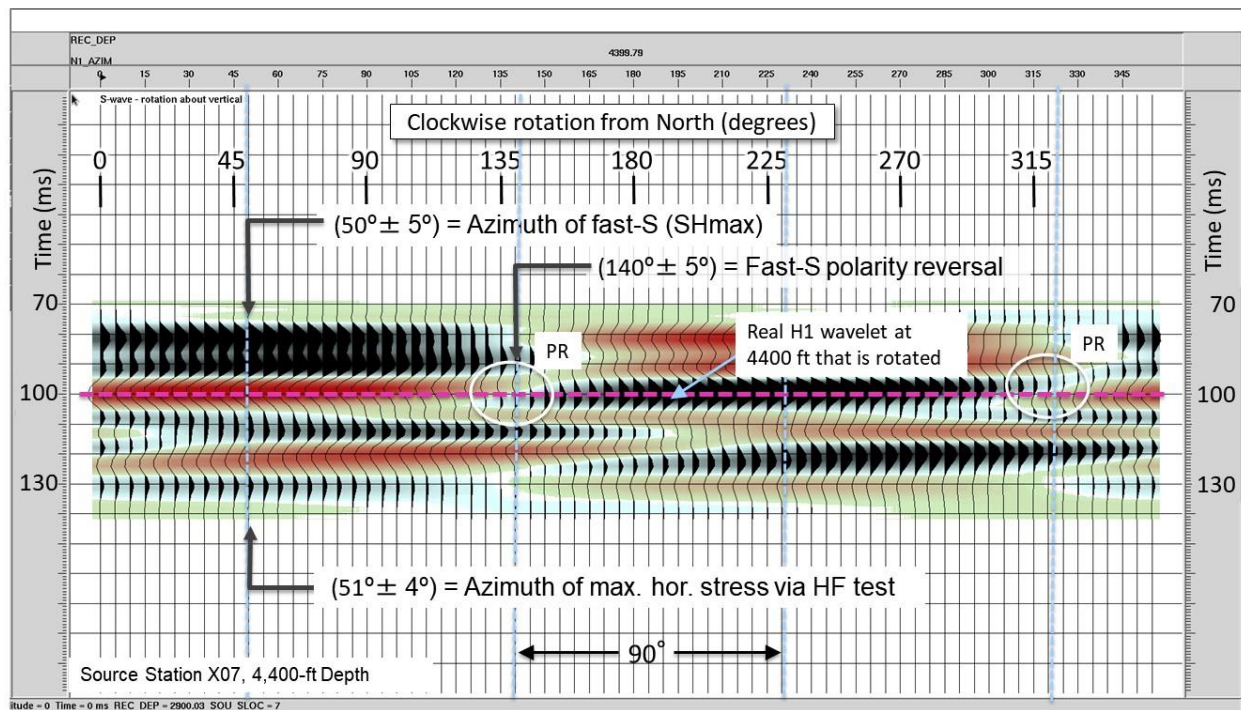
Figure 3-9. Estimate of Shmax azimuth using only H1 rotated direct-S wavelets. The vertical vibrator source was positioned at station X07. Receiver depth was 4400 ft (1341 m). Shmax azimuth is 50 degrees (+/- 5º), the azimuth displaced 90 degrees from azimuth 140 degrees where the H1 (fast-S) wavelets undergo a polarity reversal.

Displays of rotated, direct-S, H1, VSP wavelets generated at source stations X07, X15, and X16 are displayed as Figures 3-9, 3-10, and 3-11, respectively. Refer to the source-station map in Figure 3-2 to understand the azimuths and offset-distances associated with these four VSP source stations. The red-dash, zero-time line in Figure 3-9 is another example of an ideal zero-phase reference line selected by the VSP data processor. In this case, the real wavelet that was rotated to create the H1 wavelet panel is identified at azimuth 180 degrees. This real wavelet recorded by the transverse-horizontal geophone at depth 4400 ft is already an almost-perfect zero-phase wavelet. As a result, the data processer could correctly position the zero-phase reference line, and the red-dash line shown in this display does not have to be adjusted. The fast-S polarity reversal at an azimuth of 140 degrees is correctly identified. The fast-S azimuth (i.e., the Shmax azimuth) is then at 50 degrees, an azimuth shift of 90 degrees from the azimuth where a fast-S polarity shift occurs.

The term "genesis wavelet" is appropriate for the single wavelet that is phase rotated to create the rotated-wavelet panels exhibited in this section, and will now be used frequently. The genesis wavelets recorded by transverse-horizontal geophones that are rotated to create the H1 rotated-wavelet panels in Figures 3-10 and 3-11 are far from being zero-phase wavelets. For example, the 100-ms reference line used by the VSP data processor cuts through the black peak of the real transverse-horizontal geophone wavelet in Figure 3-10 at azimuth 355 degrees, but unfortunately, this black peak is not a symmetrical peak like one should see for a zero-phase wavelet. However, if the reference time line is moved up from 100-ms to the red-dash line at 94-ms, then that red-dash line passes exactly through the peaks of symmetrical black peaks centered around azimuth 50 degrees, as well as through the peaks of symmetrical red troughs centered around azimuth 230 degrees. A polarity reversal then occurs at an azimuth of 140 degrees. The result is that Shmax azimuth is again shown to occur at 50 degrees (+/-5°), after the zero-phase reference line is correctly positioned.
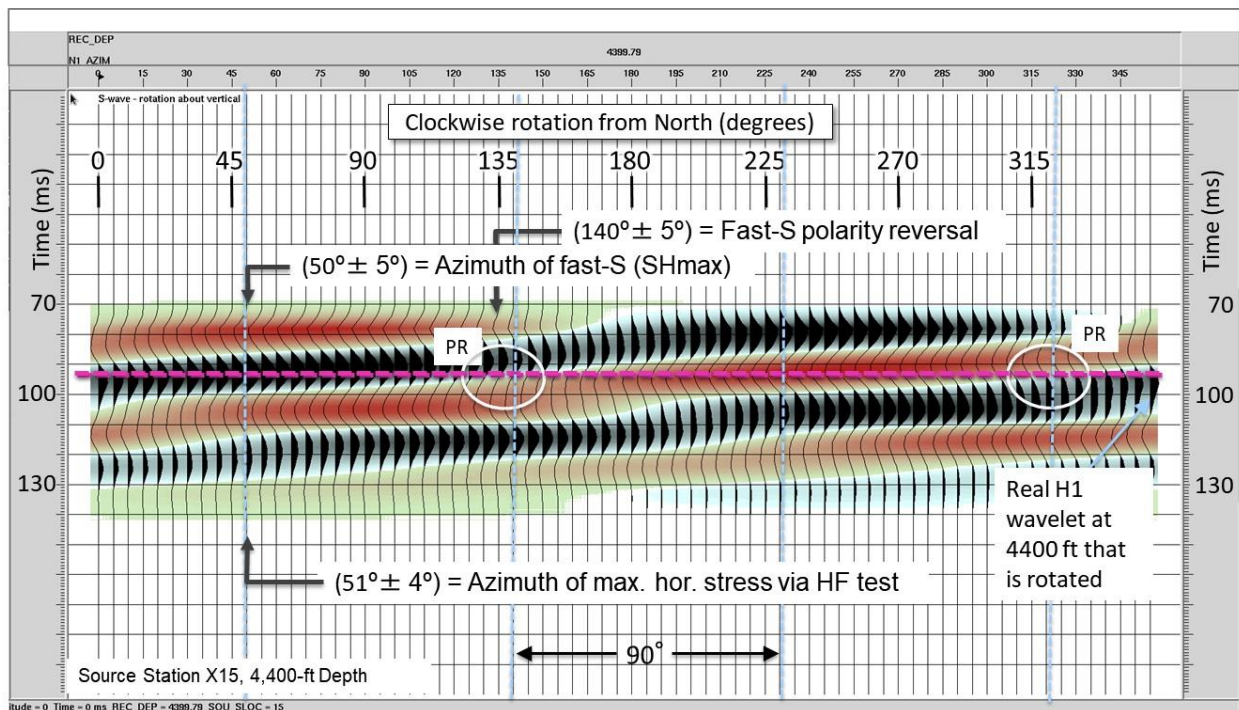
Figure 3-10. Estimate of Shmax azimuth using only H1 rotated direct-S wavelets. The vertical vibrator source was positioned at station X15. Receiver depth was 4400 ft (1341 m). Shmax azimuth is 50 degrees (+/- 5°), which is the azimuth displaced 90 degrees from azimuth 140 degrees where the H1 (fast-S) wavelets undergo a polarity reversal, after the zero-phase reference line is moved up 6 ms to pass through the apex of high-amplitude, zero-phase wavelets.

This analysis illustrates two important principles:

(1) If the genesis wavelet used to create a rotated-wavelet panel is not a "reasonable" approximation of a zero-phase wavelet, the zero-phase reference line used to search for polarity reversals of rotated versions of that genesis wavelet will almost always not be positioned correctly.

(2) This outcome means that the original zero-phase reference line can be moved up or down "a few" milliseconds to compensate for the fact that a genesis wavelet is not a proper zero-phase wavelet.

When the phase properties of a genesis wavelet deviate from the properties of a true zero-phase wavelet, the cause usually is that there is interference from a second wavelet of a different wave mode that occupies some of the same time-space coordinates as the genesis wavelet. When this data behavior occurs, the best solution would be to move the wavelet-rotation procedure to a different receiver station where there is no, or minimal, noise interfering with a potential genesis wavelet.
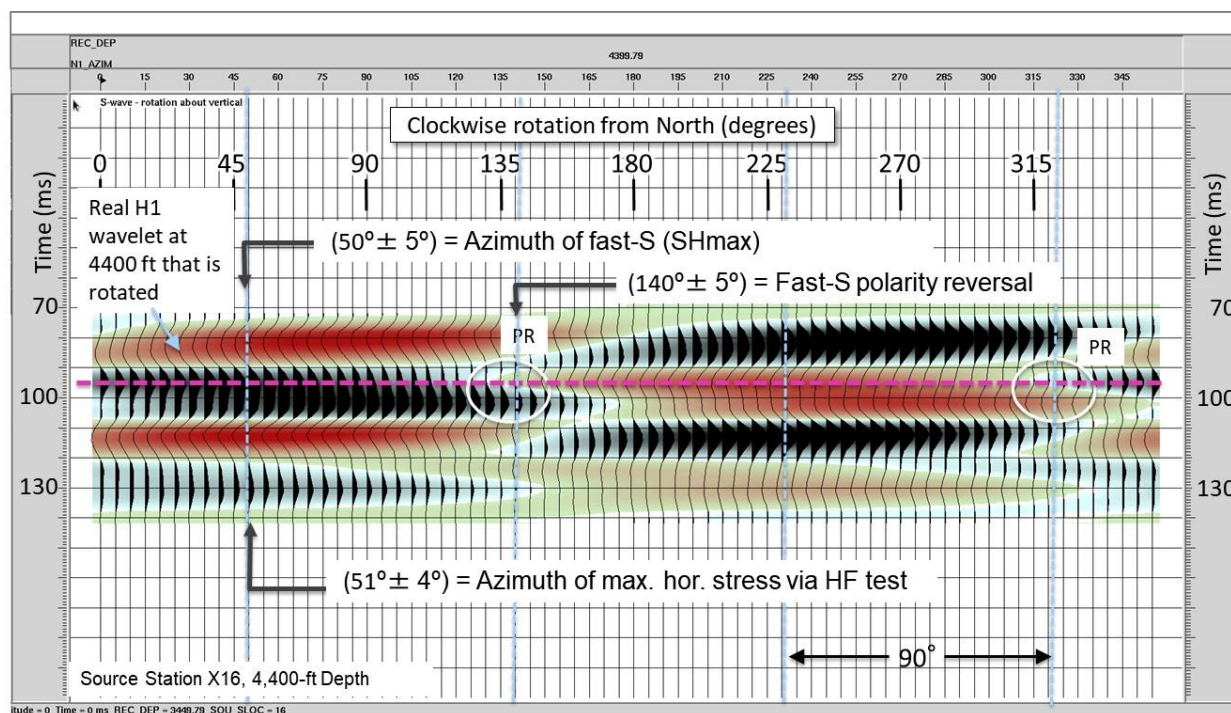
Figure 3-11. Estimate of Shmax azimuth using only H1 rotated direct-S wavelets. Vertical vibrator was positioned at source station X16. Receiver depth was 4400 ft (1341 m). Shmax azimuth is 50º(+/- 5º), which is the azimuth displaced 90º from azimuth 140º where the H1 (fast-S) wavelets undergo a polarity reversal, after the zero-phase reference line is moved up 4 ms.

The genesis wavelet used for wavelet rotation that is recorded by the transverse geophone for source station X16 (Figure 3-11) is indicated at a wavelet-azimuth of 25 degrees. Again, the original reference-time line at 100-ms passes through a black peak of this genesis wavelet that is asymmetrical, not symmetrical as it should be for a zero-phase wavelet. The zero-phase reference line is thus moved up 4 ms to be the red-dash line displayed in Figure 3-11 that passes through the apex of the black peaks between 340 to 355 degrees of azimuth. All phase behavior of data in the wavelet panel of Figure 3-11 is now measured relative to this repositioned red-dash line. The results are that a fast-S polarity reversal is identified at azimuth 140 degrees, which means Shmax azimuth (i.e., fast-S polarization azimuth) is 50 degrees (+/-5º).

This example again emphasizes the importance of paying close attention to the wavelet chosen for azimuth rotation. In this case, the genesis wavelet identified at 25 degrees of wavelet-rotation is far from being a zero-phase wavelet. Instead, it appears to be a complex wavelet formed by a mixture of two wavelets. The early part of this genesis wavelet appears to be a zero-phase wavelet, so the apex of this "apparent" zero-phase wavelet was chosen as a possible zero-phase line. This speculation turned out to be correct, particularly when it is noted

how the red-dash line passes exactly through the apices of rather good-quality zero-phase wavelets clustered around azimuths of 0 and 180 degrees. However, it would be better practice to push this particular rotated-wavelet example aside and search for a genesis wavelet recorded at a different receiver station that had better zero-phase properties.

When zero-phase reference lines are properly adjusted from where they were positioned during standard VSP data processing, Shmax azimuth for data generated at these three far-offset source stations (X10, X15, X16) have a consistent value of 50 degrees (+/-5°).

3.10   Summary of VSP Predictions of Shmax Azimuths

Table 3-2 summarizes the Shmax analyses presented in this section. Data are arranged in columns so that source offset distance from the VSP receiver well increases from left to right in the second line of the table. Straight-line travel paths from the surface source to the receiver station chosen for analysis imply that the approach angle of the down-going genesis wavelet used to calculate full-azimuth rotated wavelets varies from 2.6 to 44.5 degrees from vertical (fourth line of the table). All approach angles other than the 2.6-degree angle for zero-offset station ZVSP differ significantly from the zero-degree approach angle used in Sondergeld and Rai's laboratory test (Figures 2-4 and 2-5). The upscaling of this seminal laboratory test to real-world VSP data demonstrates a valuable principle – that being that the rotation of down-going S wavelets produced by a P-wave source does not have to be constrained to wavelets that arrive at zero-degrees incident angle on stressed rocks.

Table 3-2. Source station test parameters.

Source azimuth (degrees)	52	278	311	275	87	115
Source offset (ft)	195	2041	2675	3393	3955	4326
Geophone depth (ft)	4225	3750	3750	4400	4400	4400
Approach angle (degrees)	2.6	28.6	35.5	37.6	42	44.5
Shmax azimuth (degrees)	50 (+/- 5)	55 (+/- 5)	50 (+/- 5)	50 (+/- 5)	50 (+/- 5)	50 (+/- 5)

Noting that Shmax azimuth at the FutureGen2 site as determined by down-hole hydraulic fracturing tests is 51 degrees (+/-4°), an additional observation of importance is that the wavelet-rotation procedure proven in this project provides accurate estimates of Shmax azimuth regardless of the azimuth-approach angle of a genesis wavelet at a stressed-rock interval. Examination of Table 3-2 shows that azimuth-approach directions of a genesis wavelet relative to the 51 degree azimuth of Shmax varied from 1 to 124 degrees. Because transverse-geophone wavelets are used as genesis wavelets, the orientation of the shear displacement produced by each genesis wavelet in Table 3-2 differs by 90 degrees from the approach-azimuth direction of that wavelet (i.e., the S displacement applied to stressed rocks at the FutureGen2 site varied from 91 to 214 degrees relative to Shmax azimuth). The consistently correct estimates of Shmax azimuths provided by this S-wavelet rotation procedure imply that the wavelet-rotation concept allows deep stressed rocks to be analyzed with vibrator sources positioned at azimuths of convenience away from a VSP receiver well.

3.11   Conclusions about VSP Analyses

A concept demonstrated in this research is that vertical vibrators produce down-going direct-S wavefields that are ideal for VSP wavelet-rotation purposes, and that it is not necessary to deploy a specialized S-wave seismic source to generate down-going direct-S VSP wavelets unless an S-wave source option is preferred by an investigator. An attraction of determining

fast-S (Shmax) azimuth by rotation of down-going, direct-S, VSP wavelets is that it is not necessary to follow traditional practice of making a series of S-mode images with horizontal geophones oriented in different azimuths, and then measuring image-time positions of S-mode reflections in order to determine fast-S (Shmax) and slow-S (Shmin) azimuths.

In previous industry efforts to estimate Shmax from VSP data, it is often necessary to make images that show arrival times of S-mode reflections in several azimuth directions, search these images to decide if there is an azimuth where S reflections arrive earliest, and if there is a second azimuth where those same reflections arrive at a latest time. The azimuth of the earliest arrival times should be the azimuth of Shmax. The azimuth of the slowest arriving reflections should be the azimuth of Shmin. These two azimuths should also differ by 90 degrees. To execute these procedures, a S-wave source was preferred, and that source needed to be at as many offset azimuths from the receiver well as possible. This data acquisition was expensive and impossible to do at some locations. Likewise, the data processing was expensive and demanding. In contrast, the methodology we introduce is fast, simple, low cost, and can involve only one source station if necessary.

The principal challenges to determining Shmax via direct-S VSP wavelet rotation are to ensure that the VSP direct-S wavelet that is used is a good approximation of a zero-phase wavelet, and then that a zero-phase reference line is properly positioned across each panel of rotated wavelets that need to be analyzed. The rotated-wavelet examples presented in this section illustrate and emphasize the importance of these two data-analysis requirements.

VSP data used in these demonstration analyses have not been subjected to significant data-processing procedures. The direct-S VSP wavelets that are mathematically rotated are essentially raw, unprocessed wavelets. Raw and unprocessed wavelets were used to emphasize that this wavelet-rotation methodology does not require that complicated data processing steps be applied to VSP data. However, when this procedure is expanded to numerous application areas, we recommend that researchers apply any modest data processing procedures that will enhance the zero-phase character of direct-S wavelets.

There will also be situations where data-processing procedures will definitely have to be applied to VSP data before proper S-wavelet rotation can be performed. Examples would be when a land-based VSP source is a buried explosive, a vertical impact, or an air gun in a mud pit, not a vertical vibrator as was used in this study. These types of impulsive P sources produce either one-sided, minimum-phase wavelets or mixed-phase wavelets, not symmetrical zero-phase wavelets. Wavelet-shaping operators must be applied to these types of VSP data to convert all wavelets embedded in down-going and up-going VSP wavefields to zero-phase wavelets. Another example would be when up-going events such as P-P reflections and/or P-SV reflections cut across a down-going direct-S wavelet at a key depth where a Shmax estimate must be made. These overlapping wavelets produce a mixed-phase S-wavelet that, in some cases, cannot be altered into an appropriate zero-phase waveshape. In such a case, wavefield separation procedures must be applied to attempt to extract an essential direct-S wavelet from its interfering wavefield.

It should be emphasized that this wavelet-rotation methodology is strictly a land-based strategy for non-invasive measurement of stress effects in deep rocks. The methodology cannot be applied in marine areas because no seismic source positioned in water can produce a direct-S wavefield. The shear modulus of water is zero, thus shear waves will not propagate in water.

One possibility for marine application of this concept of mathematically rotating a down-going direct-S wavelet would be to utilize the down-going S wavelet created by P-to-SV mode conversion at the seafloor or at a sediment interface near the seafloor. A follow-up study should first be considered for land-based VSP data in which a down-going P-to-SV converted mode produced at a subsurface interface is used as a substitute for down-going direct-S wavelets produced directly at the baseplate of a vertical vibrator. Only direct-S wavelets produced at a vibrator's baseplate were used in this study to emphasize that such a direct-S illuminating S-wave exists.

When S-waves propagate in a medium that has weak anisotropy, there is essentially no measurable difference in fast-S and slow-S velocities determined from VSP data or from any form of S-mode seismic data. In such instances, it may be difficult to decide if a reversal in a VSP direct-S wavelet polarity identifies a Shmax (isotropy axis) azimuth or a Shmin (symmetry axis) azimuth. It will be important in such situations to obtain some type of reliable, independent estimate of Shmax azimuth to influence one's decision as to which reversal in a VSP direct-S wavelet polarity is associated with Shmax azimuth.

Examination of Table 3-2 shows that consistent estimates of 50 to 55 degrees with a measurement error of (+/-5°) for Shmax azimuth were obtained for VSP data generated at six different source stations distributed around a central VSP receiver well. The vertical-vibrator source that created the down-going, direct-S wavelets used for wavelet rotation was positioned in a different azimuth direction, and at a different offset distance, from the VSP receiver well at each source station. All of these non-invasive VSP estimates of Shmax azimuth agreed with an independent, and invasive, measurement of Shmax azimuth of 51 degrees (+/-4°) determined by a hydraulic fracture test conducted in this same VSP receiver well in 2013. These analyses confirm that mathematical rotation of direct-S wavelets produced by a vertical-vibrator source is a simple, never-used-before, non-invasive, procedure for measuring Shmax azimuth in deep stressed rocks.

4.0 Non-invasive Extraction of Stress Information from 3D Seismic Data: Methodology

4.1 Introduction

The goal of this 3D seismic portion of this research project is to derive estimates of the azimuth directions of Shmax horizontal-stress vectors from traditional, non-invasive, 3D seismic data. The objective is to ensure that anyone who wishes to replicate these procedures can do so without having to acquire any special type of 3D seismic data. This methodology can be repeated with common, 3D, vertical-geophone, seismic reflection data that are widely available to anyone.

This second phase of this stress-from-seismic investigation is particularly important because the research data used are the type of 3D seismic data that have been acquired around the globe for the past several decades. Specifically, "P-wave" seismic data, which means the data are generated by a "P wave" source, such as a vertical vibrator or a shot-hole explosive, were used and are recorded with only vertical geophones. Quote signs are placed around the term "P-wave" in this paragraph because almost all users of seismic reflection data do indeed think that vertical-geophone data that have been generated by vertical vibrators, or by shot-hole explosives, contain only P-wave reflections. The sources that generated the 3D data used were buried explosives deployed in a grid of shot-holes. This report will show that the assumption that vertical-geophone data generated by buried-explosives contain only P-P reflection is not correct by utilizing down-going S-wave illuminating wavefields produced directly at each shot cavity in the 3D seismic area examined. This important concept about the illuminating P and S wavefields produced by a buried explosive has been documented in Figures 2-7 and 2-8.

4.2 Emphasis on Shear Waves

It is widely accepted by geophysicists that shear (S) waves are more sensitive to stress conditions and fracture orientations in rocks than are compressional (P) waves (Alford et al., 1989; Hardage et al., 2011; Mueller, 1992; Winterstein and Meadows, 1991; Xu and King, 1989). The 3D seismic investigation thus places a strong emphasis on S waves. A key objective of this research to extract stress azimuths from 3D seismic data is to illustrate that shot-hole explosives send a down-going S wave into the earth directly from each shot-hole cavity, and that these down-going S waves can be used for imaging deep rocks in the same manner that traditional P-waves produced by these same buried explosive sources are used. This direct-S imaging principle by buried explosive sources is explained in Sections 2.7 through 2.10 of this report.

The specific S-mode utilized in this 3D seismic section is the SV-P mode, which is a seismic imaging option that has been ignored by geophysicists. An SV-P mode involves a down-going direct-S illuminating wavefield produced by a P source and up-going P reflections generated by that down-going S wavefield by SV-to-P mode conversions at deep rock interfaces. These mode-converted, up-going, P reflections are recorded by surface-based vertical geophones, just as are up-going P reflections that are generated by a down-going, illuminating, P wavefield. Alternate terminology that could be used for the SV-P mode would be to refer to it as a "converted-P" mode. This terminology is a parallel to the name "converted-S" that has been

widely adopted to refer to the P-SV mode that is recorded by horizontal geophones when 3C geophones are deployed on the earth surface.

This fact, that SV-P reflections are recorded by surface-based vertical geophones, means that tens of thousands of square miles of legacy 3D vertical-geophone data that are already preserved in digital data libraries can be retrieved from data storage and reprocessed for SV-P imaging when S-wave information is needed. In fact, this legacy-data option is exactly what will be discussed in this section. Specifically, the project area where this 3D seismic research was done spanned the Perch 3D survey area in the Michigan Basin that is described in Section 1 of this report (Figures 1-3 and 1-4). The Perch 3D data that are processed here are thus legacy 3D "P-wave" data acquired previously.

Two approaches for estimating Shmax azimuth are described in this section. The first approach will utilize SV-P reflections embedded in the Perch 3D vertical-geophone data. The second technique is based on a rather sophisticated inversion technique that is applied to the Perch 3D P-P reflection data. This inversion concept is rather new, has excited some geophysical researchers, and certainly needs to be investigated for stress-field applications. Both approaches are based on the anisotropic earth model depicted in Figure 4-1. The type of rock anisotropy described by this model is called horizontal transverse isotropy (HTI).

4.3   Anisotropic Rocks

The term *anisotropy* is used in geophysical literature to refer to physical properties of a rock that vary when those properties are measured in different directions, i.e., in different azimuths. The rock model in Figure 4-1 shows a series of vertical extensional fractures (not shear fractures) and the azimuths of Shmax and Shmin horizontal stresses associated with those extensional fractures. As shown earlier, in Figure 2-1 and its related text, the direction in which extensional fractures are oriented is the same as the azimuth of Shmax. Shmin azimuth is perpendicular to Shmax, and thus, is perpendicular to extensional fractures. Rock physicists define the vertical coordinate plane that parallels the vertical plane of extensional fractures as an *isotropy plane* of an anisotropic medium. A vertical plane oriented perpendicular to aligned extensional fractures is defined as a *symmetry plane* (refer to Figure 4-1).

Seismic waves that propagate through anisotropic rock exhibit the unique characteristic that their propagation velocity varies, depending on the horizontal angle between their displacement vector and the direction in which isotropy planes are oriented. Numerous studies show that velocities of P-waves that travel through anisotropic rock vary in only a minor way regardless of whether their P displacement vectors are oriented parallel to the isotropy plane, or parallel to the symmetry plane (for example, refer to the data displayed as Figure 2-9). Only when fracture density is high do P waves that travel in the direction of the isotropy plane have velocities that are slightly faster than velocities of P waves that propagate in the direction of the symmetry plane. However, even in densely fractured rock, the difference between P velocities in these two orthogonal directions is so small that it is challenging to use P-wave velocities, and azimuth-dependent arrival times of P-P reflections. to identify isotropy and symmetry azimuths.
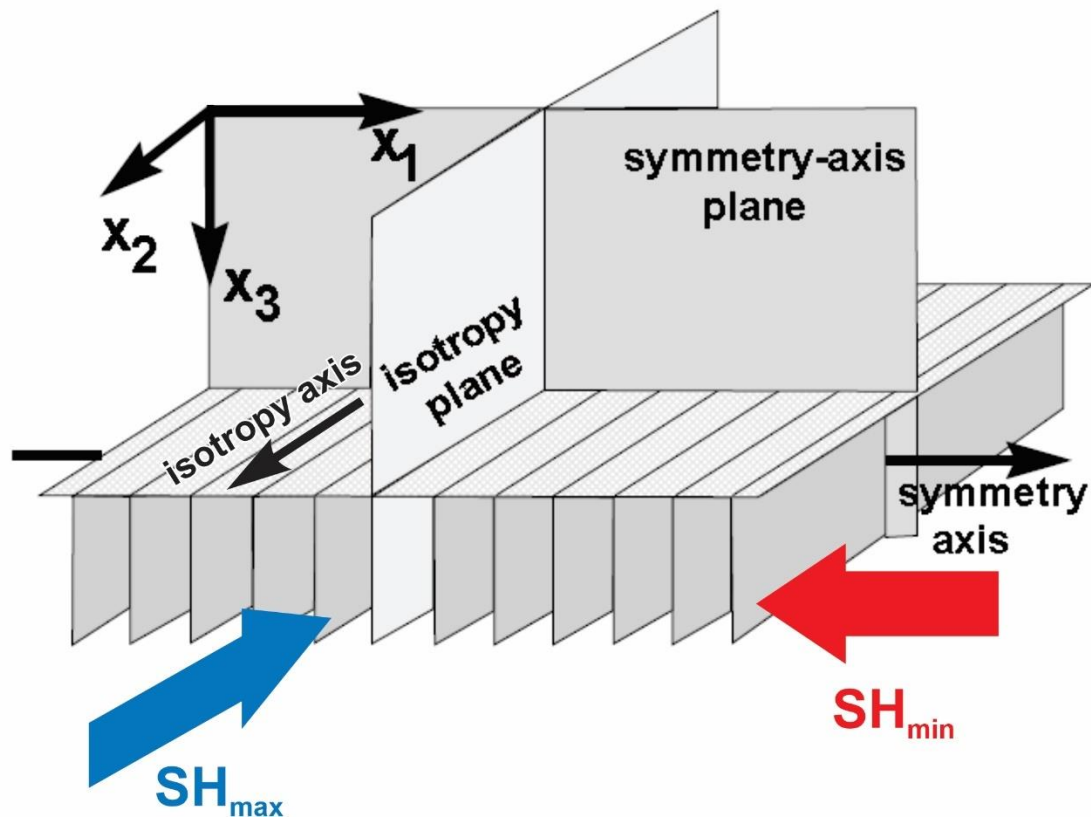
Figure 4-1. This drawing describes an HTI (horizontal transverse isotropy) type of anisotropic rock medium and introduces terminology commonly used to describe seismic wave propagation in such a medium. Principles that will be illustrated are: (1) as an S wave travels through an anisotropic medium, it segregates into two daughter S waves (S1 and S2) that travel with different velocities (refer to Figure 2.5), (2) the fast-S mode (S1) is polarized in the same direction as the SHmax azimuth, and (3) the slow-S mode (S2) is polarized in the same direction as the SHmin azimuth.

In contrast, S-wave velocities are observed to vary significantly if their displacement vectors are oriented in the isotropy plane, which has a faster S velocity, rather than in the symmetry plane, which has a slower S velocity. This S-wave propagation physics is also documented in Figure 2-9. The faster S velocity will be denoted as V_{S1}; the slower S velocity will be indicated as V_{S2}. The difference in V_{S1} and V_{S2} velocities in stressed rocks is usually large enough to create measurable differences in azimuth-dependent travel times of seismic S wave modes through anisotropic rocks. Terms used in geophysical literature to describe this unique S-wave behavior of an S-wave separating into two distinct shear waves in anisotropic rocks are *shear wave splitting*, and in some terminologies, S-wave *birefringence*. These principles about S-wave velocity behavior in stressed rock form the basis of the first analysis method that was used in this section to determine the azimuth of Shmax at the Perch 3D seismic area.

4.4   Are Fractures Required in Order to Have Rock Anisotropy?

The anisotropic rock model in Figure 4-1 was developed by rock physicists and exploration geophysicists to aid in mapping fractures with seismic reflection data. The model is valuable, but it can be misunderstood when considering the question - "Do fractures have to be present in rocks in order to have rock anisotropy and shear-wave splitting?". The answer is "No", but the presence of fractures seems to always dominate any discussion of this popular rock model.

Shear-wave velocity is controlled by the stiffness coefficients that exist in a rock unit. Velocities of both P waves and S-waves increase as rock stiffness increases. Rock anisotropy will thus occur whenever there is any azimuthal change in rock stiffness coefficients for whatever reason. Aligned vertical fractures certainly create an azimuthal variation in rock stiffness. Stiffer rock, and thus faster velocities, occur in the direction of aligned fractures. Weaker stiffness coefficients, and thus slower velocities, occur normal to aligned fractures. The result of azimuth-dependent S-wave propagation through a fractured rock produces the classical shear-wave splitting that is such a valuable tool for identifying and quantifying fracture populations.

A broader question that needs to be considered is "What conditions other than aligned fractures can create rock anisotropy?". Several possibilities could be proposed, but one of the most obvious conditions is simply the presence of Shmax and Shmin horizontal stress fields in a rock unit. Because of the difference in the magnitudes of Shmax and Shmin stresses, shear-wave displacement vectors will find it more difficult to displace rock fabric against a Shmax constraining stress than to move that rock fabric against a smaller-magnitude Shmin constraining stress. S waves sense this stress-induced azimuthal difference in rock stiffness even when there are no fractures in a rock unit. Thus, fast-S modes will be polarized in the direction of Shmax, as shown in Figure 4-1, even when embedded, oriented, fractures are removed from that diagram.

Use of fast-S polarization direction to define Shmax azimuth is a principle that can be used in fractured rock or in non-fractured rock. This understanding is particularly important if seismic S waves are to be used to monitor stress changes in deep CO_2 storage reservoirs because these reservoirs are deliberately located where there supposedly are no fractured rock. This no-fractured-rock precaution is taken to ensure that there is an optimal, leak-proof, reservoir sealing unit that will ensure long-term CO_2 sequestration. The research results presented in this section are thus particularly important for non-invasive monitoring of stress fields in deep CO_2 reservoirs. Methods that can be used to define Shmax azimuth in deep stressed rocks, even when those rocks have no fractures, or only a merger population of fractures have been shown.

4.5   Basic 3D Data Processing Flow

This section will not present all of the steps and parameters that were used in processing the Perch 3D data but rather will focus only on the key data-processing steps that have to be done to extract SV-P reflections from vertical-geophone data. Seismic data processing that is done to extract both P-P and SV-P reflections from 3D vertical-geophone data involves three basic procedures. These three essential steps are:

1. Apply procedures to vertical-geophone data, where SV-P and P-P wavefields are intermingled, that will extract the P-P wavefield and place it in data-processing stream 1, and that also extracts the SV-P wavefield and places it in data-processing stream 2.

2. Estimate and apply P-static corrections at source stations and at receiver stations that adjust P-P reflections in P-P data-stream 1 to a common reference datum, and then estimate and apply S statics corrections at source stations and P statics corrections at receiver stations in SV-P data-stream 2 that adjust SV-P reflections to a common reference datum.

3. Determine appropriate velocity fields across the survey area. This step must be done twice, first for P-P data, and then for SV-P data.

4.6 Static Corrections

The mean surface elevation across the Perch 3D area was used as the reference depth datum in this study. During data acquisition, some sources and receivers were above this arbitrary depth datum, and some sources and receivers were below the depth datum. Static corrections are travel-time adjustments that convert field traces to traces that would be present if all sources and receivers were positioned on this selected reference datum plane. The velocity field must also be referenced to this same depth datum. Proper static changes made to seismic reflection data usually make astounding improvements in seismic reflection quality. If static corrections are not made, then seismic reflections are controlled by variations in surface elevation, and by lateral changes in near-surface velocities, and do not relate to deep geology.

The Perch 3D survey presented unique problems that complicated determining static corrections and velocity wavefields needed to create proper trace gathers and to conduct accurate migration velocity tests. These problems occurred because the earth surface across the Perch area is covered with a thick (approximately 800-ft to 1000-ft) layer of glacial drift material, sometimes also referred to as glacial till material. The thickness of this glacial drift layer changed erratically over short distances, and the internal fabric in near-surface layers also varied unpredictably over short vertical and horizontal distances, just as one would expect that material that is pushed by ice glaciers would behave. Basically, the glacial till layer across the Perch 3D survey can be likened to the material that a giant bulldozer, with a blade width of several tens of kilometers, would deposit if it started pushing material southward from interior Canada and spread it across the Michigan Basin. The resulting surface layer is a complex mix of boulders, crushed rock, and unconsolidated and consolidated sediments that varies vertically and horizontally over short distances. These surface conditions were present across the Perch 3D seismic area. The Michigan Basin glacial till layer is considered by most seismic data processors to be the most challenging condition that can be found for determining correct static adjustments to apply at source and receiver stations.

P-P data-processing procedures overcame these drift-layer complications rather well because shallow, but sparse, P-wave sonic log data were available that provided some guidance about near-surface, P-wave, velocity behavior that helped determine P-wave static corrections at both source stations and receiver stations. However, it was difficult to determine SV-P statics because there were no measurements of S-wave velocities across the shallow glacial till material to provide guidance as to the near-surface S velocities that need to be estimated to calculate S statics at each source station.

S velocities in the shallow glacial-till material varied dramatically over short distances. The Vp/Vs ratio in sedimentary and evaporite rocks is confined to a range of about 1.6 to 2.2. In near-surface weathered layers, and particularly in the surface glacial debris across the Perch 3D area, the Vp/Vs ratio can vary over a wide range extending from values as high as 10 or 12

to values as low as 3. Fortunately, Vp velocities in high-porosity, water-saturated, near-surface, sediments remain relatively stable because P-waves travel through material by two travel paths: (1) by grain-to-grain contact, and (2) by transmission through water-filled pores. Because P-wave velocity in water is constant, the wet, high-porosity, surface layers across the Perch area usually do not allow huge variations in P velocities to occur over short distances. The resulting, reasonably stable, near-surface, P velocity allowed acceptable-quality P-wave statics to be determined.

In contrast, S waves travel only through grain-to-grain contacts; S waves cannot travel through pore water. Thus, S velocities have no constant, stabilizing, water-velocity, dependency in surface sediments like P waves do. As a result, S-wave velocity varies rapidly and wildly in the shallow, uncompacted glacial-till layer. Essentially all of the velocity variations in near-surface material that causes Vp/Vs velocity ratios to vary from a low value of about three to values as high as 10 or 12 are caused by large-magnitude, short-distance, changes in S velocity, not by changes in P velocity.

Good practice dictated that the first data-processing tasks for the Perch 3D data was to determine reliable P-wave static corrections and accurate P-P stacking velocities, before initiating any SV-P data processing. High-quality stacks of common mid-point (CMP) P-P data then provided an SV-P data processor trace-gather targets to match by applying iterative S-wave static-correction procedures to SV-P trace gathers. More importantly, CMP stacks of P-P data provide information that helped data processors determine SV-P stacking velocities. The SV-P velocity that has to be determined is the converted-wave velocity that converts dominant SV-P reflections to the same depths as their companion P-P reflections.

A way to summarize the SV-P data-processing challenge is that an important deliverable of this study is to create accurate estimates of the azimuths in which S velocity is "fast" and estimates of the azimuths where it is "slow". These decisions are made by measuring the arrival times of an S-mode reflection at a fixed (X, Y) coordinate in image space as a function of azimuth approach directions to that (X, Y) imaging point. However, the arrival time of a S-mode reflection observed in azimuth #1 can be affected by an incorrect S-static applied to source-to-receiver travel paths oriented in azimuth #1, and that static effect can be as large as, and perhaps even larger than, the effect caused by an actual change in S-mode velocity that occurs in azimuth #1.

4.7   Extracting and Separating P-P and SV-P Wavefields

The entanglement of P-P and SV-P reflection events in a common P-P trace gather of vertical-geophone data acquired at a Texas prospect is shown in Figure 4-2. The energy source was a buried explosive similar to the buried-explosive sources used to generate the Perch 3D vertical-geophone data. These Texas data are shown as a common-depth-point (CDP) trace gather after one initial pass of reflection migration has been applied. The flattened reflections that extend across the trace gather are P-P reflections, which are positioned at the same image time for all source-to-receiver offsets after this data migration step. Each P-P reflection appears at the same image time across this vertical-geophone trace gather because the migration process used an accurate P-P migration velocity. All P-P traces in this display are located at the same CDP spatial coordinates in the subsurface; the traces simply have not yet been summed to create a single image trace at those CDP image coordinates.

The curved events that appear in this same vertical-geophone trace gather are SV-P reflections. These SV-P reflections have not been corrected to flat events by the P-P velocity used in the migration process because SV-P velocities are slower than P-P velocities. Traditionally, P-P data processors have assumed that these slower-velocity events were inter-bed P-P multiples created at shallow depths. Such interbed multiples would also have a slower velocity than P-P primary reflections. However, researchers at The University of Texas at Austin demonstrated that these ubiquitous events are SV-P converted-mode reflections, and almost never are interbed multiples. This finding is a game-changing observation that allows S-wave reflection seismology to be practiced with vertical-geophone data created by P sources (Graul, 2017; Gupta and Hardage, 2017; Hardage et al., 2014; Hardage and Wagner, 2014a, 2014b; Hardage, 2017a, 2017b, 2017c, 2017d; Karr, 2017; Li and Hardage, 2015; Li et al., 2017).
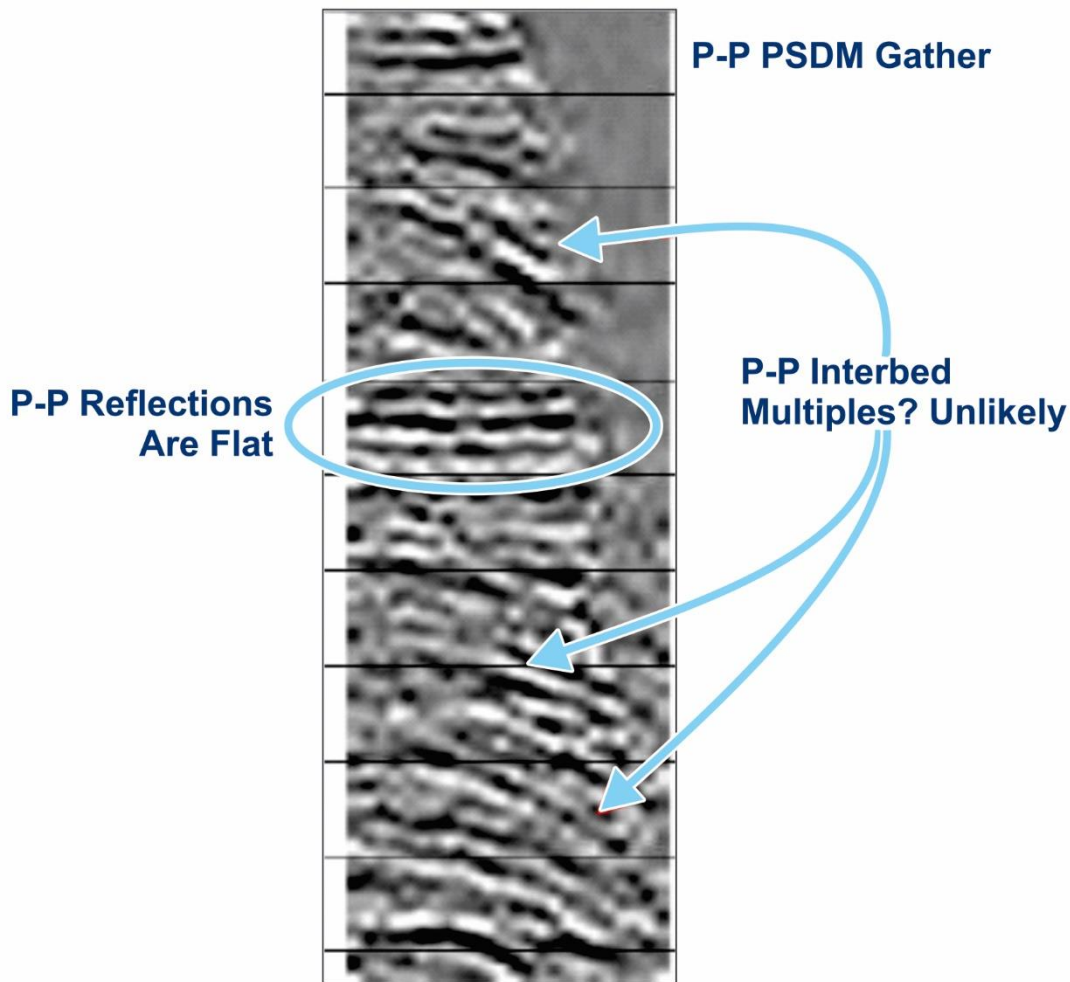
Figure 4-2. P-P, common-depth-point, vertical-geophone data after one application of P-P migration velocities. P-P reflections are flat, as they should be. The down-curving reflections are slower-velocity SV-P reflections that are embedded in the same vertical-geophone data. This gather is an excellent example of the manner in which P-P and SV-P reflections are entangled in vertical-geophone data.

The separation of SV-P data from P-P data in vertical-geophone data can be accomplished by iterative subtraction operations that create outputs which are essentially pure P-P or pure SV-P trace gathers. Data processors have a variety of procedures that could be applied to the data in

Figure 4-2 that would enhance flat, constant-time events and reject curved events. Any of these procedures can be used for wavefields separation.

As an example, model data are used in Figure 4-3 to illustrate the suppression of SV-P reflections that allows coherent P-P reflections to be properly emphasized (panels A, B, C). Panels D-E-F illustrate the same methodology, but now SV-P reflections are flattened (panel D) because the data are migrated with the slower, correct, converted-wave velocity. P-P reflections now curve upward because they have faster velocities than SV-P velocities (panel E). An iterative subtraction process then suppresses the P-P reflections and enhances the SV-P reflections, which are now flattened by migration that uses the correct converted-wave velocity. The end result is wavefield separation, with panel C showing the P-P wavefield, and panel F showing the SV-P wavefield. Both wavefields co-existed in the raw vertical-geophone data (panels A and D).
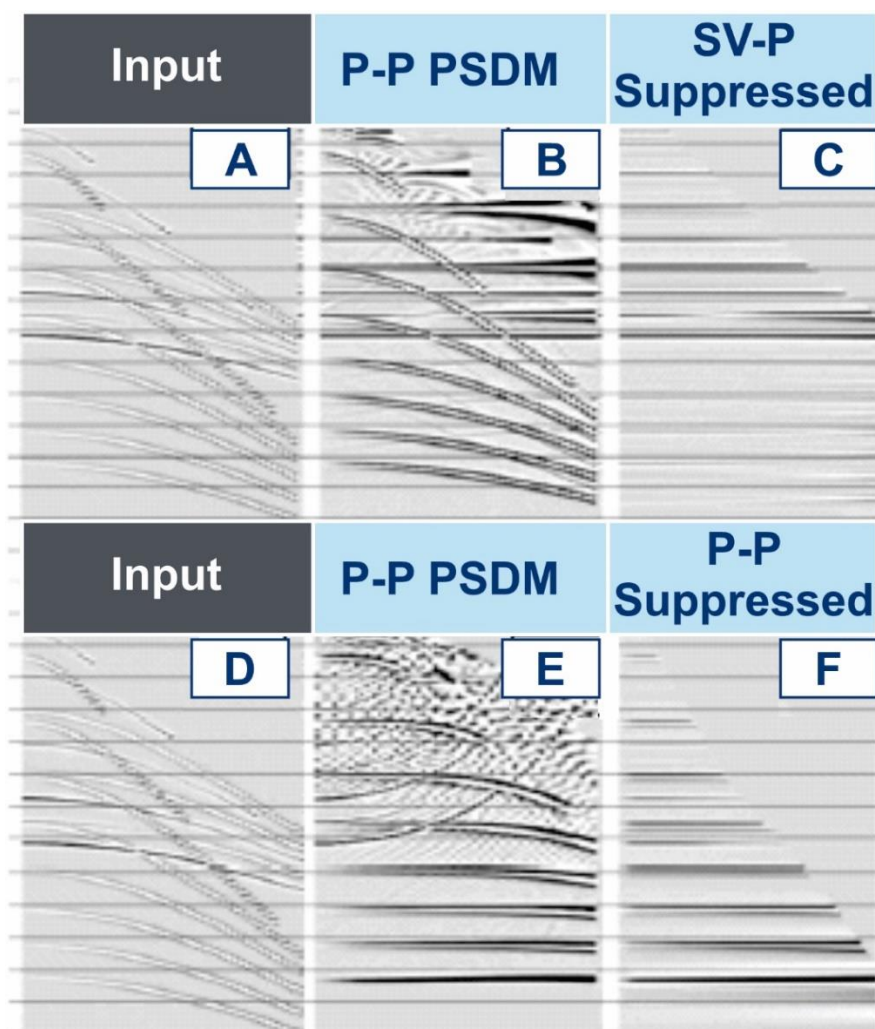
Figure 4-3. A modeled trace-gather of vertical-geophone data (panels A and D). In panel B, P-P velocities have been used to flattened P-P reflections. SV-P reflections are still curved downward. Panel C is the result of applying filters that suppress curved events, enhance flat events, and leaves a high-quality P-P reflection gather. Panel E shows the effects of applying SV-P velocity corrections that flatten SV-P reflections and over-correct P-P reflections. Panel F shows the SV-P reflection field after curved P-P reflections are suppressed. Taken from Graul, 2017.

A real-data example is illustrated in Figure 4-4. Panel A is an original pre-stack depth migration (PSDM) depth migration, constructed with P-P velocities, at a stacking bin in 3D P-P image space. P-P reflections are flat, as they should be. However, the buried explosive sources used in this Texas-basin 3D survey created robust down-going SV illumination wavefields, and obvious, down-curving, SV-P reflections are intermingled with the flattened P-P reflections in this migration of vertical-geophone data. Panel B shows the same data after an iterative subtraction process is implemented to remove the curved SV-P reflections and expose the pure P-P reflections. These data are a beautiful example of the mixing of P-P and SV-P reflections in data generated by a P source and recorded with only vertical geophones. This intermingling of P-P and SV-P reflections occurs repeatedly in vertical-geophone data. Research teams have now observed this dual-wavefield behavior in vertical-geophone data acquired in 10 different basins.
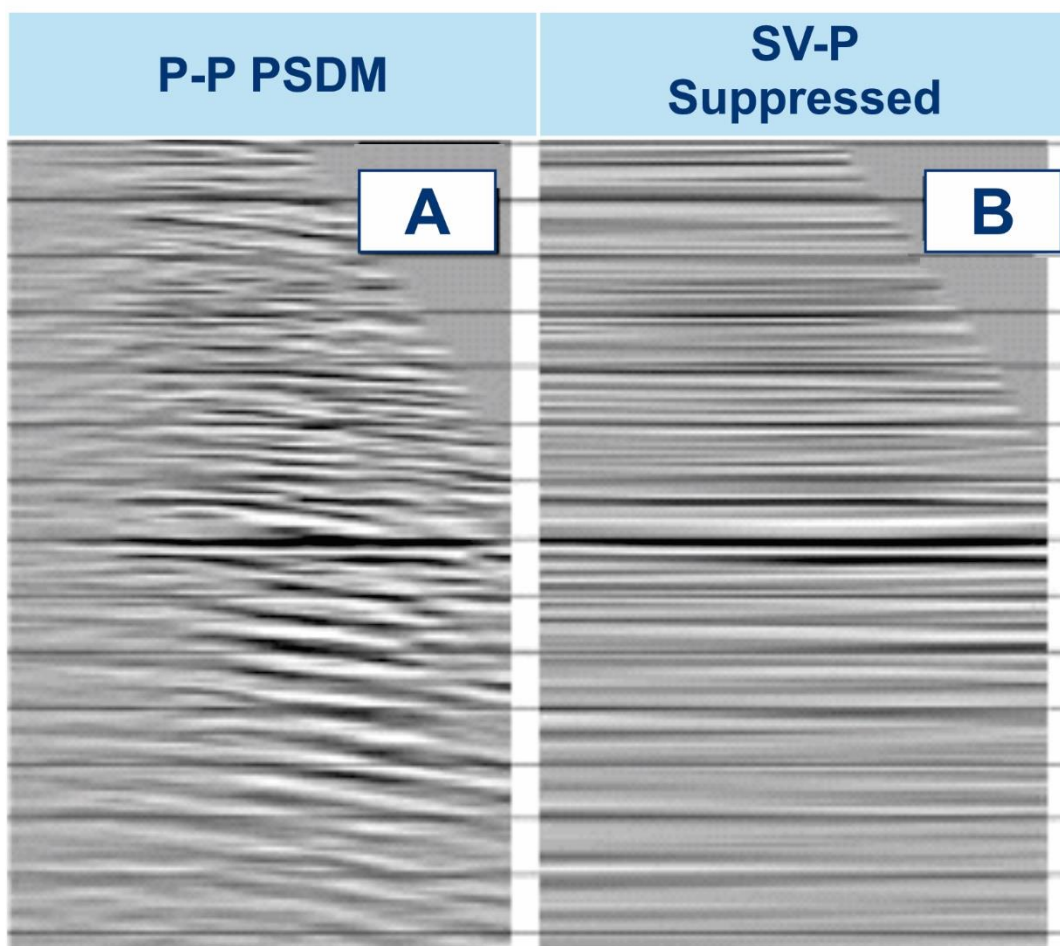
Figure 4-4. Panel A shows a real P-P trace gather at a stacking bin that has been subjected to a PSTM migration in which P-P velocities were used. P-P reflections are flat as they should be. However, robust SV-P reflections were also produced by the P source (buried explosives), and these SV-P reflections appear as down-curving reflections. Panel B shows the P-P trace gather after the curved SV-P reflections are removed by a wavefield subtraction procedure. Taken from Graul, 2017.

4.8   Rotating Azimuth Sectors

The concept of determining Shmax azimuth with 3D converted-mode data is summarized in Section 2.11. The basis of the concept is to analyze converted-mode reflections created by source-receiver pairs that are confined to be inside in a narrow, rotating, corridor of data-acquisition space that spans only 20 or 30 degrees of azimuth. The origin of this rotating corridor should be positioned at a number of stacking bins inside 3D data-acquisition space. In Section 2, P-SV converted-mode data, retrieved from horizontal geophones in a 3D deployment of 3C geophones, were used to illustrate the rotating-corridor concept (Figure 2-9). This long-standing practice of using azimuth-dependent P-SV trace gathers had to be used in Section 2 because, until this present study, there were no published examples of using 3D SV-P data in any manner to define Shmax. That same rotating, narrow-corridor, concept described in Section 2.11 will now be used to determine Shmax by using SV-P data acquired in the Perch 3D deployment of vertical (not horizontal) geophones. The results summarized here will apparently be the first public exposure of using SV-P data to detect Shmax azimuth in anisotropic rocks.

The fundamental requirement for implementing this rotating-corridor type of Shmax data analysis is to segregate 3D data space into narrow, rotating, azimuth corridors as illustrated in Figure 2-10, and then to use a trace-gather, data-processing, strategy that will illustrate the arrival times of key, targeted, SV-P reflections inside each of these rotating data corridors. If earliest-arriving SV-P reflection times occur in a consistent azimuth direction at a significant number of X-Y coordinates across data-acquisition space, it is reasonable to conclude that this earliest-arrival azimuth direction is probably the azimuth of Shmax.

4.9   Azimuth Sector Migration

A basic principle in seismic data processing is that the down-going wave from a seismic source is scattered upward, by reflection, from each point in the subsurface it encounters. These scattered data then arrive at surface receivers that are deployed around each source station. Migration is the process of gathering these surface-recorded, back-scattered, reflection data and then summing the data at their common scattering points across a deep rock interface. This migration procedure is performed for all data samples recorded in a 3D seismic survey. Migration of any 3D seismic data that span several square kilometers thus involves trillions of numerical operations and may have to be repeated several times in order to update and improve the accuracy of the velocity field that guides data movements to their correct scattering coordinates.

The numerical process which accomplishes this imaging task can be either pre-stack time migration (PSTM) or pre-stack depth migration (PSDM). One of these migration options has to be done to create a P-P image from vertical-geophone data, and a separate migration procedure then has to be done to create an SV-P image from the same vertical-geophone data. The difference between these two procedures is that a P-P velocity field is used to migrate P-P data, but a second, separate SV-P velocity field is used to migrate SV-P data.

To determine Shmax azimuth at the Perch 3D survey site, each 3D dataset (both P-P and SV-P) was migrated an additional six times because both P-P and SV-P data were analyzed in 30-degree azimuth corridors in order to search for Shmax and Shmin azimuths. Regardless of what angle width is used for a rotating data corridor, it is essential that narrow-corridor analyses span at least 180-degrees of data-acquisition azimuth. In each narrow-corridor migration, the only

data that are migrated are those data that involve source-receiver pairs that are positioned inside each fixed azimuth corridor. The angle width of the narrow-azimuth corridors used for the Perch 3D data was 30 degrees, thus six azimuth corridors had to be used to span 180 degrees of azimuth in order to utilize all of the Perch 3D data.

In analyzing the Perch data, the origin point of each rotating azimuth corridor was centered on a targeted stacking bin. The center lines of the six corridors radiating away from that stacking bin were then oriented, respectively, at azimuth angles of 0, 30, 60, 90, 120 or 150 degrees measured clockwise from north.

Each azimuth corridor oriented in these azimuths of 0, 30, 60, 90, 120 or 150 degrees at each stacking bin represents positive-offset sources and positive-offset receivers for that stacking bin (Figure 2-10). Their respective counterpoint corridors, oriented at azimuths of 180, 210, 240, 270, 300, and 330 degrees, respectively, from that same stacking bin, represent negative-offset sources and negative-offset receivers (Figure 2-10).

4.10   Examples of P-P and SV-P Migrated Data from the Perch 3D Survey

A PSTM of P-P data along Inline 1320 is shown as panel (a) in Figure 4-5. This migration involved shot-hole sources and vertical geophones distributed in all azimuth directions away from each P-P image coordinate along this inline. Three important stratigraphic units are marked on the profile; these being the Bass Islands (BI), Niagaran (N), and St. Peter (SP). P-P image quality is rather good in this example. The Bass Island unit is positioned at approximately 700 ms in P-P image space. The Niagaran and St. Peter are positioned at deeper P-P image times of approximately 1,000 and 1,200 ms, respectively. Note that these image times are correct for both P-P data (Figures 4.5 and 4.6) and SV-P data (Figures 4.7 and 4.8) because a time warp of the SV-P data was done that converted SV-P image time to approximately equivalent P-P image time.

Figure 4-5. (a) Inline 1320 from the P-P Perch 3D data after the data have been imaged using a full-azimuth pre-stack time migration (PSTM) procedure based on P-P velocities. (b) Inline 1320 from the P-P Perch 3D data after the data have been imaged using a PSTM procedure limited to sources and receivers positioned inside a 30-degree corridor with its center line oriented from 0 to 180 degrees on the azimuth compass. (c) Inline 1320 from the P-P Perch 3D data after the data have been imaged using a PSTM procedure limited to sources and receivers positioned inside a 30-degree corridor with its center line oriented from 60 to 240 degrees on the azimuth compass.

The companion profiles in panels (b) and (c) of Figure 4-5 are PSTM stacks of P-P data along these same image coordinates except these data are generated by only those positive-offset and negative-offset sources that are within a narrow azimuth corridor spanning 30 degrees, and that are then recorded by positive-offset and negative-offset receivers also positioned within that same 30 degree-wide azimuth corridor. The image qualities in panels (b) and (c) are degraded, compared to the image in panel (a), because stacking folds in (b) and (c) are reduced by a factor of approximately six compared to the stacking fold in panel (a). This fold reduction occurs because the positive-offset and negative-offset portions of an azimuth corridor of 30 degrees spans 1/6 of the full 360 degrees of azimuth that surround each image bin.
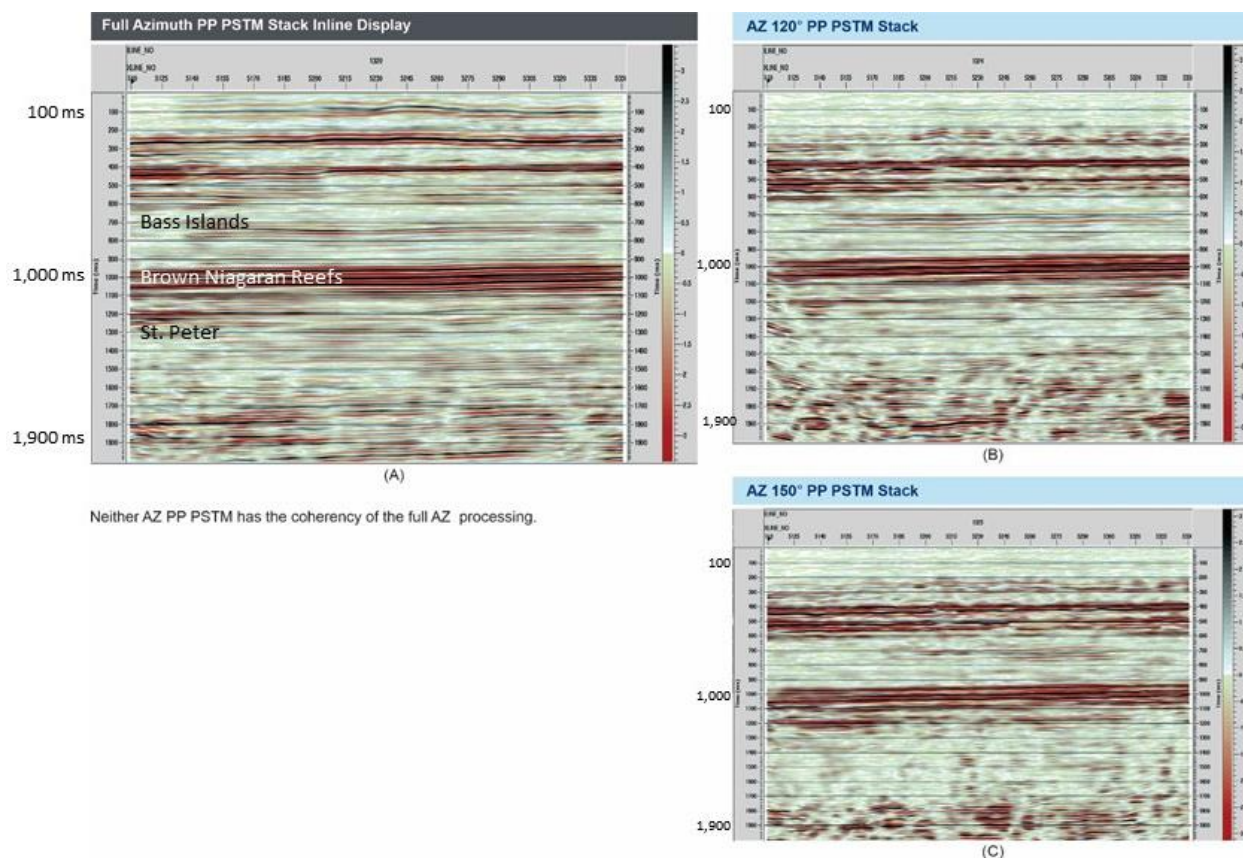
Figure 4-6. (a) Inline 1320 from the P-P Perch 3D data after the data have been imaged using a full-azimuth pre-stack time migration (PSTM) procedure based on P-P velocities. (b) Inline 1320 from the P-P Perch 3D data after the data have been imaged using a PSTM procedure limited to sources and receivers positioned inside a 30-degree corridor with its center line oriented from 120 to 300 degrees on the azimuth compass. (c) Inline 1320 from the P-P Perch 3D data after the data have been imaged using a PSTM procedure limited to sources and receivers positioned inside a 30-degree corridor with its center line oriented from 150 to 330 degrees on the azimuth compass.

The objective of using sources and receivers that are restricted to a narrow azimuth corridor is to ensure that P-P reflection arrival times are controlled by velocities along ray paths that are forced to travel in a specific azimuth direction through stressed rocks. By examining P-P data in narrow-corridor data, azimuth variations in P-wave velocity and in P-P reflectivity can be recognized and analyzed. Panel (b) of Figure 4-5 shows P-P velocity behavior in a narrow 30 degree corridor whose center line is oriented in a north-south direction. Panel (c) then shows P-P velocity behavior in a narrow 30 degree corridor whose center line is oriented from 60 to 240 degrees on the azimuth compass.

The data in panel (a) of Figure 4-6 are the same full-azimuth data along Inline 1320 that are displayed in Figure 4-5a. Data panels (b) and (c) in Figure 4-6 show two more narrow corridor stacks. The center line of the 30 degree-azimuth corridor in Figure 4-6b is oriented from 120 to 210 degrees on the azimuth compass. The center line of the data corridor used to produce the image in Figure 4-6c is oriented from 150 to 330 degrees on the azimuth compass.
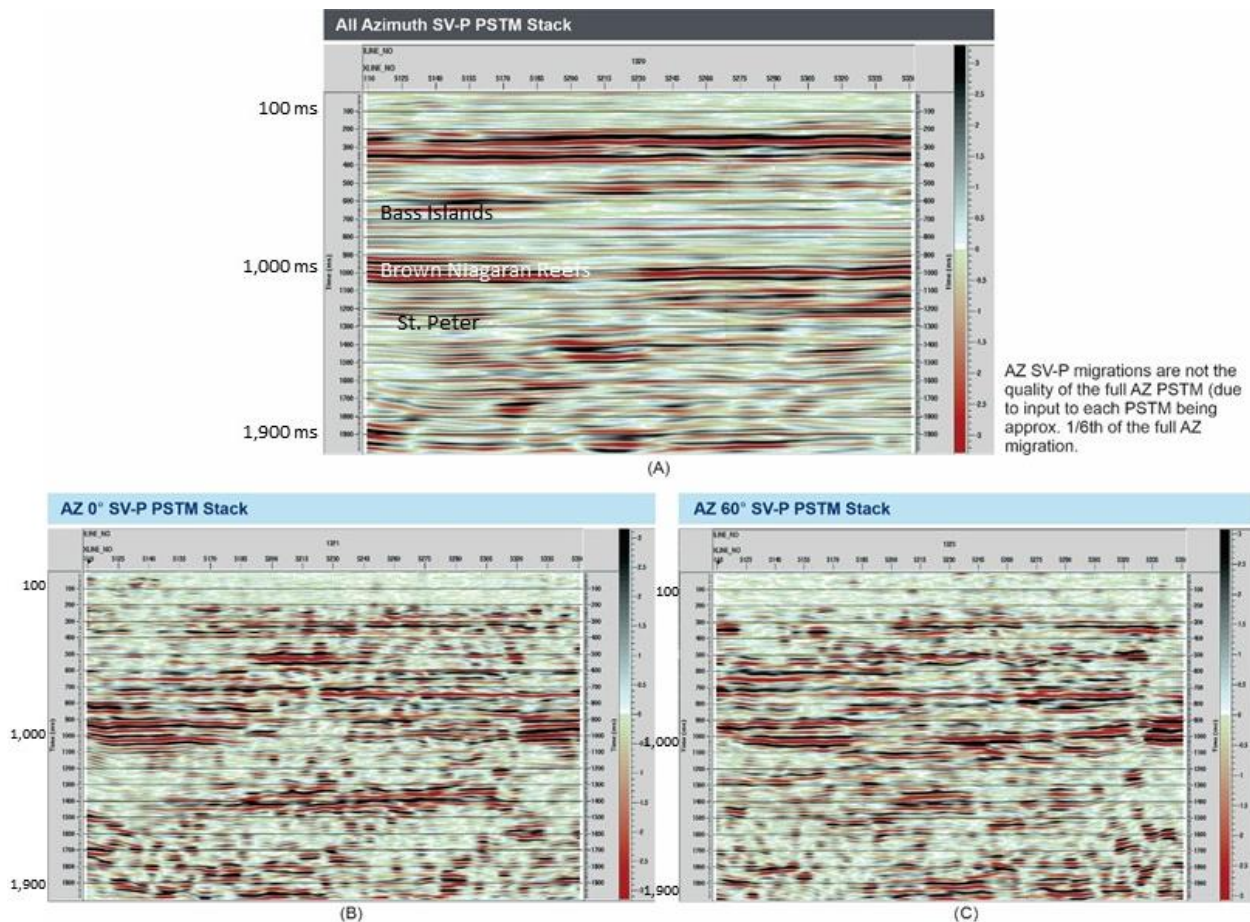
Figure 4-7. (a) Inline 1320 from the SV-P Perch 3D data after the data have been imaged using a full-azimuth pre-stack time migration (PSTM) procedure based on SV-P velocities. (b) Inline 1320 from the SV-P Perch 3D data after the data have been imaged using a PSTM procedure limited to sources and receivers positioned inside a 30-degree corridor with its center line oriented from 0 to 180 degrees on the azimuth compass. (c) Inline 1320 from the SV-P Perch 3D data after the data have been imaged using a PSTM procedure limited to sources and receivers positioned inside a 30-degree corridor with its center line oriented from 60 to 240 degrees on the azimuth compass.

Figures 4-7 and 4-8 show SV-P examples of full-azimuth and narrow-corridor images that mimic the P-P data in Figures 4-5 and 4-6. The full-azimuth SV-P image displayed in panel (a) in each figure is reasonable-quality data. However, images made from the SV-P narrow-corridor data are obviously lower quality than are their companion P-P narrow-corridor images in Figures 4-5 and 4-6, which illustrates the damaging effects of not being able to determine optimal S-wave static corrections at source stations. It will be necessary to reference back to the random increases and decreases in signal-to-noise behavior inside these narrow-corridor SV-P images when later sections are discussed.
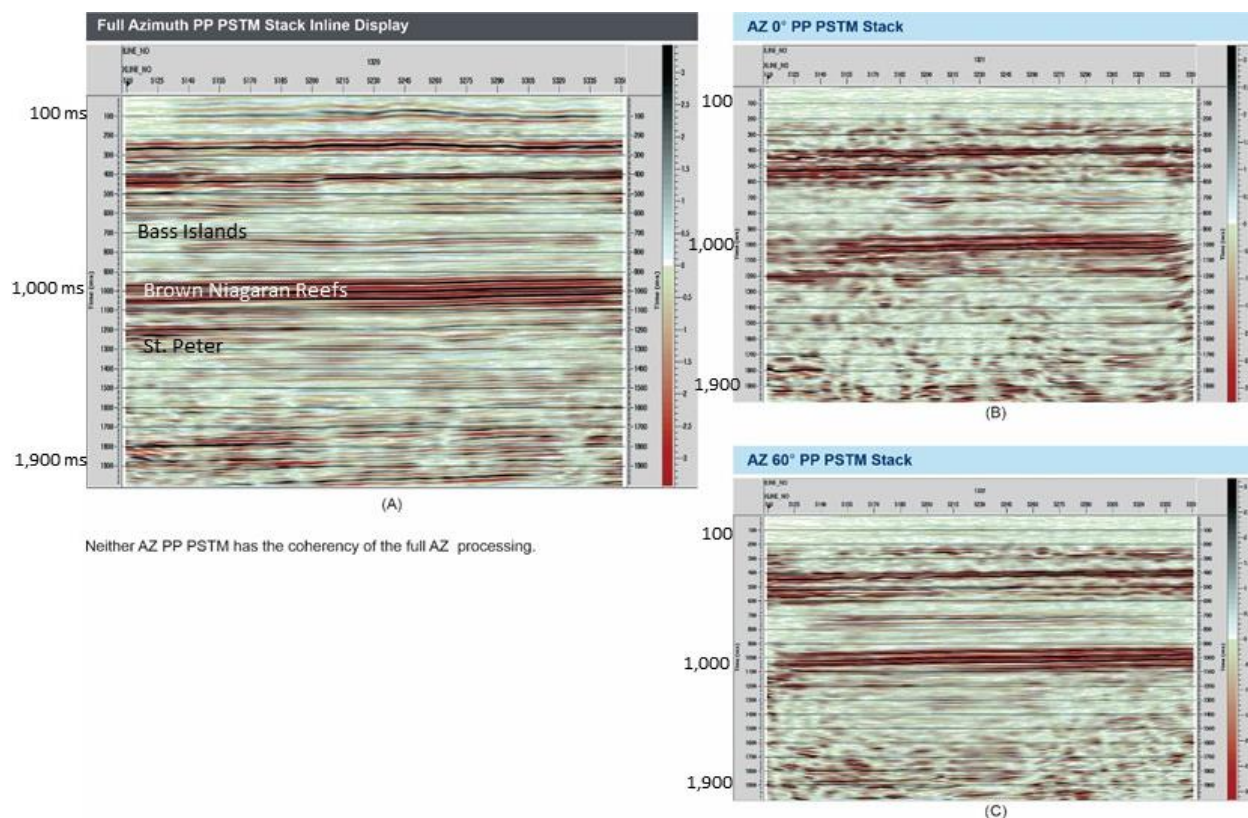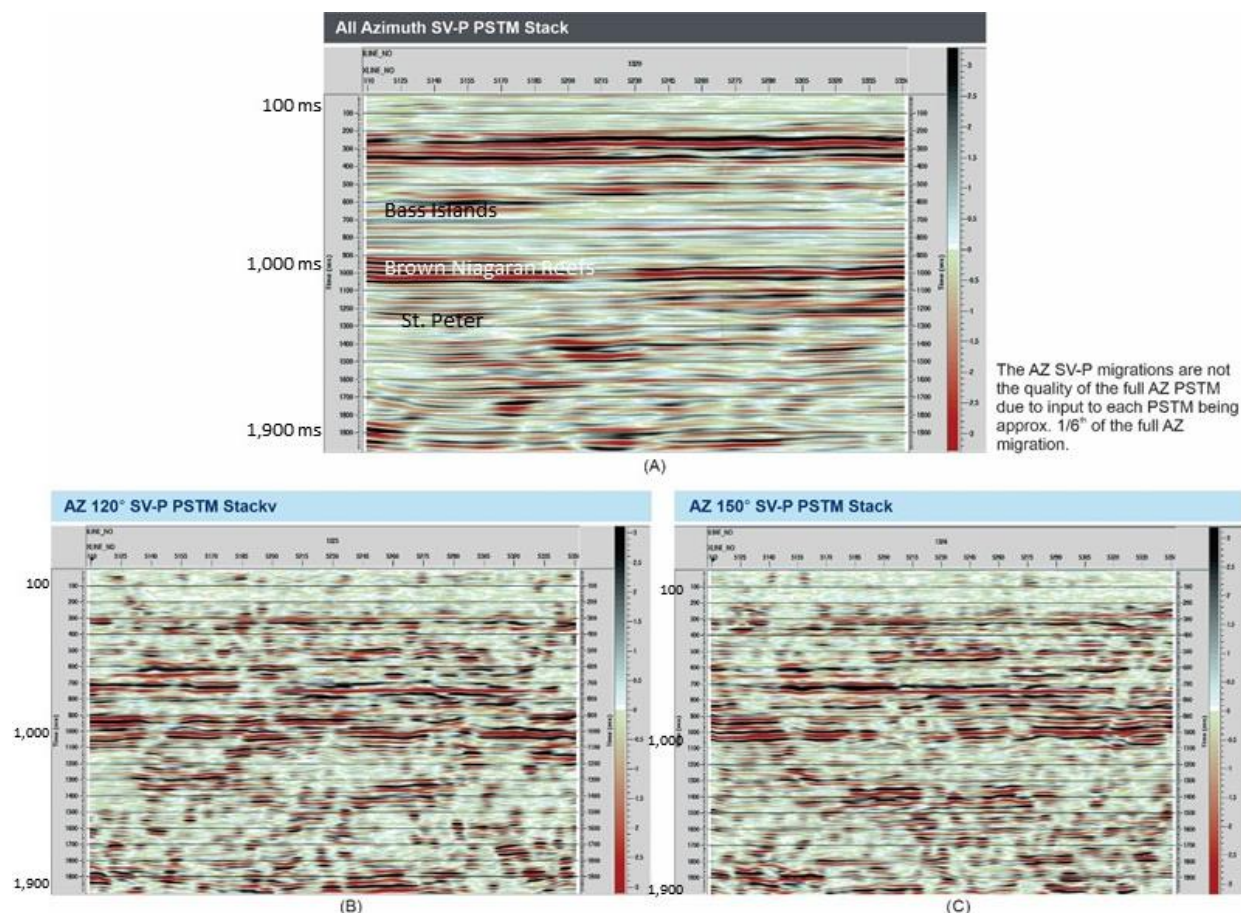
Figure 4-8. (a) Inline 1320 from the SV-P Perch 3D data after the data have been imaged using a full-azimuth pre-stack time migration (PSTM) procedure based on SV-P velocities. (b) Inline 1320 from the SV-P Perch 3D data after the data have been imaged using a PSTM procedure limited to sources and receivers positioned inside a 30-degree corridor with its center line oriented from 120 to 300 degrees on the azimuth compass. (c) Inline 1320 from the SV-P Perch 3D data after the data have been imaged using a PSTM procedure limited to sources and receivers positioned inside a 30-degree corridor with its center line oriented from 150 to 330 degrees on the azimuth compass.

4.11 Past versus Present Methods of Detecting Azimuthal Changes in S-Wave Velocities

Distinction 1: P-SV Data versus SV-P Data

The example of azimuthal variations in P-SV reflections illustrated in Figure 2-9 represents a first-generation (circa 1998) strategy for defining fast-S and slow-S polarization directions with converted-mode seismic data. In the late 1990s, when investigators wished to study fast-S and slow-S behavior, they used a P-wave seismic source and deployed both vertical and horizontal geophones. They then used the up-going SV portion of the P-SV mode, which was recorded by horizontal geophones, to investigate slow-S and fast-S behavior. However, only vertical geophones were deployed across the Perch 3D data area, so fast-S and slow-S behaviors in this project had to be analyzed by utilizing the down-going SV portion of the SV-P mode. This Perch 3D study is the first known effort to use SV-P data to analyze anisotropic rocks.

Distinction 2: NMO and Super Bins versus PSTM and Standard Bins

Pre-stack time migration of seismic reflection data was not an established data-processing procedure in the 1990s. Fast-S and slow-S analyses were performed in a rudimentary way. First, a super-bin was constructed in the middle of the X-Y area that was imaged. This super bin was a square area spanning a 2-by-2 group, or a 3-by-3 group, or even a 5-by-5 group, of standard stacking bins. A super-bin trace-gather summed many more traces than did a standard-bin trace gather, and super-bin reflections thus had higher signal-to-noise ratios than lower-fold reflections produced in single-bin gathers. The only procedure applied to a super gather was that normal moveout (NMO) corrections, which had been practiced for decades, were applied to flatten reflection events. A simple visual examination of azimuth-dependent, super-bin reflection arrival times was usually sufficient to determine fast-S/slow-S azimuths, if anisotropy was strong. Differentiating between fast-S and slow-S azimuths was difficult when rocks had weak anisotropy. Whatever fast-S/slow-S behavior was determined visually at this one, centrally located, super bin was then assumed to apply across the total 3D survey area.

A much more rigorous methodology was utilized in analyzing the SV-P reflections embedded in the Perch 3D vertical-geophone data. Specifically, PSTM procedures were performed sequentially in six narrow-azimuth corridors centered on each standard-size, Perch 3D, stacking bin. It should be emphasized that stacking bins across the Perch survey had dimensions of only 82.5 ft x 82.5 ft, which is not a large data collection area. Each data corridor at each stacking bin had an azimuth width of 30 degrees. PSTM procedures were based on SV-P velocities in each corridor and were applied to data generated by only those source-receiver pairs that were positioned inside that narrow corridor. The central axes of adjacent corridors were rotated clockwise by 30 azimuth degrees relative to each other so that, at each stacking bin, the positive-offset directions of the six corridors created for that stacking bin spanned 180 degrees of azimuth coverage of the Perch 3D data space. The companion, negative-offset, portions of these six rotating corridors spanned the other 180-degree portion of the Perch data space.

Figure 2-10 illustrates positive-offset and negative-offset portions of a narrow-azimuth data corridor. By constraining source-receiver pairs used in PSTM calculations to be inside this type of narrow-azimuth corridor, data processors know that SV-P source-to-receiver ray paths are confined to the azimuth direction in which an azimuth corridor is oriented. SV-P reflection times determined by PSTM can then be influenced by rock velocities that exist in only that particular azimuth direction.

Distinction 3: Minor Data Computations versus Massive Data Computations

Early-day methods of searching for fast-S and slow-S azimuths required only the creation of narrow-corridor trace gathers in one super bin, followed by the application of NMO corrections to those gathers, all of which are relatively minor data manipulations by today's standards. In contrast, the use of PSTM at every standard stacking bin is a massive data-processing effort.

The number of stacking bins across the Perch 3D survey area was of the order of 100,000. Several hundreds of data traces were included in each PSTM procedure at each of these stacking bins. Six azimuth corridors were analyzed at each bin. The number of migrated data samples in each SV-P data trace was 1000 or more. These numbers combine to illustrate that the number of data sample movements performed in the SV-P PSTM procedures applied to the Perch 3D data reached into the trillions.

4.12 Procedure for Determining Azimuth-Dependent SV-P Velocities

When PSTM movements of SV-P reflection-data samples are completed in 3D image space, six migrated SV-P traces exist at each stacking bin; one trace being contributed by each of the six SV-P azimuth corridors that radiate away from each SV-P imaging bin. The task is then to decide which of the six traces in each stacking bin has the earliest arrival time. The azimuth corridor that contributes the earliest arriving version of a targeted-reflection event will be oriented in the direction in which the fast-S mode is polarized. This azimuth will also be the Shmax azimuth at that stacking X-Y coordinates.

Figure 4-9 shows a set of model calculated traces that will be used to illustrate the numerical procedure that was used to determine fast-S direction (Shmax azimuth) across the Perch 3D survey area.

Figure 4-10a then uses these model traces to illustrate the numerical procedure that was used to determine Shmax azimuth across the Perch 3D area. Although the earliest-arriving and latest-arriving wavelets can be recognized by visual inspection, decisions based on visual inspection are not a practical approach to evaluating azimuth influence on wavelet arrival times across a 3D data space containing 100,000 or more of such image bins. A quick, efficient, and accurate numerical procedure must be developed. Additional challenges faced when decisions are made by visual inspection are that many data traces will be contaminated by noise, refection wavelets will not have consistent shapes, correct wavelet arrival times will be difficult to determine and to adjust, and paper bookkeeping work will be massive and burdensome.

The method created by Texseis, the company that did the SV-P data processing for this project, is a correlation technique in which a reference trace is produced first by shifting the azimuth-dependent arrival times of the six reflection wavelets in a stacking bin to a constant arrival time (Figure 4-10b). These six time-aligned wavelets are then summed to create an improved-quality reference wavelet for that specific image bin. Note how this time shifting and summing of traces allow the reflection wavelet in each individual corridor trace to increase the signal-to-noise character of the summed wavelet, and simultaneously, causes the random noise portions of the narrow-corridor traces above and below the reflection wavelet to cancel each other in the summed trace.
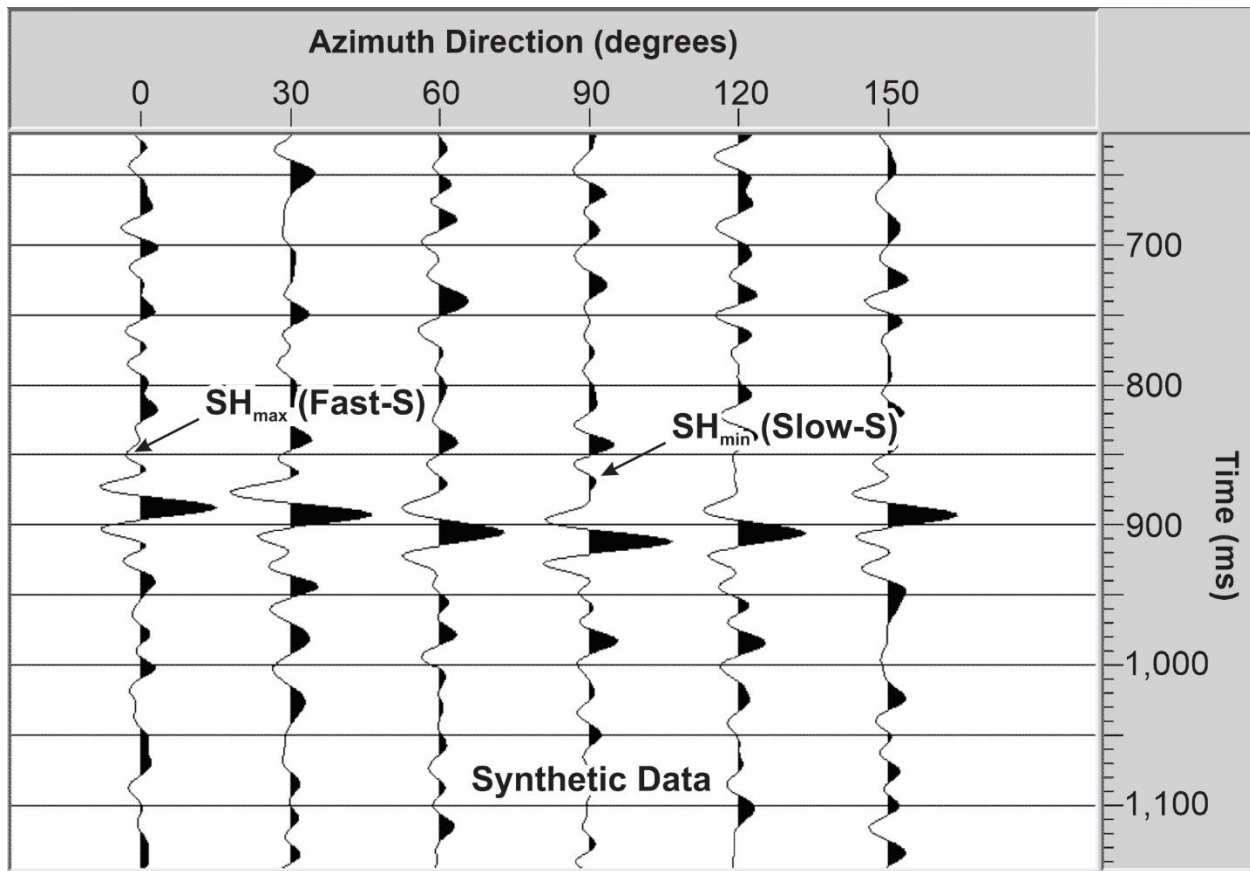
Figure 4-9. Synthetic SV-P traces calculated for an anisotropic medium like that illustrated in Figure 4-1. Each trace is an image trace, positioned at the center of an image bin, that is created by migrating all SV-P reflection traces produced by source-receiver pairs that are constrained to azimuth corridors that are only 30 degrees wide. Fast-S direction in this model was oriented at an azimuth of 0 degrees, and slow-S direction was oriented at an azimuth of 90 degrees.
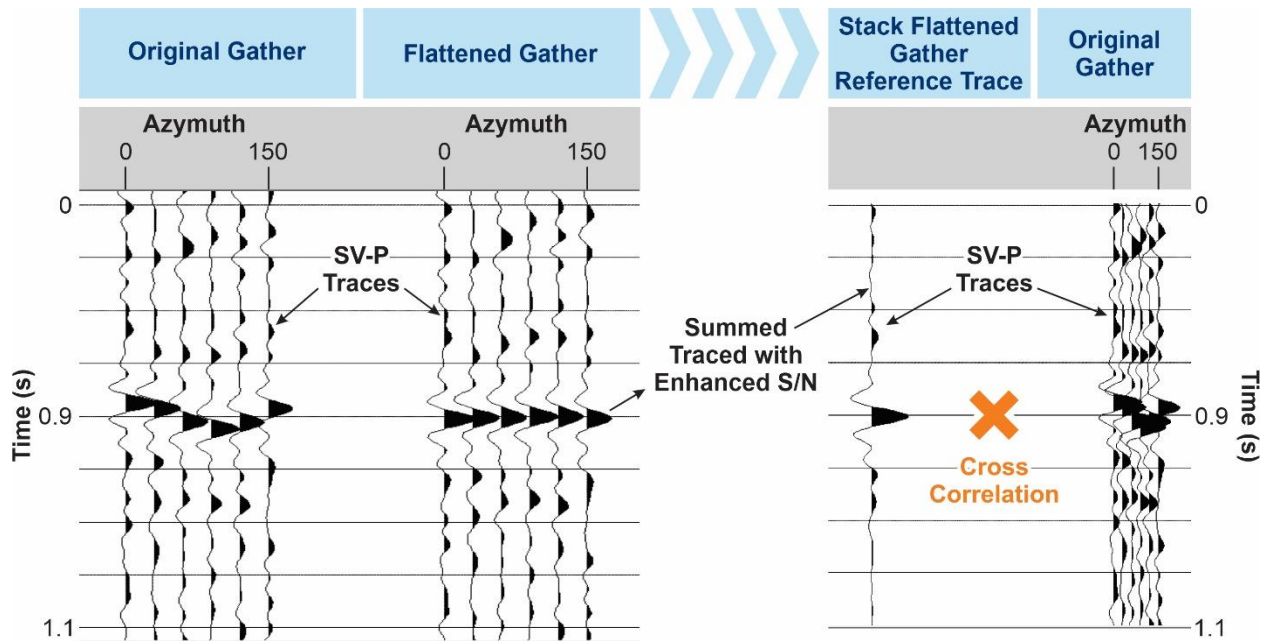
Figure 4-10. (Left) SV-P model traces from Figure 4-9. (Center) All 6 SV-P reflections are shifted to a constant arrival time so they can be summed to enhance the signal-to-noise ratio of the wavelet that images the targeted interface. (Right) The summed trace is then cross-correlated with the original data traces to obtain a higher-quality measure of the differences in arrival times of each reflection wavelet.

Next, this new reference trace, with its optimal-quality SV-P reflection wavelet, is cross correlated with each of the six original, azimuth-dependent, traces as shown by the model traces in Figure 4-11. In this second model, fast-S azimuth is repositioned at 30 degree azimuth not at 0 degree azimuth as in Figures 4-9 and 4-10. This trace correlation provides two important parameters: (1) a correlation time shift (ΔT) for each azimuth-dependent wavelet arrival that is based on an optimized reference wavelet, and (2) a normalized correlation coefficient that can be used as a reliability factor to judge the confidence of each estimated ΔT time delay. The sign convention of cross-correlation is such that the least-negative time shift in the cross-correlation output corresponds to the polarization direction of the fast-S mode (which is also the Shmax azimuth), and the most-positive time shift corresponds to the polarization direction of the slow-S mode (which is the Shmin azimuth).

Examples of real SV-P data traces extracted from four Perch 3D image bins are displayed in Figure 4-12. Visual inspection confirms that SV-P reflection wavelets that travel different azimuths to each image bin do indeed arrive at different times at targeted interfaces at 600 ms and 700 ms. These azimuth-dependent SV-P arrival times indicate Shmax and Shmin azimuth effects are embedded in the Perch 3D SV-P data. The data also illustrate typical noise backgrounds and wavelet irregularities that are embedded in real data traces across the Perch 3D area.
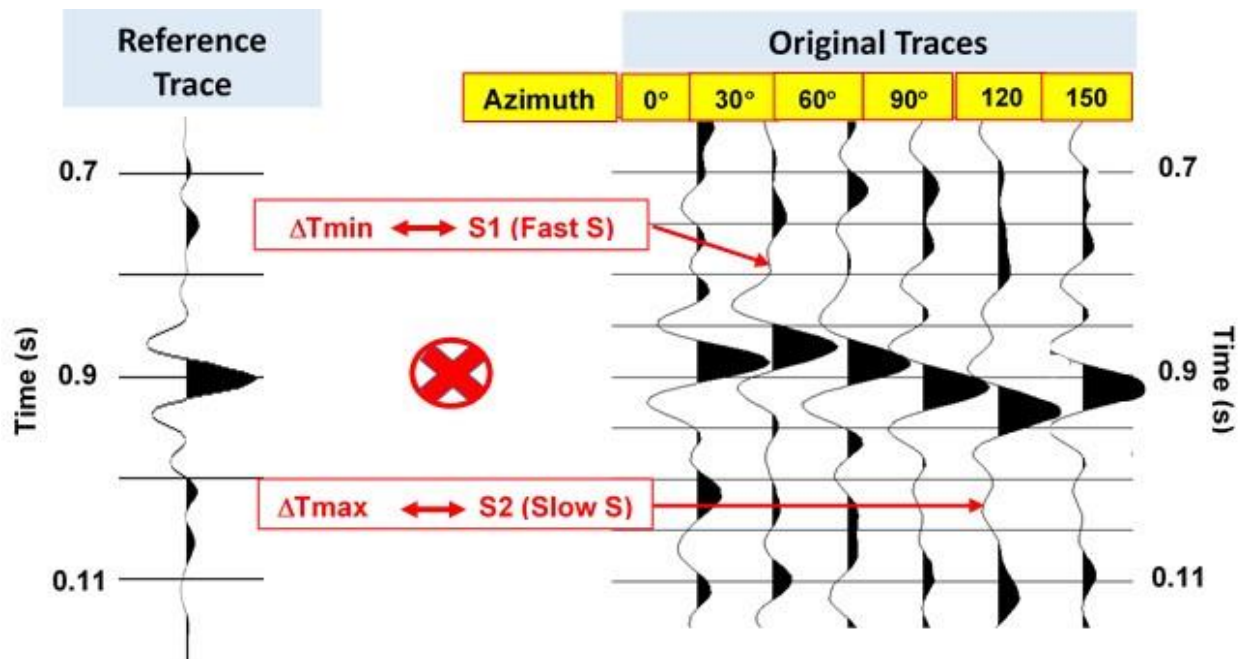
Figure 4-11. Cross-correlation procedure used at each SV-P stacking bin to estimate azimuth-dependent arrival times of SV-P reflection wavelets from a targeted interface. The reference wavelet on the left is a summed wavelet such as illustrated in Figure 4-10. The six traces on the right are cross-correlations between this reference wavelet and the six azimuth-dependent reflection wavelets placed in a hypothetical stacking bin by PSTM data movements.

The SV-P reflection at 700 ms in Figure 4-12 is a good example of azimuth-dependent arrival time. Detailed examination of the six-trace groups on the left-side of Figure 4-12 shows that the wavelet that is embedded in the third trace from the left in each data panel arrives earliest. This consistent SV-P travel time behavior implies Shmax azimuth is oriented approximately 60 degrees CW from north. In the six-trace SV-P reflection groups at 600 ms, it is difficult to decide whether the SV-P wavelet in the third trace or in the fourth trace arrives earliest because two interfering wavelets create a complex-shaped wavelet that makes it difficult to define wavelet arrival time.

This type of wavelet interference will cause an automatic, software-based, selection of SV-P arrival time to provide a "noisy" estimate of Shmax azimuth, as will be seen in maps that follow.
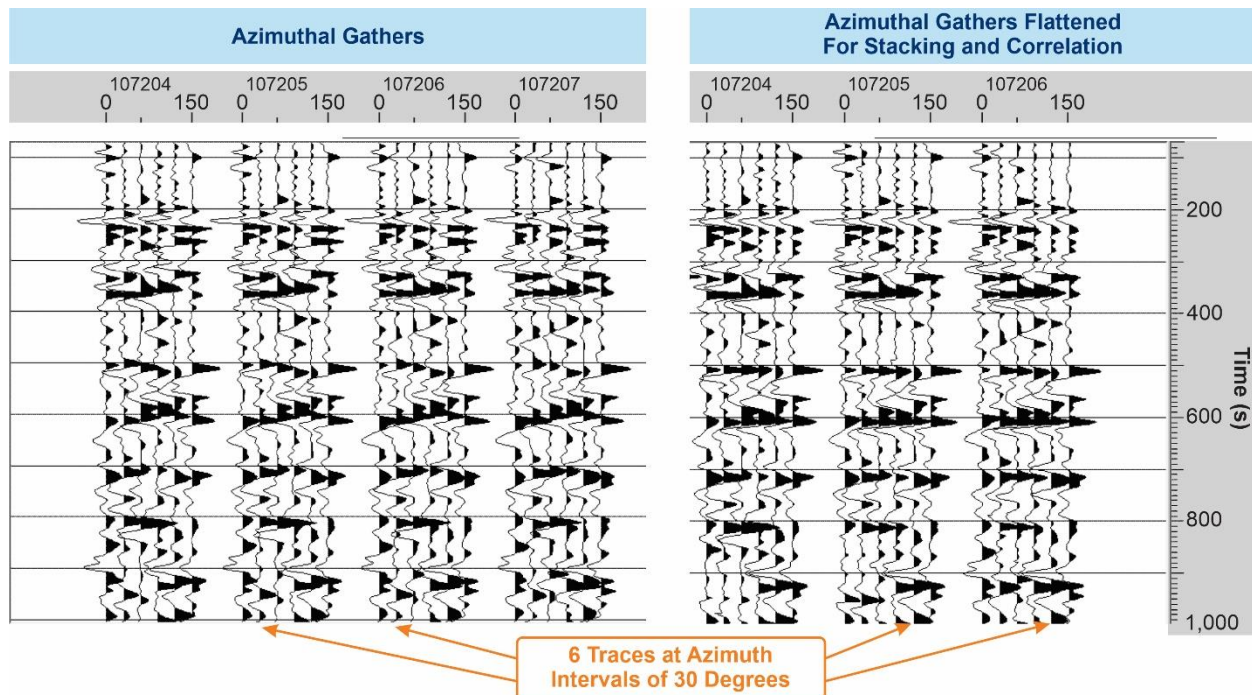
Figure 4-12. (Left) Real SV-P data traces from the Perch 3D data that illustrate the complex shapes of azimuth-dependent SV-P reflection wavelets that arrive at four consecutive SV-P stacking bins. These inconsistent waveshapes are the reason that a wavelet-summing procedure is used to create a best-estimate for the SV-P imaging wavelet at each stacking bin (Right). Targeted reflections at 600-ms and 700-ms exhibit obvious azimuth-dependent SV-P arrival times in the unshifted traces on the left. The six-trace gather at bin 107207 (Left) is not repeated as a flattened version (Right).

4.13 Mapping Azimuth-Dependent SV-P Velocities

The numerical trace-correlation methodology described in the preceding section was applied at almost every SV-P stacking bin across the entire Perch 3D seismic area. At each stacking bin, analyses were done for SV-P reflections associated with three key stratigraphic units: Bass Island, Niagaran, and St. Peter. The Bass Island unit is positioned at approximately 700 ms in SV-P image space. The Niagaran and St. Peter are positioned at deeper SV-P image times of approximately 1,000 and 1,200 ms, respectively. Note that these image times are correct for both P-P data and SV-P data because Texseis did a time warp of the SV-P data that converted SV-P image time to approximately equivalent P-P image time.

This study goes a step beyond what any previous determination of Shmax and Shmin analysis with S-mode reflection data has ever done – this being that Shmax was estimated at almost every stacking bin across a rather large area at three different depth levels. Each SV-P stacking bin is a small area of only 82.5 ft x 82.5 ft, and there are more than 100,000 stacking bins across the Perch 3D survey area. Previous seismic-based stress studies have almost always followed less-demanding strategies. Usually an analysis was done in only a small area of S-mode image space where S-mode reflection data were optimal quality and at only one targeted horizon.

The limited-corridor stacks of SV-P data exhibited in Figure 4-12 are harbingers that indicate difficulties will be encountered in these efforts to do narrow-corridor analyses at a large number of stacking bins across the Perch image space. The SV-P image data in Figures 4-7 and 4-8

illustrate how SV-P reflection character changes from poor-quality to good-quality in abrupt, erratic fashions when SV-P data are examined in low-fold, narrow-azimuth corridors. These variations in SV-P reflection quality are, in large part, due to the fact that precise S-wave static corrections are so difficult to determine when there is no supporting near-surface S-wave velocity information to use for guidance. In contrast, the full-fold SV-P images in Figures 4-7 and 4-8 are reasonable quality, which shows the power that high-fold trace stacking has in re-enforcing time-aligned reflection energy and in suppressing mis-aligned energy arrivals. The message provided by Figures 4-7 and 4-8 is that any analysis of SV-P data that is performed in narrow-azimuth corridors will be a battle between Shmax azimuth predictions determined in zones of reliable SV-P reflection data and in zones of noisy SV-P reflection data.
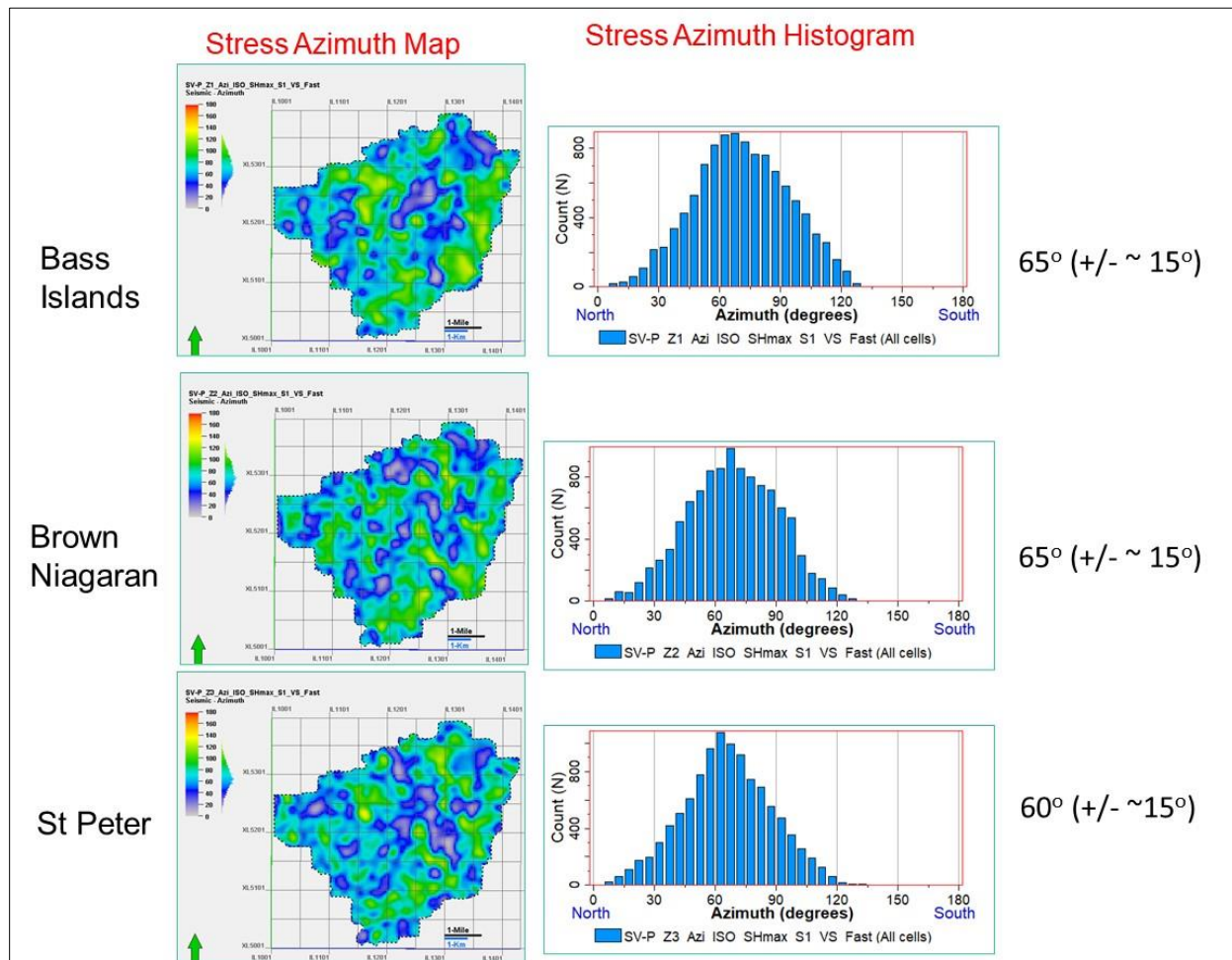
Figure 4-13. Maps of estimates of Shmax azimuth based on azimuth-dependent, arrival-time, analyses of SV-P reflections. Information on the right are the approximate mean and standard deviation values of each histogram.

The cross-correlation procedure illustrated in Figure 4-11 was helpful in constructing the maps of Shmax azimuths in Figure 4-13. The magnitude of the cross-correlation coefficient associated with each trace in a six-trace set (such as the data in Figure 4-12) was used as a reliability factor to decide if the arrival time of an SV-P reflection wavelet created in a stacking bin should be accepted or rejected. The family size and spatial distribution of acceptable and not-

acceptable SV-P reflection wavelets varied, depending on the cutoff level used to define "rejected" for a cross-correlation value. A cross-correlation value of 0.5 or greater was used to define reliable SV-P arrival times that were used to construct the three maps in this figure.

The estimates of Shmax azimuth shown in Figure 4-13 are quite encouraging. First, note that the vertical dimension of each histogram plot is approximately 1000. Each histogram is thus based on several thousands of estimations distributed across the SV-P image space. Further, each data point used to construct the histograms represents the average-azimuth estimate inside a 3 x 3 size super-bin that moves across all of the normal-size SV-P image defined by the maps on the left side of the illustration. The use of this super-bin adds another factor of 9 to the number of total normal-size image bins that are involved in these Shmax azimuth estimates.

Another way to obtain a feel for the number of normal-size stacking bins inside the SV-P image space is to look at the maps on the left side of Figure 4-13. Each square area in the background grid of these maps is a square mile. Inspection of these grid squares will show that the image area spans approximately 40-mi^2. There are 4096 normal-size stacking bins per square mile, which means there are about 160,000 normal-size stacking bins across the SV-P image space. Not all of these bins were used in the analyses of Shmax azimuth estimation. For example, bins that are close to the edges of the image space cannot be used because full-azimuth trace gathers cannot be constructed in these bins. Even so, the estimates of Shmax azimuth in Figure 4-13 involves many 1000s of individual stacking bins.

In summary, the estimates of Shmax azimuth displayed in Figure 4-13 are powerful evidence of the robustness of using azimuth-dependent SV-P arrival times to define fast-S azimuth (i.e., Shmax azimuth). These estimates were made at three different depths of approximately 3500 ft, 5500 ft, and 7500 ft. Each depth-based estimate was also based on analyses of azimuth-dependent SV-P arrival times at several tens of 1000s of stacking bins. Even with concerns that inaccurate S statics might not allow azimuth-dependent SV-P arrivals times to be recognized, the methodology practiced in this study was sufficiently robust to produce a consistent estimation that indicated Shmax azimuth at the Perch 3D seismic area is approximately 65 degrees clockwise from north.

4.14   Travel-Time Analyses versus Reflection-Amplitude Analyses

There are two standard approaches to using seismic data to extract physical properties from deep rocks: (1) use seismic attributes that can be extracted from travel-time measurements, or (2) use seismic attributes that can be extracted from wavelet-amplitude behavior. Experienced geophysicists seem to be united in their opinions that travel-time measurements are always more reliable than are wavelet-amplitude measurements. There are simply far more factors that affect amplitudes of wavelets that reflect from deep rocks than there are factors that affect travel times of reflected wavelets from those same rocks. Given the option of obtaining the same information from deep rocks (e.g., Shmax stress azimuth) with a technique based on travel-time information, or with a technique based on wavelet amplitude behavior, experienced seismic data processors would always prefer the travel-time option.

Sections 4.12 and 4.13 described a procedure to estimate Shmax azimuth from SV-P travel-time measurements. A procedure that utilizes an approach that is based on P-P wavelet-amplitude behavior will now be implemented. An important difference between these two approaches is that the travel-time measurements utilize SV-P reflections, but the wavelet-

amplitude approach that will follow will utilize P-P reflections. Both sets of reflections are extracted from the same vertical-geophone data.

4.15   Determining Shmax and Shmin from P-P Amplitude Inversion

The P-P amplitude inversion procedure that we implemented across the Perch 3D area was developed by Ruger (1997). Ruger's concept potentially could provide the same fracture analyses of deep rocks that, up to that time, could be obtained only with S waves, so his theory raised much interest across the geophysics community. However, the computational procedures that had to be done were demanding and not easily understood. Consequently, a book was soon published to expedite implementation of the technology (Ruger and Gray, 2014). Only the most basic principles of the inversion procedure are summarized here. Readers who wish more detail are directed to these Ruger references.

The analysis focuses on P-P PSTM data in which migrated P-P traces are assembled into CDP gathers at each P-P imaging bin. These gathers are collections of all traces that contribute to the P-P image at that stacking bin, with the traces positioned, in sequence, according to their source-to-receiver offset distances. The offset distance is regularized into intervals, typically on the order of several 100 ft, starting at 0 and ending at a maximum offset distance usually between 20,000 ft and 30,000 ft. Only P-P data are analyzed in this inversion procedure.

The procedure requires that binned P-P reflection data be assembled as functions of incidence angle (θ) rather than as functions of offset distance. Using velocity and geometric information, each offset distance is converted to an angle-of-incidence on a targeted reflecting interface, with that interface defined as a function of either depth or reflection time. For the Perch data, this procedure produced 40 to 60 angle traces that covered an incident angle range from 0 to about 45 degrees. P-P reflection amplitude, Rpp(θ), varies slowly with increasing incident angle θ, so a small-degree increment of angle sampling is not needed. Instead, reflection traces are usually stacked (averaged) to form a single trace at incident-angle intervals of usually 5 degrees. This averaging also enhances the SNR of the P-P data trace positioned at each incident angle, θ.

At a boundary separating two isotropic rock layers, P-P reflection behavior from that boundary can be described, as a function of incident angle, by the following equation that geophysicists have used for years:

$$(4.1) \quad Rpp(\theta) = A + B \sin^2(\theta).$$

In this equation, **Rpp** is the P-P reflection coefficient, **θ** is the incident angle of the down-going illuminating P ray path at the rock interface (measured relative to the normal to the interface), **A** is the P-P reflection coefficient at normal incidence, and **B** is the **gradient**, a quantity that defines how the magnitudes of P-P reflection amplitudes change as the incident angle swings away from normal incidence.

Ruger (1997) and Ruger and Gray (2014) showed that in an HTI medium (a medium that has horizontal transverse isotropy as illustrated in Figure 4-1), Equation 4.1 needs to be altered to read as:

$$(4.2) \quad Rpp(\theta,\varphi) = A + [Biso + Bani \cos^2(\varphi - \varphi sym)] \sin^2(\theta).$$

In this equation, **φ** is the azimuth direction from source to receiver, **φsym** is the azimuth direction of the rock **symmetry** axis, which is also the azimuth of Shmax (and the azimuth of any aligned extensional fractures that may be present [Figure 4-1]). **Biso** is the same gradient of reflection amplitude as **B** in Equation 4.1. **B** is altered to this new notation **Biso** to emphasize that **Biso** is a gradient that describes how magnitudes of reflection amplitudes vary with incident angle for **isotropic** rocks. This assumption means **Biso** is a constant that does not change with azimuth. In contrast, **Bani** is a separate gradient term that defines how the magnitude of reflection amplitudes vary with azimuth. All of the terms inside the square brackets of Equation 4.2 form an azimuth-dependent form of Equation 4.1 which can be written as:

$$(4.3) \quad Rpp(\theta,\varphi) = A + B(\varphi_k) \sin^2(\theta).$$

In this simplified equation, **B(φ$_k$)** is the gradient of P-P reflection amplitudes when the azimuth direction from a source to a receiver is azimuth φ_k.

When P-P trace gathers are examined in narrow, rotating, azimuth corridors, Equation 4.2 shows that the gradient term $B(\varphi_k) = [(Biso + Bani \cos^2(\varphi_k - \varphi sym)]$ has the following values when the source-to-receiver azimuth φ has the following values:

- $B(\varphi_k)$ = (Biso + Bani), when φ = φsym (the fast-S azimuth)

- $B(\varphi_k)$ = Biso, when φ = φsym +/- 90 degrees (the slow-S azimuth), and

- $B(\varphi_k)$ values range from Biso to (Biso + Bani) for all other azimuths.

Reference back to Figure 4-1 which provides graphical illustrations of some of this terminology. These bullet-point principles show that if a methodology can be implemented that will estimate **B(φ$_k$)** from azimuth-dependent P-P trace gathers, then Shmax azimuth can be determined. It needs to be emphasized that gradient values determined from real P-P trace gathers are controlled by variations in reflection-wavelet **amplitudes** as a function of azimuth, not on changes in wavelet **arrival times** with azimuth as has been used in the analyses described for SV-P data in Sections 4.12 and 4.13 (Figures 4-9 through 4-13).

The diagram in Figure 4-14 depicts synthetic, angle-dependent, trace gathers of P-P reflection data (black traces), and synthetic, angle-dependent, trace gathers of SV-P data (red traces). Each wiggle-trace gather shows reflection-wavelet amplitude values at their actual reflection time, which is the narrow, dashed, time-coordinate line extending across each set of traces. This reference timing line passes through the single data point on each trace where the amplitude of the dominant peak or trough of a wavelet is positioned. It must be emphasized that the red curve labeled Rsvp and the black curve labeled Rpp are not reflection coefficients. They are, instead, the single amplitude-value extracted from each of the wiggle traces along the dashed-line time coordinate that passes through the exact apex of each reflection wavelet's peak or trough. Rpp black-curve values are thus directly proportional to P-P wavelet-amplitude values. Similarly, Rsvp red-curve values are directly proportional to SV-P wavelet-amplitude values.
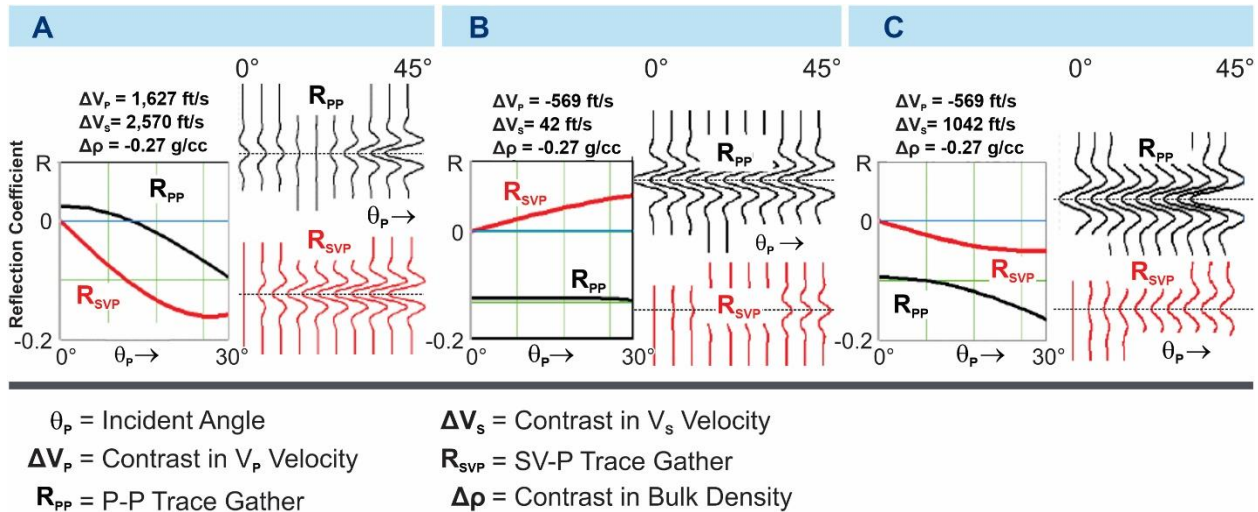
Figure 4-14. Calculated amplitude versus angle trace gathers at stacking bins where there are different impedance contrasts. Incident angles vary from 0 to 45 degrees at increments of 5 degrees. P-P traces (black wiggles) and SV-P traces (red wiggles) are shown in this example. These traces represent a full-azimuth stack. The remainder of this section will focus on P-P trace gathers only.

This technique for measuring the correct amplitude of a reflection wavelet is valid ONLY IF reflection wavelets are zero-phase wavelets and if all procedures that affect reflection amplitudes are properly executed and monitored. This zero-phase requirement is important and requires that careful wavelet processing be done when conditioning P-P data for amplitude-inversion purposes. This challenge of creating zero-phase wavelets is emphasized because the only true information about rock reflectivity occurs **exactly at the peak (trough) reflection time of each reflection wavelet**. The rest of the reflection wavelet that spans most of each data trace is just along for the ride. Whatever variations in wavelet amplitudes occur away from this single-data-point reflection time are essentially meaningless. Variations in reflection wavelet amplitudes are, unfortunately, inescapable complications that always exist when processing and interpreting real-world seismic wiggle-trace data.

Only P-P trace gathers will be considered in this discussion because the amplitude-inversion theory developed by Ruger (1997) and Ruger and Gray (2014) uses only P-P reflection amplitudes (Equations 4.2 and 4.3) to estimate the azimuth of Shmax. The amplitude-versus-angle (AVA) gathers shown in Figure 4-14 are synthetic P-P traces that simulate a collection of full-azimuth, pre-stack, time-migrated P-P traces (designated as an **ALL AZ PSTM** procedure). In other words, the source-to-receiver ray paths that contributed traces to the gather were allowed to follow any azimuth direction between 0 and 360 degrees to reach the stacking bin.

However, to create data that are appropriate for using Equation 4.2 to determine azimuth orientation of Shmax, it is important that P-P gathers be constructed from PSTM data that are constrained so that source-to-receiver travel paths that contribute to each gather remain inside a narrow azimuth corridor. These narrow-azimuth data will be designated as **PP AZ AVA** gathers. An example of such gathers, which again uses synthetic data composed of idealized zero-phase wavelets, is shown in Figure 4-15.
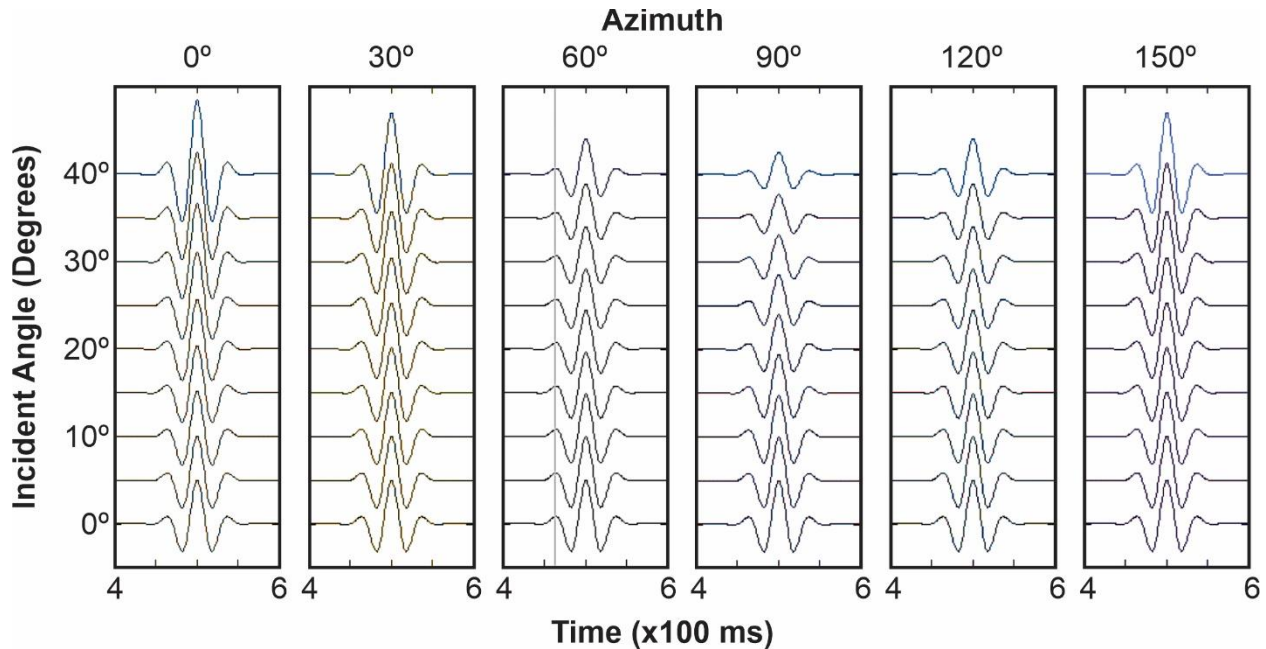
Figure 4-15. Synthetic traces representing narrow-azimuth gathers of P-P AVA traces collected at the same stacking bin. Each trace-gather corridor has an azimuth width of 30 degrees. Each corridor radiates away from the same stacking bin in positive-offset and negative-offset directions. Six such corridors provide a full 360-degree azimuth gather of traces around each stacking bin and allow azimuth-dependent P-P reflectivity to be analyzed.

There is significant variation in the calculated Rpp (θ,Φ) data illustrated in Figure 4-15. Wavelets that arrive at incident angles ranging from 0 to 15 degrees are essentially constant amplitude for all six azimuth-approach corridors because these wavelets travel at near-vertical incident angles. Wavelets that approach a reflecting interface at near-normal incidence encounter only small amounts of anisotropy. In contrast, anisotropic conditions have significant effects on oblique ray paths that travel long, slanted-ray-path, distances through anisotropic rock.

Most of the rock information contained in these P-P trace gathers can be determined from two trace-gather parameters: (1) the rate of change of the wiggle-trace amplitudes with incident angle, which is called the **Gradient**, and (2) the value of the wiggle-trace amplitude at normal incidence, which is called the **Intercept**. Because these two quantities (**Gradient** and **Intercept**) are derived from scaled values of real P-P data traces, their values are only proportional to the true Intercept value **A** and the true Gradient value **B** in Equation 4.1. Consequently, the term **Rpp(0, Φ)** will be used for **A**, and the term **Gradient** will be used for **B**, to distinguish these real-data terms from their model-derived equivalents in Equation 4.1.
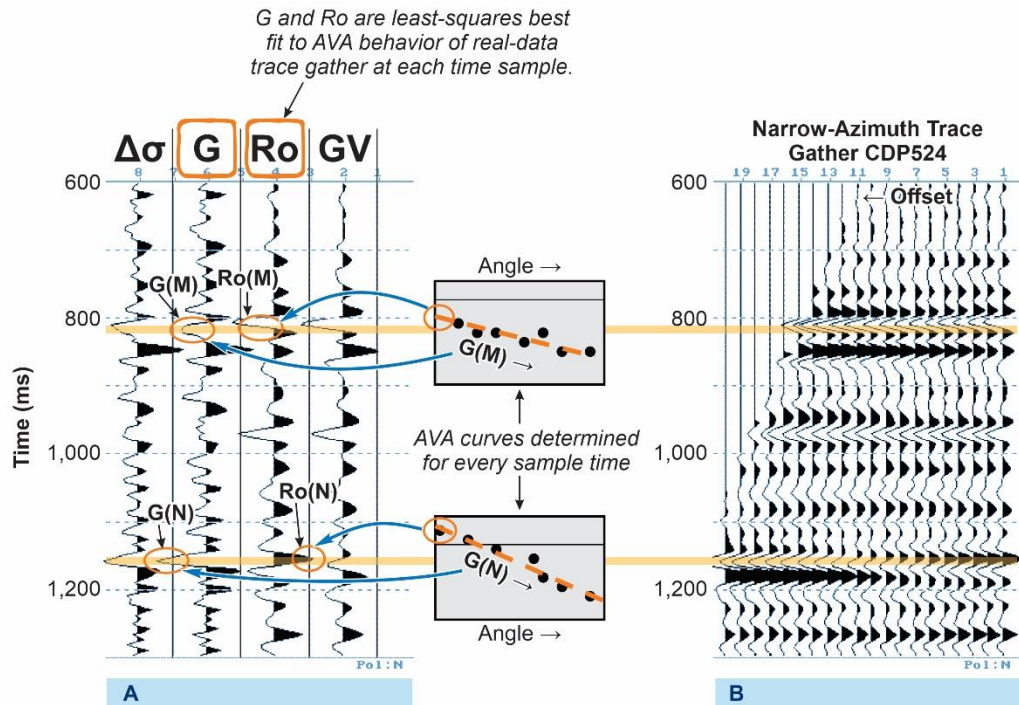
Figure 4-16. Real, migrated, Perch P-P traces (B) assembled at a stacking bin. The amplitudes of the traces are gathered from right-to-left along a fixed time line, such as indicated by the two yellow lines, and then displayed as an amplitude-versus-angle plot shown by the black dots in the two central boxes. A best-fit straight line is then calculated to fit the black-dot trend. The slope of this straight line is the Gradient (G), and the amplitude value when the straight line reaches 0-degree angle is the Intercept (Ro), which is circled at the left side of each gray box.

Inspection of Figure 4-15 shows that the largest **Gradient** influence on reflection-wavelet amplitudes occurs for the traces gathered in the two narrow corridors oriented at 0-degree azimuth and at 90-degree azimuth. One of these azimuths is the Shmax direction, and one is the Shmin direction. The explanation of how to define which azimuth is the Shmax direction and which is the Shmin direction will be delayed until Figure 4-17 is presented. First, this discussion will make a short detour to examine a real P-P trace gather from the Perch 3D survey, which is displayed as Figure 4-16.

Figure 4-16 shows the methodology used to determine AVA attributes **Intercept** and **Gradient** (introduced in Equations 4.1, 4.2, and 4.3) using real P-P trace-gather data from the Perch survey. Panel B shows a real P-P, narrow-azimuth corridor, trace gather at a single Perch-survey stacking bin. Traces in panel B are plotted from right-to-left as a function of increasing offset, or increasing incident angle, depending on a data processor's preference. Neither offset distances nor incident angles are labeled for any of the traces. Incidence angle 0 degree starts at the right-most trace of panel B and increases to the left across the trace gather to a value of approximately 45 degrees.

Note the analyses documented in the two boxes between the two panels of wiggle-trace data. The information in each box summarizes the amplitude behavior of the P-P trace data in the right-side panel that occurs across a constant-time coordinate of the traces. Two arbitrary constant-time-coordinate lines are chosen for illustration. They are emphasized by yellow

horizontal lines and will be referred to as reference line M (top) and reference line N (bottom). The black dots in each box indicate the P-P trace-amplitude behavior as the migrated traces are examined from right-to-left along each of these constant-time-coordinate lines.

The slope of the best-fit straight-line to the amplitude values intersected by each yellow line defines the **Gradient** of the trace amplitudes along that reference timeline. These gradients are labeled **G(M)** and **G(N)**, respectively, in each box. The amplitude value where each best-fit line intersects the left side of each box (which is where the 0-degree incident-angle value for the gradient plot is located) is the **Intercept** value for the trace amplitude behavior. Each **Gradient** value is placed in its proper time coordinate in a new trace labeled **G** (left panel) Each **Intercept** value is placed in its proper time coordinate in a new data trace labeled **Ro** (left panel). These two new data traces (**Gradient** and **Intercept**) provide the information needed for inverting P-P AVA behavior into estimates of Shmax and Shmin azimuths.

Synthetic model data will now be used to illustrate how a **Gradient** trace extracted from azimuth-corridor trace gathers of P-P data is used to determine the azimuth of Shmax. Because the *Biso* term previously discussed (Equation 4.2) is constant, and is independent of azimuth, it can be subtracted from the B(Φk) term in Equations 4.2 and 4.3 without negatively affecting the detection of the *φsym* azimuth. Each **Intercept** and **Gradient** symmetry axis is then defined with only the *Bani* term, which is multiplied by a cosine function (Equation 4.2). Inspection of Equation 4.2 shows that this cosine function will have a maximum when Φk = **Φsym**, where Φk is the azimuth of narrow-corridor **k** used to determine **Intercept** and **Gradient**, and Φ**sym** is the azimuth of Shmax (which is the same as the azimuth of the symmetry axis, Figure 4.1).

The effect of this cosine weighting is demonstrated in Figure 4-17 where the amplitudes of the **Gradient** trace extracted from synthetic model traces are strongly affected by cosine-term weighting. The earth model used in this example is altered from the model that created the synthetic traces in Figure 4-15. In this second earth model, the Φsyn direction (Shmin azimuth) occurs at 30 degrees, and the Φiso direction is 120 degrees (SHmax azimuth). These two stress axes are emphasized by maximum values of the **Gradient** values, which are produced principally by the cosine footprint that are embedded in the data (Equation 4.2).
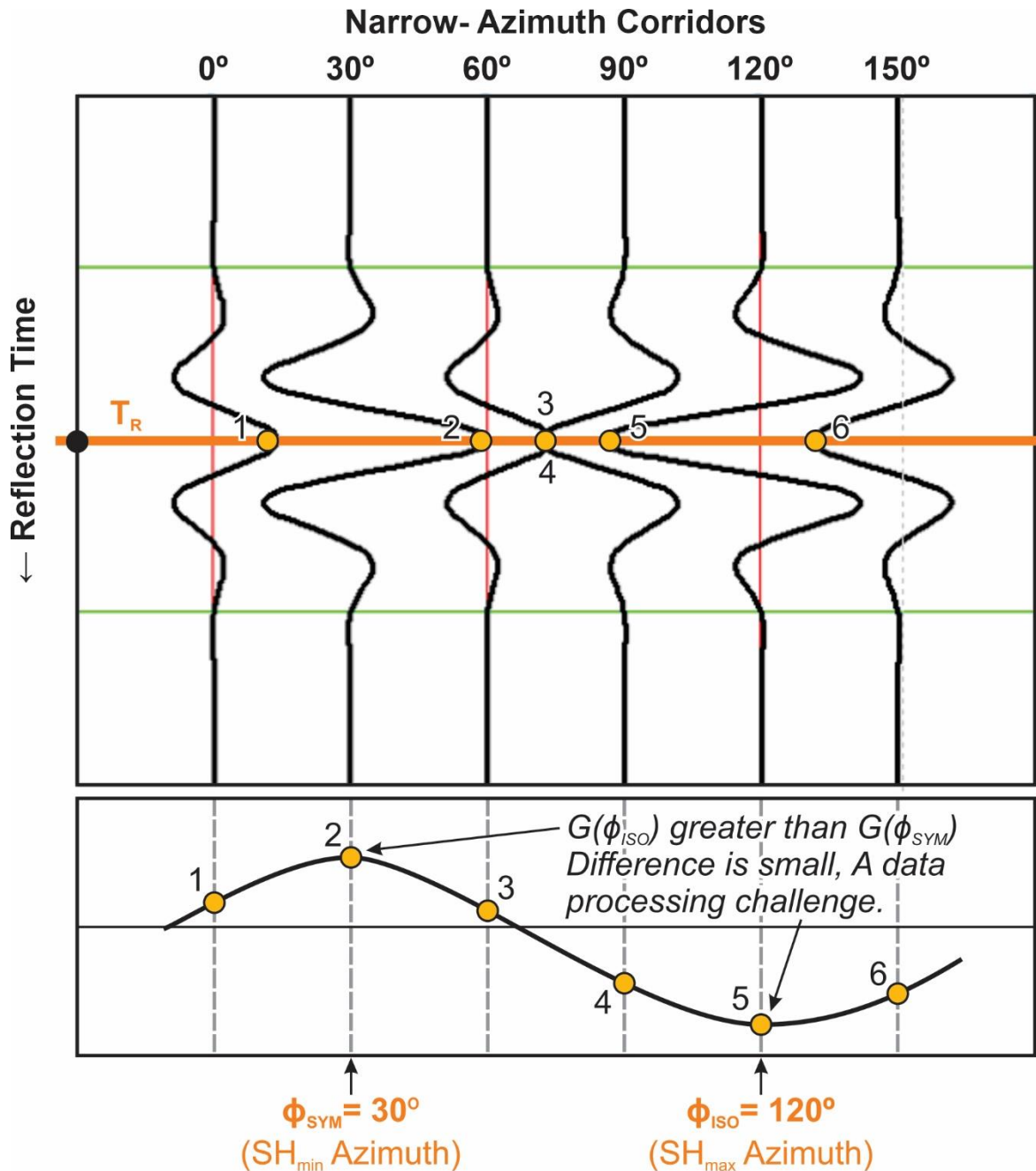
Figure 4-17. Model-based calculations of azimuth-corridor gradient traces. This model involved a symmetry axis oriented at an azimuth of 30 degrees and an isotropy axis oriented in an azimuth of 120 degrees. Even though the data traces use ideal, zero-phase, absolutely-noise-free, wavelets, it is still challenging to distinguish which axis (symmetry or isotropy) creates the higher amplitude response.

The numbered data points (1 through 6) identify the extrema of the Gradient trace created for this simplified earth model. When these data points are plotted to exhibit the cosine nature of their values (bottom of Figure 4-17), it is possible to see that the extrema of the Gradient function extracted from the narrow-corridor oriented at an azimuth of 90 degrees (which is the Shmax azimuth in this model) has the largest magnitude of any of the Gradient traces. However, the difference between the Gradient values for 90-degree azimuth (Shmax) and for 0-

degree azimuth (Shmin) is small. In real-data analyses, factors such as random noise, basic wavelets that are not exactly zero-phase, incorrect static adjustments, etc. affect reflection amplitudes and can easily cause the Gradient value in the Shmin azimuth to have a larger value than the Gradient value in the Shmax azimuth. The result will be an incorrect interpretation of Shmax azimuth.

With these observations in mind, Φsyn and Φiso values can now be extracted from inversions of real, narrow-azimuth corridors across the Perch 3D survey area and then individually plotted in a convenient map format for interpreters to use to determine Shmax and Shmin azimuths. Such maps now follow.

4.16   Maps of SHmax and SHmin Azimuths Created by P-P Amplitude Inversion

Displays of AZ PP AVA amplitude inversion results are now presented as Figure 4-18 for three zones that are centered on the Bass Island, Niagaran, and St. Peter formations. Estimates of Shmax azimuths are presented as histograms and as color-coded maps in the same formats used for the SV-P reflection-time maps in Figure 4-12. The Bass Island analysis shows that Shmax azimuth is 70 degrees (+/-15°). This result is essentially the same azimuth range predicted by the SV-P fast-S azimuth in Figure 4-12 and is an encouraging result.

The predictions of Shmax azimuth have to be described with larger standard deviations as target depths increase to the Niagaran formation, and then deeper to the St. Peter formation. A value of 70 degrees (+/-15° or 20°) has to be used for the Shmax azimuth at the depth of the Niagaran formation. This result is consistent with the Shmax azimuth prediction provided by SV-P fast-S measurements (Figure 4-13). The estimates of Shmax azimuth provided by inversions of P-P amplitudes at the deep St. Peter are simply unreliable. P-P reflections from this deepest horizon do not have the stringent wavelet-amplitude properties required for this amplitude inversion procedure.
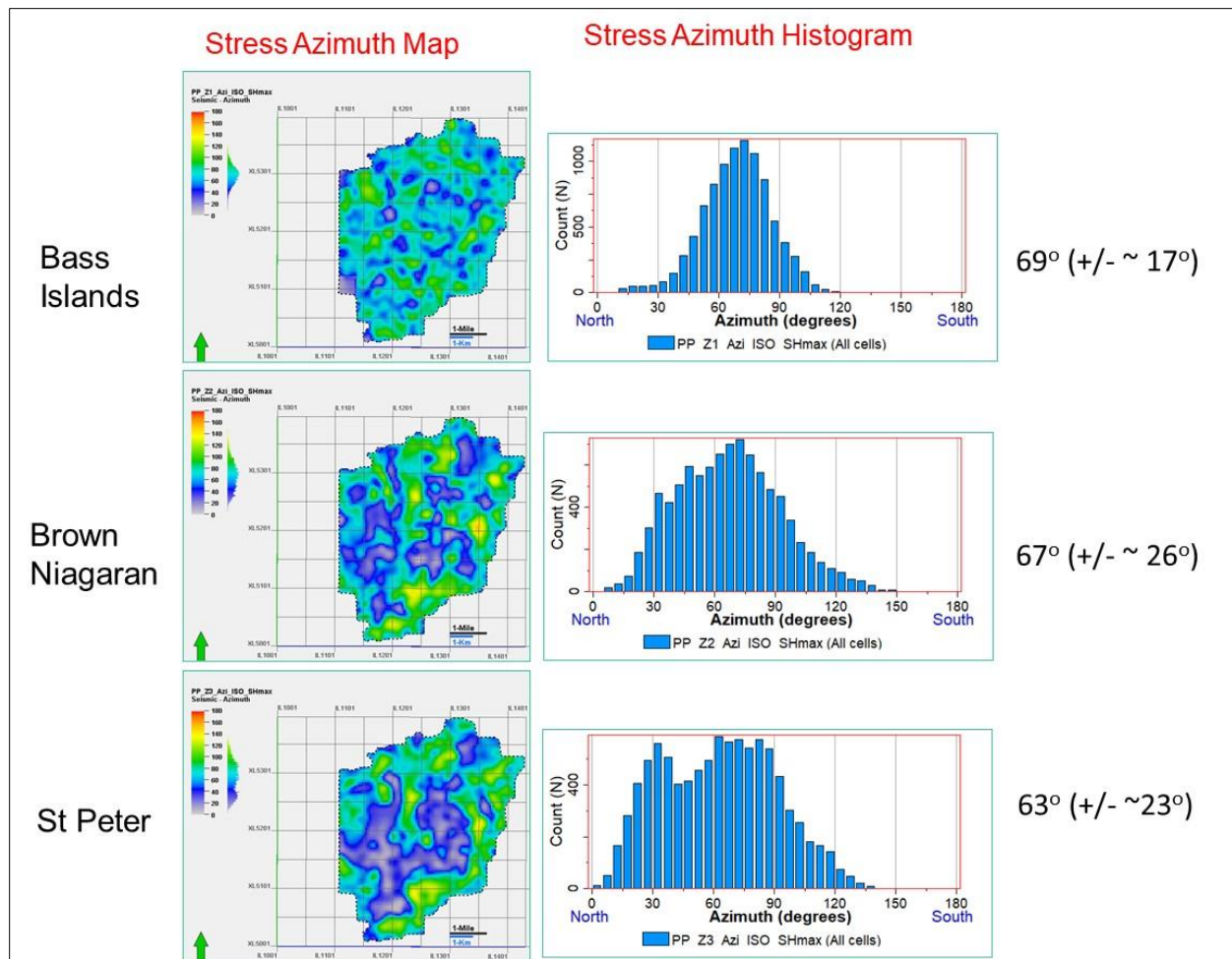
Figure 4-18. Maps of estimates of Shmax azimuth based on azimuth-dependent, arrival-time, analyses of P-P reflections. Information on the right are the approximate mean and standard deviation values of each histogram.

4.17   Conclusions About Using P-P Amplitude Inversions

The P-P amplitude inversion procedure tested at the Perch prospect requires that P-P data have a high SNR and a basic wavelet that is exactly zero phase. These two requirements are difficult to attain in any P-P data, particularly if there are any static complications or challenging velocity problems inside the area covered by the seismic image space. Both requirements become even more difficult to meet when a procedure requires that stacking fold be reduced by having to process data that are confined to narrow-azimuth corridors.

It is important to bear in mind that the preceding mathematical procedures are quite sensitive to the frequency-band limitation of seismic data and to the waveshape of the basic reflection wavelet embedded in the Perch 3D P-P data. It cannot be overstressed how important it is for data-processing procedures to create and maintain high-quality, zero-phase, relative-amplitude wavelets. Extraction of the extrema (peaks and troughs) of **Gradient** values from data which deviate from true reflection times (which require a zero-phase wavelet and error-free wavelet alignment) can lead to false values that diminish the reliability of a P-P trace inversion to determine Shmax azimuth.

Perfect alignment of zero-phase data is fraught with difficulty, and so it is anticipated that that there will be variations in the reliability of the analyses produced in this P-P azimuth-dependent approach to determining Shmax and Shmin azimuths. As Figure 4-17 demonstrates, even in numerical modeling that uses solitary, perfect-zero-phase, wavelets, the difference in the magnitudes of Shmin and Shmax extrema in the Gradient trace that is produced is still small. Even small data distortions can make the incorrect extremum in Figure 4-17 have the higher amplitude, which will result in the estimated Shmax azimuth being in error by 90 degrees. This outcome implies that in real data, it will often be challenging to decide which Gradient peaks and troughs relate to Shmax azimuth.

If P-P data are generated by vertical vibrators, the basic wavelet injected into the ground is zero-phase, by definition. However, that zero-phase character becomes distorted by interfering P multiples and by SV-P reflections and also battles with numerous noise modes when it arrives at surface receivers. Prominent among these surface noises are Rayleigh wave ground roll, wind gusts shaking weeds and trees, and local cultural activity. If P-P data are generated by buried explosives, the challenge of having a zero-phase basic wavelet is more complicated because the wavelet that leaves the shot cavity is a one-sided, asymmetrical wavelet, not a zero-phase wavelet.

These research findings indicate that a Ruger-type inversion of P-P reflection amplitudes is valuable (Figure 4-18) and should continue to be used. Users must simply be aware of its numerous pitfalls. The option of inverting P-P amplitudes for stress azimuth information will certainly be assisted by modern data-acquisition strategy, which allows tens of thousands of receivers to be deployed. Receiver arrays of this magnitude will result in stacking folds that have magnitudes that reach into the several hundreds range. These extremely high-fold data can then be segregated into narrow corridors that have stacking folds that are high enough to suppress background noise and to produce the optimal-shape wavelets that are needed for inversion.

4.18   Summary of Methodology Used to Predict SHmax from 3D Seismic Data

The most common type of seismic reflection data that will be available across a CO_2 sequestration site will be 3D seismic data. More to the point of this research focus, the most common type of 3D seismic data will be data generated by a P source (i.e., a vertical vibrator or a buried explosive) and recorded with only vertical geophones. This point is emphasized because to extract deep-rock stress information from seismic data, it is not only essential, but mandatory, that emphasis be placed on analyzing shear (S) wave modes that probe those deep rocks. The barrier that has to be overcome is then instantly faced, which is "how do you extract S-wave information from 3D data generated by a P source and recorded with only vertical geophones". The principal concepts demonstrated with this 3D seismic research are:

1. Traditional P sources not only produce illuminating P wavefields, but also produce robust, down-going, direct-S wavefields that can be used to image deep rocks. The physics that verifies this key concept is provided in Section 2, is demonstrated with vertical vibrator sources in Section 3, and now is demonstrated for buried explosive sources in Section 4.

2. Rock stress information gathered by a down-going, direct-S wavefield produced by a P source is carried back to the surface by the reflected P mode created by SV-to-P mode conversions at deep-rock interfaces. This up-going converted-P mode is recorded by

vertical geophones. Thus, it is true that invaluable, deep-rock, stress information captured by S-waves can be extracted from 3D data generated by a P source and recorded with only vertical geophones. This research thus provides the CO_2 sequestration community valuable tools for monitoring stress conditions within, and adjacent to, CO_2 reservoir rocks and their sealing units with S-wave data.

There are two fundamental approaches to extracting information from seismic reflection data. Approach 1 is to extract the information that is sought by using a method that is based on seismic travel time. Approach 2 is to extract the information that is sought by using a method that is based on seismic amplitude behavior. A general rule-of-thumb practiced by senior, battled-scarred seismic interpreters that they pass on to the next generation they tutor is "if you can get the information you seek by depending on either a travel-time technique or on an amplitude-behavior technique, always go with the travel-time technique". In other words, the number of adverse factors that affect seismic reflection amplitudes is larger than the number of factors that adversely affect reflection wavelet travel time.

In this research, both a travel-time method and a reflection-amplitude method were used to estimate Shmax azimuth at the Perch 3D seismic survey area. The travel-time-based method required analysis of the azimuth dependence of arrival times of SV-P reflections across the Perch 3D image space. The azimuth in which SV-P reflections arrived earliest at a stacking bin was the azimuth of Shmax horizontal stress at that stacking bin's coordinates. The results of this procedure are summarized in Figure 4-13.

The reflection-amplitude method used was based on concepts developed by Ruger (1997) and later expanded by Ruger and Gray (2014). This theory applies an inversion procedure to AVA behaviors observed in P-P reflections. S-wave data are not involved in this second approach; the concept is based strictly on information that can be derived from P-P reflection amplitudes. This use of P-P reflection amplitudes is an elegant, rigorous theory, and represents the optimal approach that reflection seismologists have developed to extract Shmax azimuth from P-P reflection amplitudes. P-P AVA inversion results are summarized in Figure 4-18.

4.19 Comparison between Seismic Predictions of SHmax and Ground Truth Information

Ground-truth stress data available local to the Perch 3D seismic image area are summarized in Table 4-1. These data were assembled in a previous Battelle investigation at the Perch 3D prospect (Battelle, 2019)). There is good agreement between these non-seismic measurements of Shmax azimuth and the azimuth-dependent SV-P arrival time estimates of fast-S azimuths found in these analyses.

Figure 4-13, and its accompanying text, show that the Shmax azimuth predicted by azimuth-dependent arrival times of SV-P reflections is 65 degrees (+/-15°). Examination of Table 4-1 shows the following independent measurements of Shmax azimuth that agree with these seismic-based predictions.

- Mini fracs predict Shmax values of 54 and 62 degrees. A third direction of 33 degrees is also predicted, but this measurement could be a shear fracture, not a required extensional fracture. Shear fractures are always oriented away from extensional fractures (i.e., Shmax azimuth) by approximately 30 degrees. Refer to Figures 2-2 and 2-

3 to appreciate the risks of using a small population of fractures to predict Shmax azimuth when both shear fractures and extensional fractures are detected in a borehole.

- Two drilling-induced fractures predict a Shmax azimuth of 58 degrees. There are four other drilling fractures that, again, appear to be shear fractures, not extensional fractures. They are oriented in 104 and 88 degree directions, and thus fall in the 30-degree angle range away from the orientation of extensional fractures.

- One local fault is oriented 65 degrees. Fault evidence should always be considered first unless there is compelling evidence that Shmax azimuth has been altered by later-time, regional stress dynamics.

There is, thus, rather good agreement between the three different depth levels of SV-P travel-time predictions of Shmax azimuth in Figure 4-13 and with local ground-truth data.

The shallowest P-P AVA inversion result at the Bass Island interface in Figure 4-18 also predicts a Shmax azimuth of 65 degrees (+/- 15°) just as the SV-P travel-time estimates (Figure 4-13). This is a most encouraging result for the amplitude-based option for predicting Shmax. However, the amplitude-based methodology in Figure 4-18 deteriorates as reflection depth increases to the Niagaran formation and becomes unacceptably noisy at the deeper St Peter level.

These research findings support the decades-old interpretation adage that if a seismic interpreter has a method that is based on analyzing arrival times of seismic reflections to reach a conclusion, and also a method that is based on analyzing seismic reflection amplitudes, the reflection arrival-time option is usually more reliable. No one is discouraged from using the inversion of P-P AVA reflection data even though that methodology was not as reliable in this study as was the methodology based on comparing azimuth-dependent SV-P reflection times.

This concept of determining Shmax (i.e., fast-S) azimuth by measuring SV-P reflection arrival times in narrow-azimuth gathers of SV-P traces is a wave-propagation physics that has never before been demonstrated. This new S-wave physics will not only be a valuable contribution to insert into geophysical literature, but will be a valuable, and non-invasive, procedure for monitoring stress conditions at CO_2 sequestration reservoirs.

Table 4-1. Available ground-truth stress data in the Perch 3D seismic area.

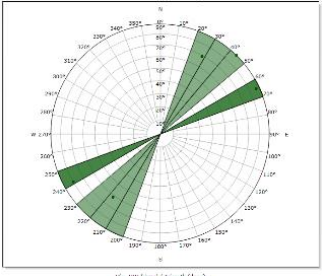| Source	Results	Comment
Mini-frac tests: three mini-frac tests successfully conducted,	Shmin magnitude: 0.76 to 0.77 psi/ft Shmax azimuth: N33E, N54E, and N62E	Shmin magnitude consistent with Haimson (1978); Shmax orientation is consistent with regional stress data

Table 4-1 (continued). Available ground-truth stress data in the Perch 3D seismic area.
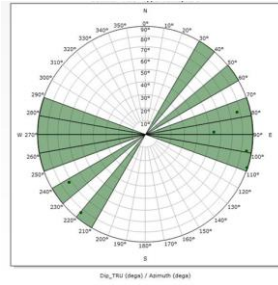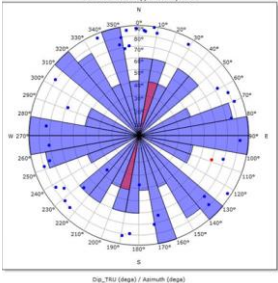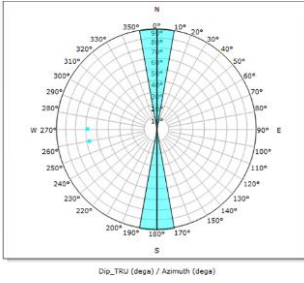
Source	Results	Comment
Image-log analysis of 6 drilling induced fractures. The 6 fractures fall into 3 groups:	Shmax azimuth: N104E avg of n=3 NW/SE fractures; N58E avg of n=2 NE/SW fractures; N88E n=1 fracture	Large amount of variability; less reliable than mini-frac test results
Image log analysis of natural fractures and faults	Conductive fractures (n=39) exhibit large amount of variability – no apparent orientation trend; may not be indicative of present-day stress condition.	
	Resistive fractures (n=2) exhibit N-S orientation; may not be indicative of present-day stress condition.	
	Faults (n=2) exhibit N-S and NE-SW orientation; may not be indicative of present-day stress condition.	
Sonic log data	Weak anisotropy was observed at one depth; otherwise, isotropic conditions prevail	Waveform dispersion plots do not provide strong evidence for stress as cause for observed weak anisostropy; therefore, no reliable data on Shmax orientation can be gleaned from the sonic data**.**
	Shmin magnitude 0.82 psi/ft, 0.76 psi/ft, and 0.69 psi/ft for the Bass Islands, Salina G, and F Unit, respectively, based on the assumption of anisotropic conditions and 0.71 psi/ft,	Anisotropic values overlap with agree better with Shmin magnitude from mini-frac tests (0.76 to 0.77 psi/ft) whereas isotropic values are lower.

Table 4-1 (continued). Available ground-truth stress data in the Perch 3D seismic area.

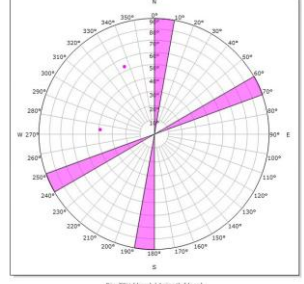| Source	Results	Comment
	0.68, and 0.68 psi/ft for the Bass Islands, Salina G, and F Unit, respectively, based on the assumption of isotropic conditions	

5.0 Summary

5.1 Overview and Objective

The research described in this report relates to only Task 2 (Extracting Stress Data from Seismic Data) of the broader DOE project titled "*A Non-Invasive Approach for Elucidating the Spatial Distribution of In Situ Stress in Deep Subsurface Geologic Formations Considered for CO$_2$ Storage (FE0031686)*". All research focused on the central challenge of extracting stress information affecting deep rocks from seismic data. Several general themes underpinned all of the research activities that were performed. These general themes can be summarized as:

1. Because S-waves are more sensitive to stress fields than P-waves, it is important to demonstrate new ways to extract S-wave information from seismic data.

2. Traditional P-wave seismic sources produce direct-S illuminating wavefields that almost always are as effective for illuminating deep rocks as are the well-known direct-P wavefields that these sources generate. Reflection seismologists have used the direct-P wavefield produced by vertical vibrators and buried explosives for decades. In contrast, they have totally ignored the companion direct-S illuminating wavefield generated by these common "P sources". This claim is easy to verify by doing a simple search of geophysical literature. Such searches will find no examples of using direct-S wavefields produced by P sources until 2014 when researchers at The University of Texas at Austin went public with research findings that they began accumulating in 2010.

3. The direct-S mode produced by P sources provides expanded S-wave applications and uses of VSP data.

4. The direct-S mode produced by P sources allows S-mode reflection seismology to be practiced with seismic data generated by traditional P-sources and recorded with only vertical geophones. This new approach to S-wave reflection seismology can be done by utilizing SV-P reflections that are intertwined with P-P reflections in vertical-geophone data.

5. Principle 3 can be practiced with legacy VSP data acquired several years in the past, and principle 4 can be practiced with legacy 3D data acquired several years in the past. These new principles of direct-S illumination with P sources can thus be practiced without expending any funds to acquire new seismic data.

6. Those who practice seismic reflection seismologists need to be shown evidence of the value of the direct-S wavefields produced by P sources.

7. Because S-waves are essential for analyzing deep stress fields, it is important to demonstrate how direct-S wavefields produced by P sources provide a non-invasive way to monitor deep stress fields.

These themes governed this research and how the investigations were executed.

5.2 Research Strategy

This research followed two simultaneous parallel paths. Path 1 was to investigate how to use the direct-S illumination embedded in VSP data generated by vertical vibrators to define and monitor changes in the azimuth of maximum horizontal stress (Shmax) in deep rocks. The

research methodology and research findings that illustrate that this objective is relatively easy to do are described in Section 2.

Specifically, these research results show that Shmax azimuth can be defined by mathematically rotating down-going, direct-S, wavelets recorded by deep, three-component, geophones and identifying the azimuths where the fast-S mode and slow-S mode reverse polarity. The azimuth where the slow-S wavelet reverses polarity is the azimuth of Shmax. In this demonstration, the Shmax azimuth predicted by this method agreed exactly with the Shmax azimuth determined in a mini-frac test in the VSP receiver well. This VSP concept and methodology have never been practiced before. These research findings provide the CO_2 sequestration community with a valuable new tool for non-invasive monitoring of stress changes caused by injection of CO_2 in deep, porous, saline, reservoir rocks. Legacy VSP data were used in this research, which demonstrates that, in many cases, others can also use existing VSP data and not have to expend funds to acquire new VSP data.

Research path 2 focused on defining fast-S azimuth with 3D seismic data generated by buried explosives and recorded with vertical geophones. Two approaches were followed. Approach 1 was to extract SV-P reflections from the 3D data and then search those reflections to determine fast-S azimuth, which is also the azimuth of Shmax. Approach 2 was to conduct an inversion of azimuth-dependent P-P reflections and then extract information from these inversion results that defined Shmax.

Approach 1 worked quite well. Shmax azimuths were determined by analyzing azimuth-dependent SV-P reflection times at three different geologic formations located at depths of 3500 ft, 5500 ft, and 7500 ft. This method provided the same Shmax azimuth (approximately 65 degrees) at all three depths. More importantly, this seismic-based estimate agreed with local ground-truth measurements of Shmax. This work is first-ever extraction and use of azimuth-dependent SV-P reflections from 3D data and provides a new and important methodology for determining fast-S azimuth (i.e., Shmax azimuth) from common 3D P-source data that are recorded by vertical-geophones.

Approach 2 yielded a correct estimate of Shmax at the shallowest formation at a depth of 3500 ft, but exhibited increasing estimation error as formation depth increased to 5500 ft and then to 7500 ft.

Similar to the VSP study, the 3D seismic data used in this research were legacy data. Others can use existing 3D, P-source, vertical-geophone data to define Shmax azimuth in deep rocks and not have to expend funds to acquire new 3D seismic data.

Important advances were achieved in this Task 2 research. Specifically, it has been verified that down-going, direct-S, wavefields produced by P sources provide low-cost and robust options for monitoring Shmax azimuth in deep reservoir rocks.

6.0   References

Alford, R.M., H.B. Lynn, and L.A. Thomsen, 1989, Seismic surveying technique for the detection of azimuthal variations in the earth's subsurface: U.S. Patent 4,817,061.

Battelle, 2019. TASK 4 (FIELD TESTING) REPORT:A Non-Invasive Approach for Elucidating the Spatial Distribution of in-situ Stress in Deep Subsurface Geologic Formations Considered for CO2 Storage DOE Award Number DE-FE0031686; Prepared by Battelle 505 King Avenue Columbus, Ohio 43201; Prepared for U.S Department of Energy National Energy Technology Laboratory, Pittsburgh, PA. December 30, 2019

Buschbach TC and DR Kolata. 1991. "Regional Setting of Illinois Basin." *In* Leighton MW, Kolata DR, Oltz DF, and Eidel JJ (eds.), *Interior Cratonic Basins*. *American Association of Petroleum Geologists Memoir* 51:29–55.

Cornet, F., 2014. Results from the In-Situ Stress Characterization Program, Phase 1: Geomechanical Tests Conducted in the FutureGen Stratigraphic Well (FGA#1). PNWD-4421. Battelle, Pacific Northwest Division, Richland, Washington.

Graul, M., 2017, AVO and interpretive processing of SV-P reflections co-existing with P-P reflections on P-wave legacy data: SEG Expanded Abstract

Gupta, M. and B. Hardage, 2017, Improved reservoir delineation by using SV-P seismic data in Wellington field, Kansas: SEG Expanded Abstract (5 pages), 87th SEG Annual International Meeting. https://doi.org/10.1190/segam2017-17559574.1

Haimson, B. C., 1978. CRUSTAL STRESS IN THE MICHIGAN BASIN, JOURNAL of GEOPHYSICALR ESEARCH DECEMBER, VOL. 83, NO. B12, December 10, 1978, pp. 5857-5863.

Hardage, B.A., M.V. DeAngelo, P.E. Murray, and D. Sava, 2011, Multicomponent seismic technology: Geophysical References Series No. 18, Society of Exploration Geophysicists, Tulsa, OK, 318 pages.

Hardage, B.A., D. Sava, and D. Wagner, 2014, SV-P – an ignored seismic mode that has great value for interpreters: Interpretation, v. 2 no. 2, SE17-SE27, httdoi.org/10.1190/INT-2013-0096.1.

Hardage, B.A. and D. Wagner, 2014a, Generating direct-S modes with simple, low-cost, widely available seismic sources: Interpretation, v. 2, no. 2, SE1-SE16, doi10.1190/INT-2013-0095.1.

Hardage, B.A. and D. Wagner, 2014b, S-S imaging with vertical-force sources: Interpretation, v. 2, no. 2. p. SE29-SE38, http://doi.org/10.1190/INT-2013-0097.1

Hardage, B.A., 2017a, Practicing S-wave reflection seismology with "P-wave" sources – concepts, principles, and overview: SEG Expanded Abstract (5 pages), 87th SEG Annual International Meeting, https://doi.org/10.1190/segam2017-17256173.1

Hardage, B.A., 2017b, Examples of SV-P images made with P sources and vertical geophones: SEG Expanded Abstract (5 pages), 87th SEG Annual International Meeting. https://doi.org/10.1190/segam2017-17430569.1

Hardage, B.A., 2017c, Real-data comparisons of direct-S modes produced by "P" sources and "gold standard" S sources: SEG Expanded Abstract (5 pages), 87th SEG Annual International Meeting. https://doi.org/10.1190/segam2017-17430461.1

Hardage, B.A., 2017, Land based S-wave reflection seismology with P sources – does it work?: SEG Expanded Abstract (5 pages), 87[th]SEG Annual International Meeting

Hardage, B.A. and D. Wagner, 2018a, Direct-SV radiation produced by land-based P sources – part 1 – surface sources: Interpretation, v. 6, no. 3, http://dx.doi.org/10-1190/INT-2018-0046.1

Hardage, B.A. and D. Wagner, 2018b, Direct-SV radiation produced by land-based P sources – part 2 – buried explosives: Interpretation, v. 6, no. 3, http://dx.doi.org/10-1190/INT-2018-0047.1

Karr, B., 2017, SV-P imaging compared to P-SV imaging – analysis of statics and velocities required to create an SV-P image: SEG Expanded Abstracts (5 pages), 87th SEG Annual Meeting.

Kusubov, A.S., 1976, Surface and body waves from surface and underground explosions: Lawrence Livermore Laboratory Report NCID-17222, 20 pages.

Li, Y. and Hardage, B. A., 2015, SV-P extraction and imaging for far-offset vertical seismic profile data: Interpretation, v. 3, no. 3, p. SW27-SW35, http://dx.doi.org/10.1190/INT-2015-0002.1

Li, Y., D. Wang, S. Shi, and X. Cui, 2017, Gas reservoir characterization using SV-P converted wave mode – a case study from western China: SEG Expanded Abstract (5 pages), 87[th]SEG Annual International Meeting

Lynn, H.B., 2004a, The winds of change: anisotropic rocks – their preferred direction of fluid flow and their associated seismic signatures, Part 1: The Leading Edge, **23**, 1156-1162.

Lynn, H.B., 2004b, The winds of change: anisotropic rocks – their preferred direction of fluid flow and their associated seismic signatures, Part 2: The Leading Edge, **23**, 1258-1268.

Miller, G. and H. Pursey, 1954, The field and radiation impedance of mechanical radiators on the free surface of a semi-infinite isotropic solid: Proceedings of the Royal Society of London, Series A, 223, 521–541, doi: 10.1098/rspa .1954.0134.

Mueller, M.C., 1992, Using shear waves to predict lateral variability in vertical fracture intensity: The Leading Edge, 11, 29-35.

Ruger, A., 1997, P-wave reflection coefficients for transversely isotropic models with vertical and horizontal axis of symmetry: Geophysics, 62, 713-722.

Ruger, A. and D. Gray, 2014, Wide-azimuth amplitude-variation-with-offset analysis of anisotropic fractured reservoirs: Society of Exploration Geophysicists, Tulsa, OK, 300 pages, https://doi.org/10.1190/1.9781560803027.entry 2.

Short, N.M., 1961, Excavations of contained TNT explosions in tuff: University of California Lawrence Radiation Laboratory Report UCRL 6445, 23 pages.

Sondergeld, C.H., and C.S. Rai, 1992, Laboratory observations of shear-wave propagation in anisotropic media: The Leading Edge, **11**, 38–43.

Twiss, R.J., and E.M. Moores, 1992, Structural geology, W. H. Freeman & Co.

Winterstein, D.F. and M.A. Meadows, 1991, Shear-wave polarizations and subsurface stress directions at Lost Hills field: Geophysics, 56, 1331-1348.

Xu, S. and M.S. King, 1989, Shear-wave birefringence and directional permeability in fractured rock: Scientific Drilling, 1, 27-33.

BATTELLE

It can be done